

REF ID: A705R-TR-89-1290

A705R-TR-89-1290

2

SC5502.FR

SC5502.FR

Copy No. 4

AD-A214 645

STUDIES OF OPTICAL MATRIX MULTIPLICATION AND RECONFIGURABLE OPTICAL INTERCONNECT CONCEPTS

FINAL REPORT FOR THE PERIOD
November 1, 1986 through April 30, 1989

CONTRACT NO. F49620-87-C-0015

Prepared for

Directorate of Electronic and Material Science
ATTN: AFOSR/NE, Dr. C. Lee Giles
Building 410
Bolling AFB, Washington, DC 20332-6448

Pochi Yeh
Principal Investigator

JULY 1989

DTIC
ELECTE
NOV 20 1989

D^{CS}

Approved for public release; distribution unlimited

"The views and conclusions contained in this document are those of the authors and should not be interpreted as necessarily representing the official policies, either expressed or implied, of the Defense Advanced Research Projects Agency or the U.S. Government."



Rockwell International
Science Center

89 11 17 031

UNCLASSIFIED

SECURITY CLASSIFICATION OF THIS PAGE

REPORT DOCUMENTATION PAGE				FORM APPROVED OMB No. 0704-0188	
1a. REPORT SECURITY CLASSIFICATION UNCLASSIFIED			1b. RESTRICTIVE MARKINGS		
2a. SECURITY CLASSIFICATION AUTHORITY			3. DISTRIBUTION/AVAILABILITY OF REPORT Approved for public release; distribution unlimited		
2b. CLASSIFICATION/DOWNGRADING SCHEDULE					
4. PERFORMING ORGANIZATION REPORT NUMBER: SC5502.FR			5. MONITORING ORGANIZATION REPORT NUMBER: AFOSR-TR-89-1290		
6a. NAME OF PERFORMING ORGANIZATION ROCKWELL INTERNATIONAL Science Center		6b. OFFICE SYMBOL (If Applicable)		7a. NAME OF MONITORING ORGANIZATION Air Force Office of Scientific Research	
6c. ADDRESS (City, State, and ZIP Code) 1049 Camino Dos Rios Thousand Oaks, CA 91360			7b. ADDRESS (City, State and ZIP Code) Bldg. 410 Bolling Air Force Base Washington, DC 20332-6448		
8a. NAME OF FUNDING SPONSORING ORGANIZATION DARPA & AFOSR		8b. OFFICE SYMBOL (If Applicable) NE		9. PROCUREMENT INSTRUMENT IDENTIFICATION NUMBER CONTRACT NO. F49620-87-C-0015	
8c. ADDRESS (City, State and ZIP Code) 1400 Wilson Blvd. Arlington, VA 22209			10. SOURCE OF FUNDING NOS.		
			PROGRAM ELEMENT NO.		PROJECT NO.
			ARPA ORDER No. 5884		TASK NO.
			60102E		01
			WORK UNIT ACCESSION NO.		
11. TITLE (Include Security Classification) STUDIES OF OPTICAL MATRIX MULTIPLICATION AND RECONFIGURABLE OPTICAL INTERCONNECT CONCEPTS					
12. PERSONAL AUTHOR(S) Yeh, Pochi; Chiou, Arthur E.					
13a. TYPE OF REPORT Final Report		13b. TIME COVERED FROM 11/01/86 TO 04/30/89		14. DATE OF REPORT (Year, Month, Day) 1989, JULY	
15. PAGE COUNT					
16. SUPPLEMENTARY NOTATION "The views and conclusions contained in this document are those of the authors and should not be interpreted as necessarily representing the official policies, either expressed or implied, of the Defense Advanced Research Projects Agency or the U.S. Government."					
17. COSATI CODES			18. SUBJECT TERMS (Continue on reverse if necessary and identify by block number)		
FIELD	GROUP	SUB-GROUP			
19. ABSTRACT (Continue on reverse if necessary and identify by block number) In this program, we studied unique computing concepts which use nonlinear optical phenomena to perform matrix multiplication and to provide reconfigurable optical interconnection. We have demonstrated several schemes for optical matrix multiplication using optical phase conjugation and nonlinear optical four-wave mixing in either the spatial or the Fourier domain. Photorefractive crystals such as barium titanate or strontium barium niobate (SBN) were used as the nonlinear media. We have also developed a unique concept of reconfigurable optical interconnection which utilizes the dynamic holograms in a photorefractive crystal in conjunction with a spatial light modulator to achieve very high energy efficiency. The same concept was validated experimentally using a BaTiO ₃ crystal. Important issues (Continued)					
20. DISTRIBUTION/AVAILABILITY OF ABSTRACT UNCLASSIFIED/UNLIMITED <input type="checkbox"/> SAME AS RPT. <input checked="" type="checkbox"/> DTIC USERS <input type="checkbox"/>			21. ABSTRACT SECURITY CLASSIFICATION UNCLASSIFIED		
22a. NAME OF RESPONSIBLE INDIVIDUAL Dr. G. Lee Giles			22b. TELEPHONE NUMBER (Include Area Code) (202) 767-21931		22c. OFFICE SYMBOL AFOSR/NE

DD FORM 1473, JUN 86

Previous editions are obsolete.

UNCLASSIFIED

SECURITY CLASSIFICATION OF THIS PAGE

UNCLASSIFIED

SECURITY CLASSIFICATION OF THIS PAGE

19. ABSTRACT (Cont'd)

such as energy efficiency, reconfiguration time, data rate, and signal-to-noise ratio have also been investigated. Our unique approach has practically eliminated the problem of fanout loss which has been regarded as one of the most critical issues in an optical crossbar switch. Future applications of this approach in various levels of the optical interconnection hierarchy (module-to-module, backplane-to-backplane, board-to-board, ...) in parallel computing and in the optical implementations of neural-like processors can be anticipated. We have also conceived several new concepts in the same area. The results are documented in eleven technical papers/presentations and four patent disclosures.

UNCLASSIFIED

SECURITY CLASSIFICATION OF THIS PAGE



TABLE OF CONTENTS

	<u>Page</u>
1.0 SUMMARY	1
1.1 Contract Description	1
1.2 Scientific Problem	1
1.3 Progress Summary	1
1.4 Publications and Presentations	2
1.5 Patent Disclosures	3
2.0 TECHNICAL DISCUSSION	4
2.1 Matrix-Matrix Multiplication	5
2.2 Matrix-Vector Multiplication	8
2.3 Reconfigurable Optical Interconnect	8
3.0 PROGRESS	12
3.1 Matrix-Vector Multiplication Using Photorefractive Four-Wave Mixing	12
3.2 Matrix-Matrix Multiplication via Color Multiplexing	14
3.3 Matrix-Matrix Multiplication using Spatial Convolution	15
3.4 Matrix-Vector Multiplication Using a Spatial Light Modulator and a Phase Conjugator	16
3.5 Optical Interconnection using Dynamic Photorefractive Holograms	17
3.5.1 Principle of Operation	17
3.5.2 Experimental Demonstration	20
3.5.3 Demonstration of High Data Rate Transmission	21
3.5.4 Energy Efficiency of Photorefractive Interconnection: Theoretical Calculation and Experimental Measurement	23
3.5.5 Maximizing Energy Efficiency by Matched Amplification via Fourier Transformation	24
3.5.6 Contrast Enhancement by Double Passage	29
3.5.7 Experimental Demonstration of Reconfigurability	33
4.0 REFERENCES	34
5.0 APPENDIX	36
APPENDIX 5.1: Optical Matrix-Vector Multiplication Through Four-Wave Mixing in Photorefractive Media	36
APPENDIX 5.2 Optical Matrix-Matrix Multiplication Using Multi-Color Four-Wave Mixing	40



TABLE OF CONTENTS (continued)

	<u>Page</u>
APPENDIX 5.3 Optical Matrix-Matrix Multiplication by Spatial Convolution via Four-Wave Mixing	48
APPENDIX 5.4 Optical Matrix-Vector Multiplication Using a Spatial Light Modulator and a Phase Conjugator	54
APPENDIX 5.5 Optical Interconnection Using Photorefractive Dynamic Holograms	59
APPENDIX 5.6 Photorefractive Nonlinear Optics and Optical Computing	64
APPENDIX 5.7 Energy Efficiency of Optical Interconnection Using Photorefractive Holograms	81
APPENDIX 5.8 On Image Amplification by Two-Wave Mixing in Photo- refractive Crystals	120
APPENDIX 5.9 Reconfigurable Optical Interconnection Using Photorefractive Hologram	135

Approved For	
Released To	
By	
Date	
Signature	
Initials	
Remarks	
A-1	



LIST OF FIGURES

<u>Figure</u>		<u>Page</u>
1	Matrix-matrix multiplication using four-wave mixing.	6
2	Matrix-vector multiplication via four-wave mixing.	9
3	Reconfigurable optical interconnection.	10
4	Optical matrix-vector multiplication using photorefractive four-wave mixing.	12
5	Experimental results of optical matrix-vector multiplication using photorefractive four-wave mixing.	13
6	Output of the detector monitoring the intensity of the optical beam representing the product vector.	14
7	Decomposition of matrix-matrix multiplication into matrix-vector multiplication.	14
8	Optical matrix-matrix multiplication via color multiplexing.	15
9	A schematic diagram illustrating the basic concept of optical matrix-vector multiplication using a photorefractive phase conjugator in conjunction with a spatial light modulator.	16
10	A schematic drawing of a $1 \times N$ optical interconnection using dynamic photorefractive holograms. $N = 4$	19
11	A schematic drawing of a $N \times N$ optical interconnection using dynamic photorefractive holograms. $N = 4$	19
12	A schematic diagram of the experimental configuration for a 1×32 interconnection using a photorefractive barium titanate crystal.	20
13	Intensity distribution at the output image plane.	21
14	Intensity distribution at the output image plane when all but three of the signal channels are "ON." The table on the right- hand side compares the energy efficiencies achieved using the conventional approach and the holographic approach.	22



LIST OF FIGURES

<u>Figure</u>		<u>Page</u>
15	(a) Signal carried by the probe beam and (b) amplified signal carried by the probe beam after undergoing two-wave mixing	22
16	A schematic diagram showing the intensities of various beams in a $N \times N$ permutational interconnection	24
17	The theoretical energy efficiency as a function of the dimension of the array as predicted by Eq. (8) for $t = 1$, $\alpha = 0$, and an optimum R	25
18	A schematic diagram of the experimental configuration for measurement of the energy efficiency of photorefractive interconnection holograms in a barium titanate crystal	25
19	Energy efficiency (η) of photorefractive two-beam coupling in a barium titanate sample as a function of the transmittance of a neutral density filter placed in the signal input arm. The transmittance is labeled $1/N$ to relate it to the fanout loss of a $N \times N$ permutation crossbar network	26
20	An experimental configuration for a 1-to- $N \times N$ (for $N = 10$) broadcasting network using photorefractive holograms at the Fourier domain	28
21	The intensity patterns of the masks for the probe and the pump beams at the image plane and the Fourier plane	28
22	Energy efficiency (η) as a function of number of signal channels (N) in a 1-to- $N \times N$ broadcasting configuration using photorefractive holograms in a barium titanate sample	29
23	An experimental configuration for contrast-enhancement by double passage	31
24	Intensity profiles and contrast of a binary image: (a) at the input plane, (b) at the output plane after double passage via phase-conjugate reflection, and (c) at the output plane after double passage via mirror reflection	31
25	Experimental results showing contrast-preserving image amplification by photorefractive two-wave mixing at the Fourier domain; (a) input intensity profile, and (b) amplified output intensity profile	32



1.0 SUMMARY

1.1 Contract Description

This contract studies unique optical computing concepts which use nonlinear optical phenomena to perform matrix multiplication and to provide reconfigurable optical interconnection. The study focuses on the use of real-time holography in nonlinear media such as photorefractive crystals for optical computing.

1.2 Scientific Problem

By incorporating the parallel nature of optics in nonlinear media, it is possible to perform parallel matrix multiplication using four-wave mixing. In addition, the dynamic holography in nonlinear optical media provides a natural candidate for the reconfigurable interconnection. The general problem in this program is to generate and investigate new concepts which use these nonlinear optical phenomena for optical computing.

Specifically, this program investigates experimentally and theoretically the multiplication of matrices using optical four-wave mixing in nonlinear media, and the possibility of using such matrix multiplication and wave mixing for reconfigurable interconnection.

1.3 Progress Summary

There are several areas of significant progress achieved under this contract that are directly related to the development of optical matrix multiplication and reconfigurable optical interconnection. These include:

1. First experimental demonstration of parallel matrix-vector multiplier using optical four-wave mixing in a barium titanate (BaTiO_3) crystal.
2. First experimental demonstration of summation process inside the nonlinear media in matrix-vector multiplications.
3. Experimental demonstration of 2×2 matrix-matrix multiplication using optical four-wave mixing in a BaTiO_3 crystal.



4. Experimental demonstration of matrix-matrix multiplication using color multiplexing.
5. Experimental demonstration of matrix-matrix multiplication using convolution.
6. Experimental demonstration of matrix-vector multiplication using a spatial light modulator and a phase conjugator.
7. Development and experimental demonstration of a new concept of reconfigurable optical interconnection using photorefractive holograms.
8. Experimental demonstration of high-efficiency interconnection using BaTiO₃ crystals.
9. Development of matched amplification at the Fourier plane to achieve maximum efficiency.
10. Experimental demonstration of high efficiency in photorefractive optical interconnection using matched amplification.
11. Experimental demonstration of reconfigurability using a liquid crystal TV in conjunction with a photorefractive barium titanate crystal.

1.4 Publications and Presentations

1. "Reconfigurable Interconnection Using Photorefractive Holograms," Proc. SPIE, Vol. 1151, Paper No. 03, to be presented at SPIE's Annual International Symposium on Optical and Optoelectronic Applied Science and Engineering (August, 1989, San Diego, CA).
2. "Energy Efficiency of Optical Interconnections Using Photorefractive Holograms," submitted to Appl. Opt. (1989).
3. "On Image Amplification by Two-Wave Mixing in Photorefractive Crystals," submitted to Appl. Opt. (1989).
4. "Photorefractive Nonlinear Optics and Optical Computing," Opt. Eng. 28(4), 328 (1989).
5. "Energy Efficiency of Optical Interconnection Using Photorefractive Dynamic Holograms," Optical Computing, 1989 Technical Digest Series, Vol. 9 (Optical Society of America, Washington, D.C.), pp. 128.



SC5502.FR

6. "Energy Efficient Optical Interconnection Using Dynamic Holograms in Photorefractive Media," OSA Annual Meeting, 1988 Technical Digest Series, Vol. 11 (Optical Society of America, Washington, D.C., 1988), pp. 178.
7. "Optical Interconnection Using Photorefractive Dynamic Holograms," Appl. Opt. 27, 2093 (1988).
8. "Optical Matrix-Vector Multiplication Using a Spatial Light Modulator and a Phase Conjugator," Spatial Light Modulators and Applications, 1988 Technical Digest Series, Vol. 8 (Optical Society of America, Washington, D.C., 1988), pp. 298.
9. "Optical Matrix-Matrix Multiplication Using Multicolor Four-Wave Mixing," Proc. SPIE, Vol. 881, paper 38, presented at OE/LASE'88 (Jan. 10-17, 1988, Los Angeles, CA).
10. "Optical Matrix-Vector Multiplication via Four-Wave Mixing in Photorefractive Media," Opt. Lett. 12, 138 (1987); Opt. Lett. 12, 373 (1987).
11. "Optical Matrix-Vector Multiplication Using Four-Wave Mixing," Paper MM5, OSA Annual Meeting (Oct. 1986, Seattle, WA), J. Opt. Soc. Am. A3 (13), 16 (1986).

1.5 Patent Disclosures

"Multicolor Matrix-Matrix Multiplier with N^3 Parallelism," M. Khoshnevisan, A.E.T. Chiou and P. Yeh, Rockwell Patent Disclosure 87SC37.

"Matrix-Vector Multiplier using Photorefractive Phase Conjugators," P. Yeh, A.E.T. Chiou and M. Khoshnevisan, Rockwell Patent Disclosure 87SC46.

"Optical Matrix-Matrix Multiplier with N^3 Parallelism by Spatial Convolution via Four-Wave Mixing," A.E.T. Chiou, Rockwell Patent Disclosure 87SC63.

"Reconfigurable Optical Interconnect using Dynamic Holograms," P. Yeh, Rockwell Patent Disclosure 87SC54.



2.0 TECHNICAL DISCUSSION

The technical problem addressed in this contract is the study of optical matrix multiplication and reconfigurable optical interconnection. By incorporating the parallel nature of optics in nonlinear media such as photorefractive crystals,^{1,2} it is possible to perform parallel matrix multiplication using four-wave mixing. In addition, the dynamic holography in nonlinear optical media provides a natural candidate for the reconfigurable optical interconnection.^{3,4}

Specifically, this program is aimed at the utilization of nonlinear optical phenomena such as phase conjugation,⁵⁻⁷ two-wave mixing,^{2,5} and four-wave mixing⁵⁻⁷ in nonlinear media^{8,9} to perform the matrix-vector and matrix-matrix multiplications and reconfigurable optical interconnection. Photorefractive crystals such as BaTiO₃ and strontium barium niobate (SBN) were used as the nonlinear media.

Generally speaking, four-wave mixing is a nonlinear optical process in which three input waves mix to yield a fourth wave. In phase-matched four-wave mixing, the three input waves consist of two counterpropagating pump waves, E_1 and E_2 , and an arbitrary probe wave, E_3 . All three couple through the third-order susceptibility, $\chi^{(3)}$, to yield a fourth wave, E_4 , which is proportional to the product of E_1 , E_2 and complex conjugate of E_3 , and can be written as⁸

$$E_4 \propto \chi^{(3)} E_1 E_2 E_3^*$$

Such a four-wave mixing can be understood in terms of the recording and readout processes which occur in holography. In the nonlinear media, one of the pump waves and the probe wave form an interference pattern which, in turn, induces an index grating. The other pump wave is diffracted from this grating and generates the fourth wave. The formation of the grating (or hologram) and readout processes take place at the same time. Thus, four-wave mixing is sometimes referred to as a real-time holography.

By using four-wave mixing in nonlinear media, multiplication of signals can take place in a subpicosecond time scale. In addition, if we use the parallel nature of optical waves, each wave can carry spatial information for the purpose of image processing using the two transverse dimensions. Such an application of four-wave mixing to



real-time image processing was recently reported using BSO crystals.¹⁰ In what follows, we will describe some unique concepts which use the two transverse dimensions to carry the matrix information for the purpose of matrix multiplication and reconfigurable optical interconnection.

2.1 Matrix-Matrix Multiplication

The matrix multiplication¹⁰⁻¹² between two $N \times N$ matrices can be stated as follows:

$$C = AB \quad (1)$$

where

$$C_{ij} = \sum_k A_{ik} B_{kj} \quad (2)$$

Note that a matrix multiplication consists of two main operations, a parallel multiplication and an addition.

Referring to Fig. 1a, let us consider a four-wave mixing configuration which is suitable for matrix multiplication.¹³ Beam 1 and Beam 2 contain the information about the two matrices $A(x,z)$ and $B(z,y)$, respectively. Beam 1 is propagating along the y -axis, and Beam 2 is propagating along the x -axis. These directions are chosen for the sake of clarity in introducing the concept. They are not the only directions for matrix multiplication. Also, these matrices can be either continuous or discrete. In the discrete case, each beam consists of a matrix of beamlets, as shown in Fig. 1b.

In the nonlinear medium, these two matrix-carrying beams form an interference pattern. As a result of the nonlinear response of the medium, a volume grating is formed. This grating contains information about the product of the matrix elements of these two matrices, and can be written as:

$$\Delta n = n_2 A(x,z) B^*(z,y) e^{i(\vec{k} \cdot \vec{r})} + \text{c.c.} \quad (3)$$



SC5502.FR

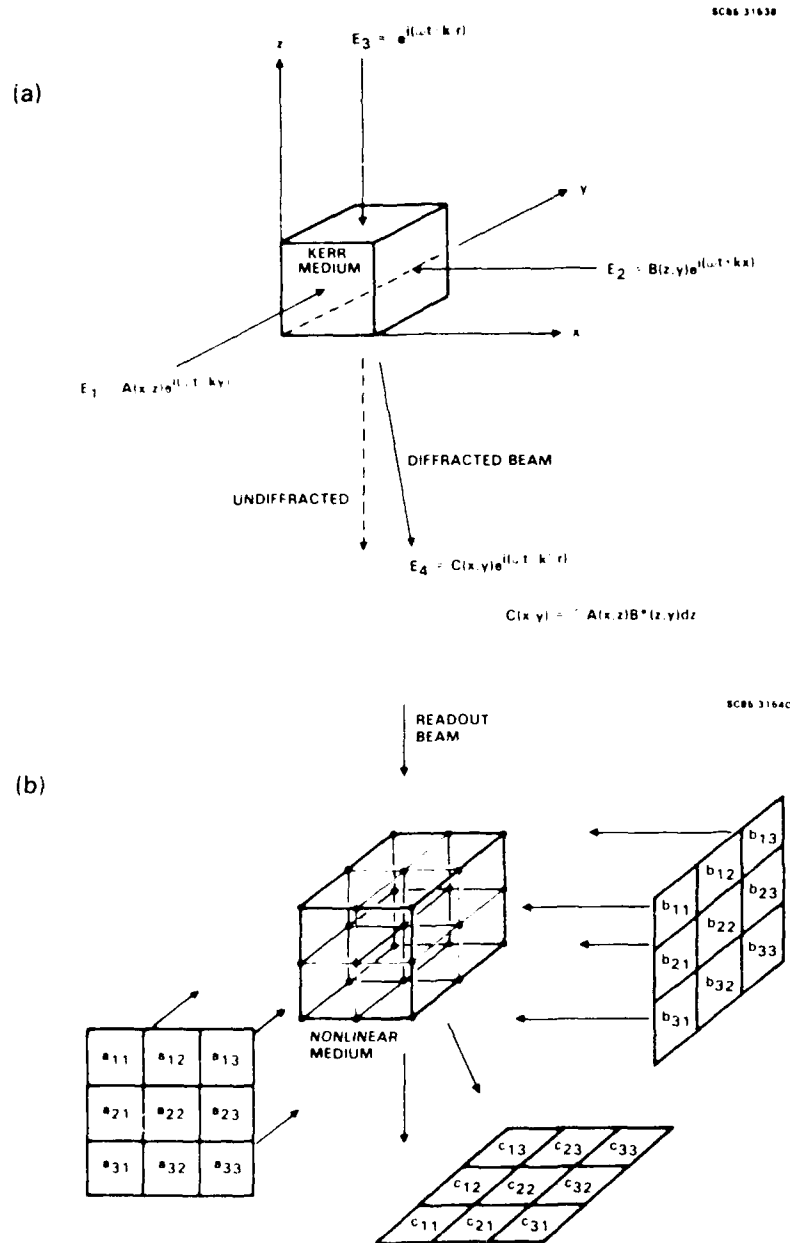


Fig. 1 Matrix-matrix multiplication using four-wave mixing.

where k is the difference of the wavevectors of the matrix-carrying beams and cc represents complex conjugation. The parameter n_2 is the Kerr coefficient and is proportional



SC5502.FR

to the third-order susceptibility $\chi^{(3)}$ of the medium. Note that the nonlinear response of the medium serves the purpose of parallel multiplication.

The volume grating is then read out by a third beam which can simply be a plane wave. The diffracted beam consists of the integrated contribution from each part of the grating along the beam path, and thus can be written

$$C(x,y) \propto \int A(x,z)B^*(z,y)dz \quad (4)$$

where the integration is carried out along the beam path. Note that the integration completes the operation of matrix multiplication. The information about the product of these two matrices is now impressed on the transverse spatial distribution of the diffracted beam.

Due to the phase matching requirement, the readout beam must be incident along the directions which satisfy the Bragg diffraction condition to achieve high efficiency. In anisotropic nonlinear media, the polarization states, as well as the direction of propagation, can be chosen such that the largest of the nonlinear susceptibilities is fully utilized.

The four-wave mixing can be either degenerate or nondegenerate. In the degenerate case, all the beams have the same frequency. In the nondegenerate case, the frequencies of the beams can be slightly different. This may be useful for the purpose of separating the diffracted beam from the undiffracted portion.

To illustrate the information capacity of such a nonlinear optical matrix multiplication, let us consider a four-wave mixing process using an Ar ion laser at 4880Å in a medium of a 1 cm cube. The grating space is of the order of 0.5 μm . Thus, 10 μm x 10 μm is enough for each pixel of information. In other words, a 1 cm cube is capable of handling 1000 x 1000 matrices. With a material response time of 1 ns, such a matrix multiplication has a potential data throughput rate of quadrillion bits per second (10^{15} bits/s)!



2.2 Matrix-Vector Multiplication

Another scheme as shown in Fig. 2 is suitable for matrix-vector multiplication.¹¹⁻¹⁴ Here, as an example, let us consider a discrete case in which we need to carry out the multiplication of an N-element vector and an N x N matrix. The vector is fanned out into N-rows of identical vectors. These N x N small beams are directed to a non-linear medium. The matrix which also contains N x N small beams is also directed to the medium in such a way that each beam of the matrix is counterpropagating in a direction relative to the corresponding beam of the vector. Thus, in the medium, there are N x N spatially separated regions which are pumped each by a pair of counterpropagating beams. Now, N x N probing beams are directed into the medium in such a way that each probe beam will propagate through an intersection region. The probe beams will be "plane wave" beamlets propagating in parallel. As a result of the four-wave mixing, each probe beam will generate a phase-conjugated beam which, within a proportional factor, can be written $M(i,j)a(j)$. By using a cylindrical lens, a summation over j can be obtained. Thus, we have

$$b(i) = \sum_j M(i,j)a(j) \quad (5)$$

where $a(j)$ is the j-th element of the vector \hat{a} and $M(i,j)$ is the matrix element. Such a scheme for matrix-vector multiplication can also be used for matrix-matrix multiplication by decomposing a matrix into column vectors and then multiplying the matrix with each of the column vectors. Using color-multiplexing, one can perform matrix-matrix multiplication with N^3 -parallelism.¹⁵

2.3 Reconfigurable Optical Interconnection

Optical interconnection will play a key role in both the optical computing and VLSI systems.^{3,4,16} There are many advantages of optical interconnect. These include high space-bandwidth and time-bandwidth products, thus, many independent channels could be exploited for demanding computations. Optical processors are inherently two-dimensional and parallel. Optical signals can propagate through each other in separate channels with essentially no interaction. Optical signals can also propagate in parallel channels without any interference and crosstalk. In the VLSI systems, optical interconnect can be used to solve the problem of communication, as well as the clock distribution.



SCSS 31841

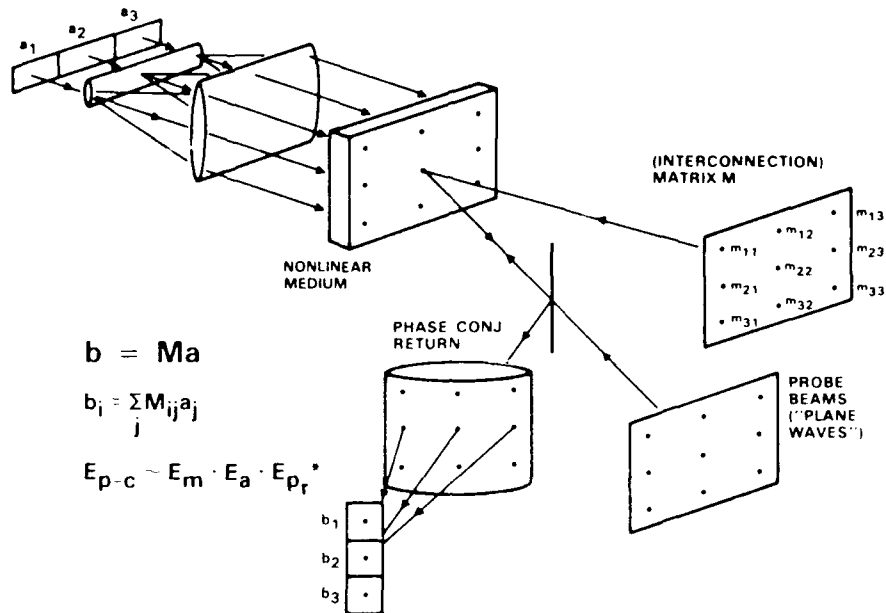


Fig. 2 Matrix-vector multiplication via four-wave mixing.

Computer-generated holograms (CGH) can be used for fixed optical interconnect. The most general CGH consists of a two-dimensional array of subholograms. Each subhologram is capable of diffracting a gate output to any gate or combination of gate inputs. Such a fixed interconnect pattern is adequate for many applications, including the point operation, matrix operation, the clock distribution and a globally synchronous systolic processor. However, there are many situations in which a dynamic optical interconnect is required.

In Fourier transform and sorting, every element of an output array is affected by all the elements of the input array, and conversely, each element of the input array affects all elements of the output array. In addition, the interconnections change at different stages of the computation. Thus, these operations require global and dynamic interconnection between different elements of the input array.

In image restoration, pattern recognition, and neural network systems, the interconnect patterns could be data-dependent, making it impossible to foresee the interconnect requirements at different stages of processing without having foreknowledge of the input. The computational throughput of parallel processor implementing



SC5502.FR

these types of operation will be critically affected by the availability of a dynamic and global interconnect network.

In Fourier transform and sorting, the requirement for dynamic interconnect can be avoided by resorting to a fixed but global interconnect pattern known as the "perfect shuffle". In the area of image restoration and pattern recognition, there is a minimum amount of regularity and structure. In addition, there is a possible data and time dependency in the interconnect requirements. A global and reconfigurable interconnect network will be vital to achieving high throughput and high efficiency with parallel processors implementing these operations.

The most general interconnect system is one in which any gate output can be connected to the input of any gate or combination of gates (see Fig. 3). The effect of such an interconnect can be represented by the matrix equation

$$O = M I \quad (6)$$

where I is a vector representing the two-dimensional input array, M is the matrix representing the interconnect, and O is a vector representing the output array. In digital optical computing,^{17,18} the input array is actually the gate output array. Each matrix element (i,j) is nonzero if, and only if, there is a connection between pixel j of the input

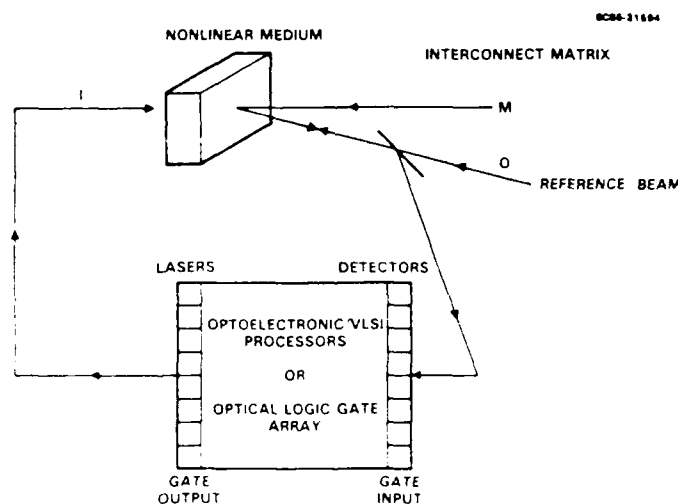


Fig. 3 Reconfigurable optical interconnection.



array and pixel i of the output array. The matrix-vector multiplication technique described in Section 2.2 can be used as an optical interconnect, which provides both local and global communication between the gate input and gate output. In the VLSI systems, the vectors I may consist of N laser beams, each containing a stream of data from a processor, and the vector O represents the output laser beams, each feeding into a processor. The main advantage of using such nonlinear matrix-vector multiplication for interconnection is that the matrix M can be easily changed for the purpose of reconfiguring the interconnect.

Equation (6) can be generalized such that both the input array I and the output array O are two-dimensional matrices. In that case, the most general interconnect matrix M must be four-dimensional (i.e., tensor of rank four). Each matrix element $(ijkl)$ represents the connection between pixel (ij) of the output array and pixel (kl) of the input array. Because of the two-dimensional nature of optical waves, it is desirable to represent the tensor M by a two-dimensional array of two-dimensional submatrices. Thus, the matrix-matrix multiplication described in Section 2.1 can be used for reconfigurable optical interconnect which provides the most general interconnection pattern. While this interconnection scheme allows complete generality, a price is paid in terms of the space-bandwidth product requirements on the nonlinear media.

3.0 PROGRESS

3.1 Matrix-Vector Multiplication

In our earlier demonstration of optical matrix-vector multiplication^{13,19} (see Appendix 5.1), we have used optical phase conjugation via nonlinear four-wave mixing in a photorefractive BaTiO_3 crystal to perform parallel multiplication. The summation required to obtain matrix-vector products is performed subsequently by using a cylindrical lens external to the nonlinear medium. With a slight modification of the experimental geometry, we have also successfully demonstrated that both the parallel multiplication and the summation can be done inside the nonlinear medium to achieve the desired matrix-vector multiplication without an external cylindrical lens.

The top view of the new experimental geometry is illustrated schematically in Fig. 4. The readout beam in this case consists of a vertical column of beamlets with equal intensity. This beam enters the crystal at an oblique angle such that each beamlet traverses, inside the crystal, all the counterpropagating pumping beamlets at the same horizontal plane. As the proper elements of the matrix and the vector are encoded in the two counterpropagating beams via the appropriate masks, the phase-conjugate output of

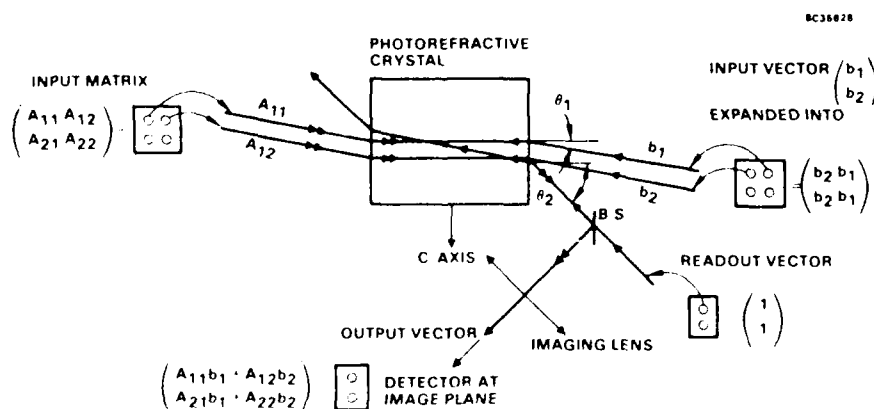


Fig. 4 Optical matrix-vector multiplication using photorefractive four-wave mixing.



each beamlet consists of the sum of the product resulting from each individual encounter. From a pure geometrical point of view, the probe beam (i.e., the readout beam) can conveniently be injected (from c-face of the crystal) perpendicular to the counterpropagating pumping beams.

The experimental results for the multiplication of a 4×4 binary matrix and a 4×1 binary vector are shown in Fig. 5. The magnified images of the masks used to encode the matrix, the vector and the probe are shown in Figs. 5a, b and c, respectively. The experimental results representing the final matrix-vector product is shown in Fig. 5d. The relative intensity of each output spot representing the element of the product vector is shown in Fig. 6. Due to the slow response time (or the order of second for optical intensity of the order of a few tens of milliwatt/cm²) and the consequential sensitivity to environmental changes of the photorefractive process, the output intensity fluctuates significantly.

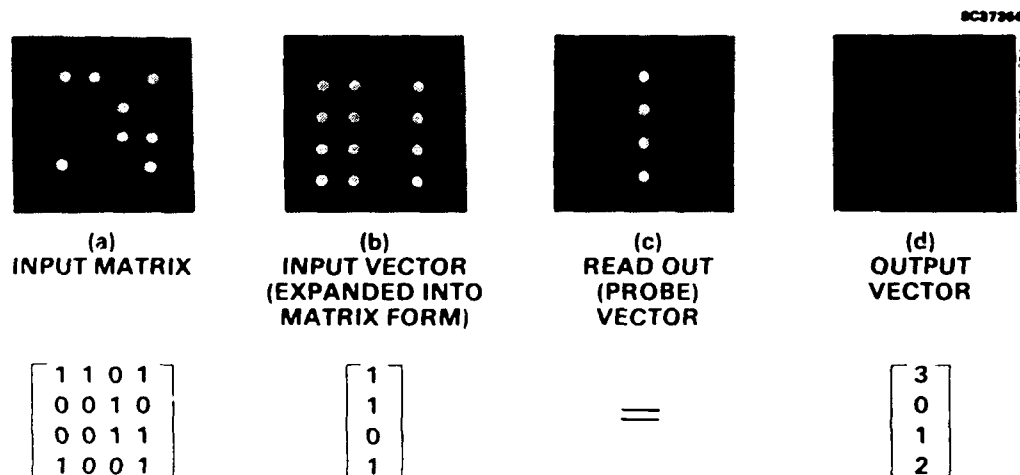


Fig. 5 Experimental results of optical matrix-vector multiplication using photorefractive four-wave mixing.



SC5502.FR

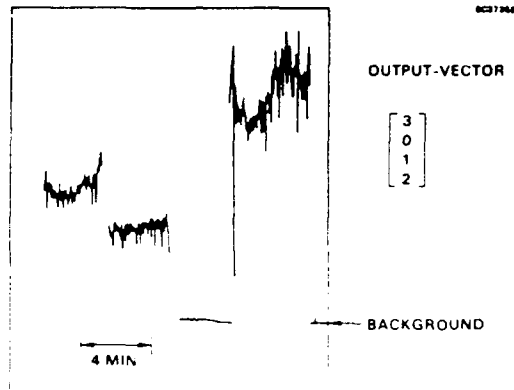


Fig. 6 Output of the detector monitoring the intensity of the optical beam representing the product vector.

$$\begin{bmatrix} m_{11} & m_{12} & m_{13} \\ m_{21} & m_{22} & m_{23} \\ m_{31} & m_{32} & m_{33} \end{bmatrix} \begin{bmatrix} a_{11} & a_{12} & a_{13} \\ a_{21} & a_{22} & a_{23} \\ a_{31} & a_{32} & a_{33} \end{bmatrix} = \begin{bmatrix} m_{11} & m_{12} & m_{13} \\ m_{21} & m_{22} & m_{23} \\ m_{31} & m_{32} & m_{33} \end{bmatrix} \begin{bmatrix} a_{11} & 0 & 0 \\ a_{21} & 0 & 0 \\ a_{31} & 0 & 0 \end{bmatrix} \\
 + \begin{bmatrix} m_{11} & m_{12} & m_{13} \\ m_{21} & m_{22} & m_{23} \\ m_{31} & m_{32} & m_{33} \end{bmatrix} \begin{bmatrix} 0 & a_{12} & 0 \\ 0 & a_{22} & 0 \\ 0 & a_{32} & 0 \end{bmatrix} \\
 + \begin{bmatrix} m_{11} & m_{12} & m_{13} \\ m_{21} & m_{22} & m_{23} \\ m_{31} & m_{32} & m_{33} \end{bmatrix} \begin{bmatrix} 0 & 0 & a_{13} \\ 0 & 0 & a_{23} \\ 0 & 0 & a_{33} \end{bmatrix}$$

Fig. 7 Decomposition of matrix-matrix multiplication into matrix-vector multiplication.

3.2 Matrix-Matrix Multiplication via Color Multiplexing

We have also extended our experimental demonstration on matrix-vector multiplication to matrix-matrix multiplication by color multiplexing^{13,20} (see Appendix 5.2). The basic idea is to decompose the problem into matrix-vector multiplications, as shown in Fig. 7, and carry out all the parallel matrix-vector multiplications simultaneously by using color multiplexing. Note that each of the operations shown on the right-hand side of the equation in Fig. 7 is in fact a matrix-vector multiplication. The basic principle of color multiplexing used to encode the component vectors with different colors is illustrated in Fig. 8 for the case of 4×4

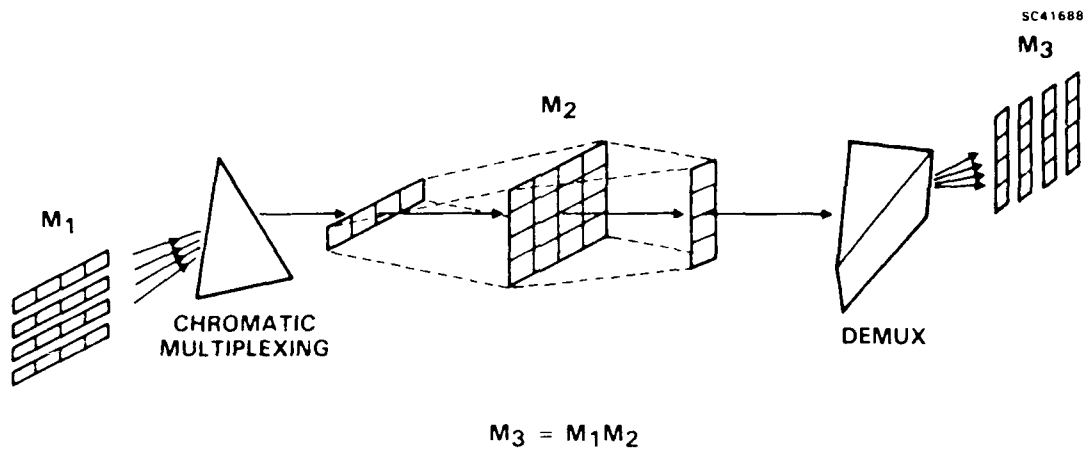


Fig. 8 Optical matrix-matrix multiplication via color multiplexing.

matrices. Each row vector of the matrix M_1 is illuminated by one color, and all the color components are then combined by the prism (angular multiplexing) into a single row prior to further expansion by anamorphic optics (not shown in the figure) to match the mask representing the second matrix. After proper element-by-element multiplications and summation (summing optics omitted) into the column, the resulting multicolor output is then demultiplexed into different color components that together represent the final product.

Using an argon ion laser that oscillates simultaneously at five colors in the blue-green and a BaTiO_3 crystal, we have demonstrated the principle described above for the case of 2×2 matrices. Details are given in Appendix 5.2.

3.3 Matrix-Matrix Multiplication using Spatial Convolution

In addition to the matrix-matrix multiplication using color-multiplexed four-wave mixing described in the previous section, we have also successfully demonstrated another scheme for matrix-matrix multiplication using spatial convolution via four-wave mixing. From the experimental point of view, the key difference between this approach and the others described above is that the nonlinear crystal is now located at the common Fourier plane, rather than the common image plane, of the input matrix masks. The encoding scheme, as explained in Appendix 5.3, is also different from those used in the earlier approaches. From the conceptual point of view, matrix-matrix multiplication in



full parallelism is achieved by space-multiplexing via spatial convolution using degenerate four-wave mixing.

3.4 Matrix-Vector Multiplication Using a Spatial Light Modulator and a Phase Conjugator

We have developed and demonstrated another new scheme for optical matrix-vector multiplication that uses a phase conjugator (with a finite storage time) in conjunction with a spatial light modulator (SLM) (see Appendix 5.4). The optical system involved is relatively simple compared with the other approaches. Without any modification, such a scheme can also perform matrix-matrix multiplication with $N^2/2$ parallelism.

Referring to Fig. 9, we use a SLM to impress the matrix and vector information in sequence to an input laser beam. This beam is directed toward a phase conjugator which has a finite storage time (a photorefractive barium titanate, for example). A cylindrical lens is inserted in the phase conjugate beam path to perform the summation.

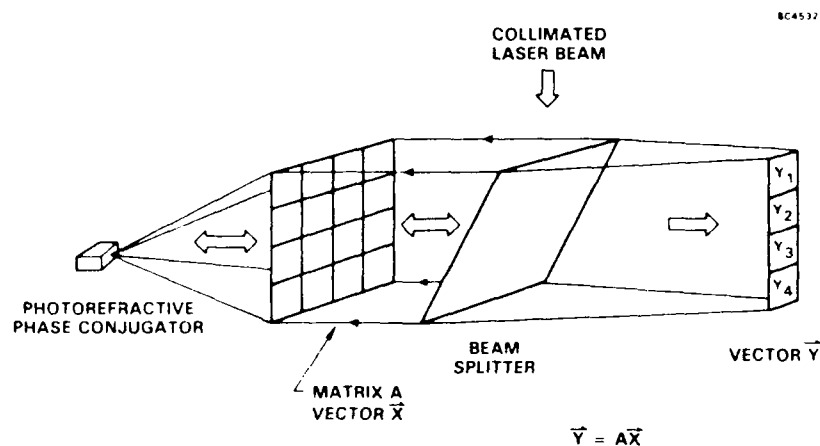


Fig. 9 A schematic diagram illustrating the basic concept of optical matrix-vector multiplication using a photorefractive phase conjugator in conjunction with a spatial light modulator.

The principle of operation is as follows: the SLM first impresses the matrix information onto the input laser beam. This beam is then incident into a phase conjugator which stores the matrix information after a finite grating formation time. When the matrix information is removed from the SLM, say by turning all the pixels into



SC5502.FR

maximum transmission condition, the phase conjugate beam which contains the reconstruction of the matrix information exists for a finite duration. This finite storage time depends on the strength of the input (read) beam. During this time, if the next frame of the SLM carries the vector information, parallel multiplication is performed as the phase conjugate beam propagates back through the SLM. Here, the vector is represented as a two-dimensional array of N identical column vectors, where N is the dimension of the vector. A cylindrical lens in the output port is used to perform the summation. The dark storage time during which the matrix information can be retrieved is determined by the photorefractive material and the pumping configuration. It ranges from seconds to microseconds.²¹

The system can also perform matrix-matrix multiplication by time multiplexing. In this case, each column vector V_i ($i = 1$ to N) which constitutes the second matrix M_2 is sequentially impressed onto the beam to multiply with the first matrix M_1 according to the matrix-vector multiplication scheme described below. To avoid the degradation of the information of M_1 stored in the photorefractive hologram during the readout, it is necessary to refresh the holographic memory with M_1 to restore its diffraction efficiency. This can be done by re-impressing M_1 onto the beam after each readout cycle. Consequently, a total of $2N$ clock cycles consisting of N cycles of write and N cycles of read, will be required to carry out the multiplication of two $N \times N$ matrices.

Using a photorefractive barium titanate crystal as a phase conjugator in conjunction with a 48×48 magneto-optic spatial light modulator (SIGHT-MOD SMD48I from Semetex Corp.), we have demonstrated the basic principle described above. The virtue of optical phase-conjugator ensures that precise pixel by pixel alignment is achieved automatically.

3.5 Optical Interconnection using Dynamic Photorefractive Holograms

3.5.1 Principle of Operation

During the first year of the program, we have developed a new concept of reconfigurable optical interconnection using photorefractive holograms²² (see Appendix 5.5). This new scheme provides an optical interconnection between an array of laser sources and an array of detectors with a very high energy efficiency.



Reconfigurable interconnection linking laser arrays and detector arrays plays a key role in optical computing. Conceptually, such interconnection can be achieved by using an optical matrix-vector multiplication.

$$v' = M v \quad (7)$$

where v is the input vector representing the signals carried by the array of lasers, and v' is the output vector representing the signals carried by the array of detectors. The matrix M represents the interconnection pattern. When a transparency or spatial light modulator (SLM) is used as the interconnection pattern, a large fraction of energy is absorbed by the transparency or SLM. This energy loss increases as the dimension of the array increases. Often, the fractional energy loss can be as large as $(N-1)/N$, where N is the dimension of the array. For a 1000×1000 crossbar switch, the loss due to fanout can be as big as 99.9%. This is not acceptable in high-speed computing because signals are passing through the SLM billion times per second and the energy loss can be enormous.

Referring to Figs. 10 and 11, we describe a new method of reconfigurable optical interconnection which uses the nonreciprocal energy transfer in photorefractive two-wave mixing to improve the energy efficiency. Figure 10 describes a one-dimensional case for the sake of clarity in explaining the concept. A small fraction of a laser beam is coupled out of the beam by using a beam splitter. This small fraction (called probe beam) is then expanded by using a cylindrical lens and passes through the SLM. In the example shown, the laser beam is to connect to Detectors b and d as prescribed by the SLM. The transmitted beam is then recombined with the main beam inside a photorefractive crystal. As a result of nonreciprocal energy coupling, almost all the energy in the main beam is transferred to the probe beam which carries the interconnection pattern. The results is an optical interconnection with high energy efficiency. Figure 11 describes the reconfigurable interconnection for laser arrays and detector arrays. In the example (a 4×4 interconnection) shown, Laser 1 is to connect to Detectors b and c, Laser 2 is to connect to Detectors a and d, Laser 3 is to connect to Detectors c and d, Laser 4 is to connect to Detector a and c. A cylindrical lens is used to focus the two-dimensional array of beams into a vector (one-dimensional array). As a result, Detector a receives signals from Lasers 2 and 4, Detector b receives signals from Laser 1, Detector c receives signals from Lasers 1, 3 and 4, and Detector d receives signals from Lasers

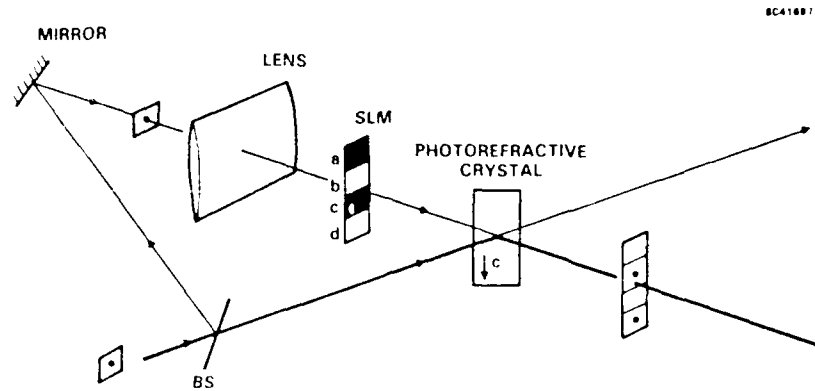


Fig. 10 A schematic drawing of a $1 \times N$ optical interconnection using dynamic photorefractive holograms. $N = 4$.

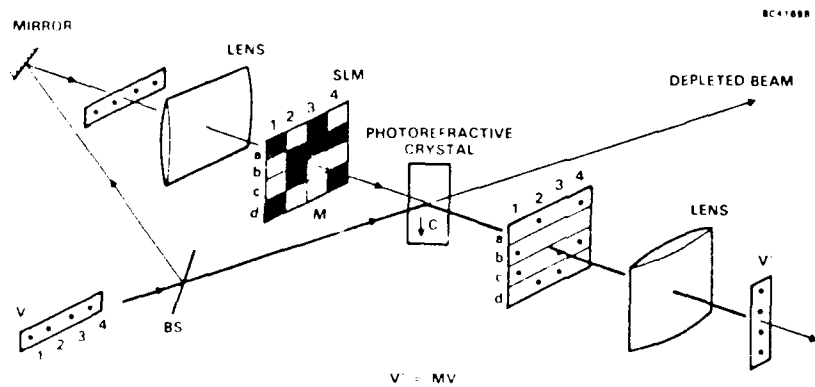


Fig. 11 A schematic drawing of a $N \times N$ optical interconnection using dynamic photorefractive holograms. $N = 4$.

2 and 3. Such a concept can be extended to interconnect N_L lasers with N_D detectors where N_L and N_D are two large numbers.

The interconnection can be reconfigured by using a different SLM pattern. The energy loss due to SLM is no more than the reflectivity of the beam splitter plus the material bulk absorption due to the photorefractive crystals. The beam splitter can be chosen such that the reflectivity is small (e.g., 5% or less) so that such energy loss is minimized. The hologram formation in the photorefractive medium will limit the recon-



SC5502.FR

figuration time. Once the interconnection pattern is formed inside the photorefractive crystal as a hologram, such a scheme is capable of providing the interconnection for high data rate transmission. In such an interconnection, the output of each laser can be input to any one or all of the detectors. Optical phase conjugation can also be used in conjunction with the two-wave mixing to correct for any phase aberration that may be caused by the crystal imperfection.²³

3.5.2 Experimental Demonstration

An experimental configuration for a 1×32 interconnection using this holographic approach is shown in Fig. 12. A Ronchi-Ruling (50 line-pairs per inch) is used as a 32-element binary vector mask. 5% of the collimated input beam transmitted through the beam splitter BS is expanded vertically by a pair of cylindrical lenses (Lc1 and Lc2) to illuminate the vector mask. 95% of the input energy reflected by the beam splitter BS serves as the pump beam which interacts with the spatially modulated signal beam inside the barium titanate crystal. The crystal and the mask are placed at the back-focal plane and the front-focal plane, respectively, of a Fourier transform cylindrical lens (Lc3). The crystal is oriented so that energy is transferred from the pump beam to the signal beam. The amplified signal output carrying the interconnection pattern is reimaged by the cylindrical lens (Lc4) on the screen SC.

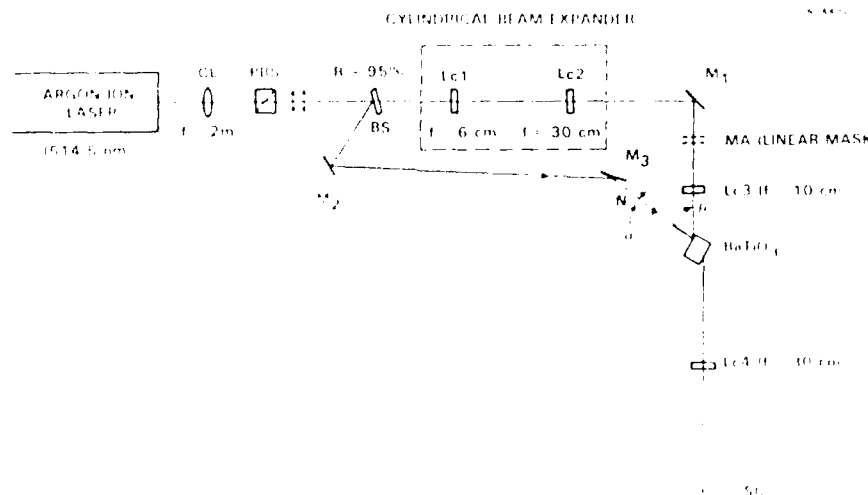


Fig. 12 A schematic diagram of the experimental configuration for a 1×32 interconnection using a photorefractive barium titanate crystal.



The intensity distribution at the output image plane is shown in Fig. 13. The experimental results is shown in Fig. 14 for the case when only three out of the 32 channels are "ON". The table in the right hand side of the figure compares the energy efficiencies achieved with and without the photorefractive holograms. For the latter case, the beam splitter BS is removed (see Fig. 12) so that all the input energy is directed into the signal channel. Note that the energy efficiency is improved by more than a factor of 7.

32 ELEMENT VECTOR MASK

SC44728

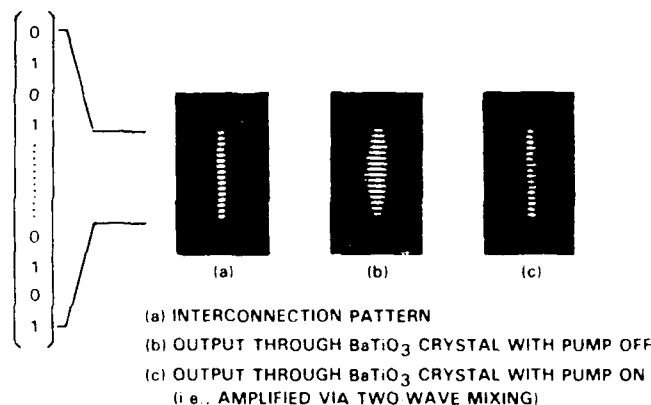


Fig. 13 Intensity distribution at the output image plane.

3.5.3 Demonstration of High Data Rate Transmission

We have experimentally demonstrated that the holographic interconnection using photorefractive holograms can accept very high data rate signals²² [see Appendix 5.5] even though the reconfiguration time is limited by the photorefractive grating formation, which is typically of the order of milliseconds at modest intensity.²¹ To demonstrate this fact, temporal modulation was impressed on a laser beam (argon, $\lambda = 514.5$ nm) using an acoustooptic device to simulate a signal, which is to be interconnected with some output. The signal used was a pulse train of frequency $f_0 = 0.833$ MHz with each pulse being ~ 0.2 μ s wide. This rate is clearly much higher than the reciprocal of the photorefractive response time. The modulated laser beam was then split into two beams and mixed in the crystal as described before, and the amplified probe beam was monitored with a photodetector. The upper oscilloscope trace in Fig. 15

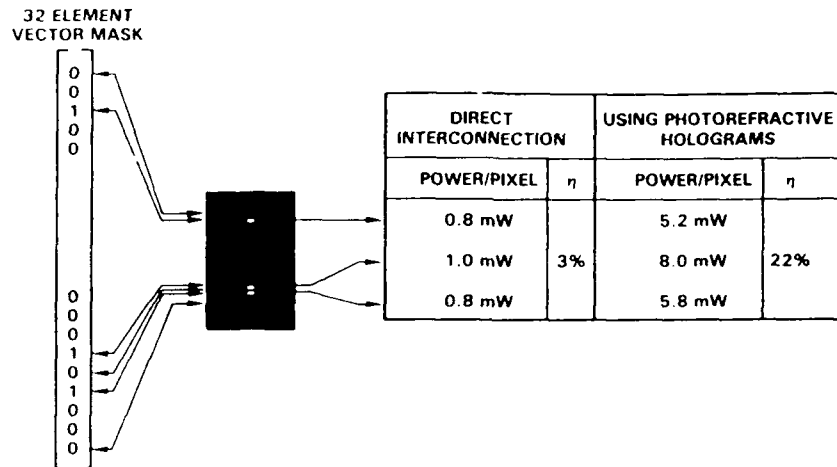


Fig. 14 Intensity distribution at the output image plane when all but three of the signal channels are "ON." The table on the right-hand side compares the energy efficiencies achieved using the conventional approach and the holographic approach.

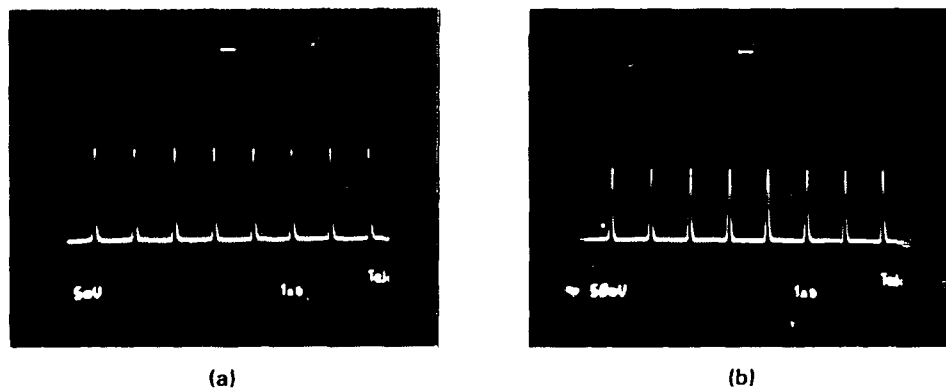


Fig. 15 (a) Signal carried by the probe beam and (b) amplified signal carried by the probe beam after undergoing two-wave mixing.

shows the input probe signal, and the lower one shows the amplified probe signal. The results show a steady-state response in which the temporally modulated pump and probe beams interact simply by diffracting off the stationary index grating that is created in the crystal after the photorefractive response time. As this experiment was performed merely to demonstrate the high signal bandwidth of the system, optimization of the parameters was not done, and the results in Fig. 15 can clearly be improved.



3.5.4 Energy Efficiency of Photorefractive Interconnection: Theoretical Calculation and Experimental Measurement [See Appendix 5.5, 5.6, and 5.7]

Referring to Fig. 16, we can estimate the energy efficiency of photorefractive crossbar switch as follows. Let I_0 be the input beam intensity and R be the reflectance of the beam splitter. It is legitimate to assume that the beam splitter is practically lossless. We may also assume that the surface of the photorefractive crystal is antireflection-coated so that the Fresnel reflection loss can be neglected. Under these conditions, the two beams that arrive at the photorefractive crystal have energies $I_0(1 - R)$ and I_0Rt/N , respectively, where t is the intensity transmittance of the "on" cells of the mask. Inside the crystal, these two beams undergo photorefractive coupling. As a result, most of the energy of the pump beam $I_0(1 - R)$ is transferred to the probe beam I_0Rt/N , which contains the interconnection pattern. The energy efficiency can be easily derived and is given by²

$$\eta = \frac{I_{out}}{I_{in}} = \frac{tR}{N} \frac{1 + m}{1 + m \exp(-\gamma L)} \exp(-\alpha L) \quad , \quad (8)$$

where m is the beam intensity ratio,

$$m = \frac{(1 - R)N}{tR} \quad , \quad (9)$$

and L is the interaction length, γ is the coupling constant, and α is the bulk absorption coefficient. For photorefractive crystals such as BaTiO₃ and SBN, the coupling constant is very large (i.e., $\gamma L \gg 1$). The efficiency can be written approximately

$$\eta = \left[\frac{tR}{N} + (1 - R) \right] \exp(-\alpha L) \quad . \quad (10)$$

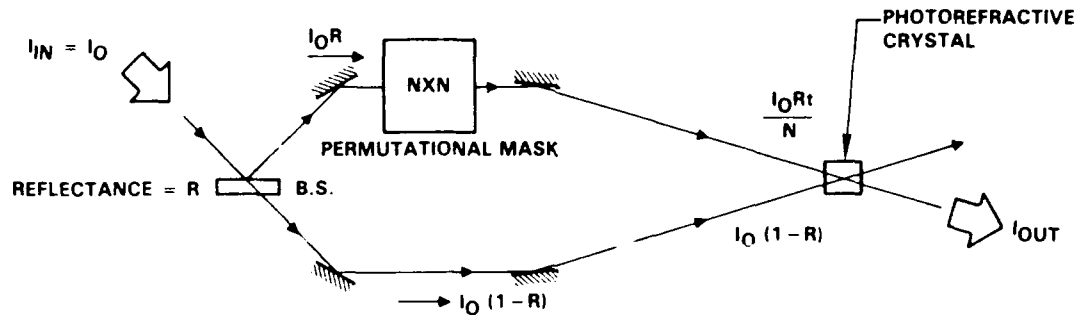


Fig. 16 A schematic diagram showing the intensities of various beams in a $N \times N$ permutational interconnection.

We notice that for large N , the energy efficiency is limited by the crystal bulk absorption $\exp(-\alpha L)$ and is maximized by using a beam splitter with a very small reflectance R (i.e., $R \sim 0$).

In Fig. 17, the maximum energy efficiency (with optimum beam splitting ratio) predicted by Eq. (8) (assuming that the insertion loss of the mask is negligible, i.e., $t = 1$ and that the absorption coefficient $\alpha = 0$) is plotted against the dimension of the array N for different coupling strength γL . The diagonal straight line represents the intrinsic fan-out loss. For cases where $\alpha \neq 0$, the curve remains valid provided that the vertical scale is multiplied by $\exp(-\alpha L)$.

Using an experimental configuration illustrated schematically in Fig. 18, we have measured the energy efficiency of the photorefractive interconnection holograms in a barium titanate crystal as a function of the fan-out loss.¹³ Instead of expanding the signal beam through a vector mask as described earlier (see Fig. 12), a neutral density filter (NDF) in the signal arm is used to simulate the fan-out loss. The experimental results are shown in Fig. 19. The solid line is a theoretical fit using Eq. (8) with αL and γL as the fitting parameter. The results ($\alpha L = 9.2$, $\gamma L = 1.1$) agree with those obtained from other independent measurements.

3.5.5 Maximizing Energy Efficiency by Matched Amplification via Fourier Transformation (see Appendix 5.7)

In the experiments discussed above, both signal and pump beams are Gaussian beams with no spatial intensity pattern. In the interconnection applications, these beams



SC5502.FR

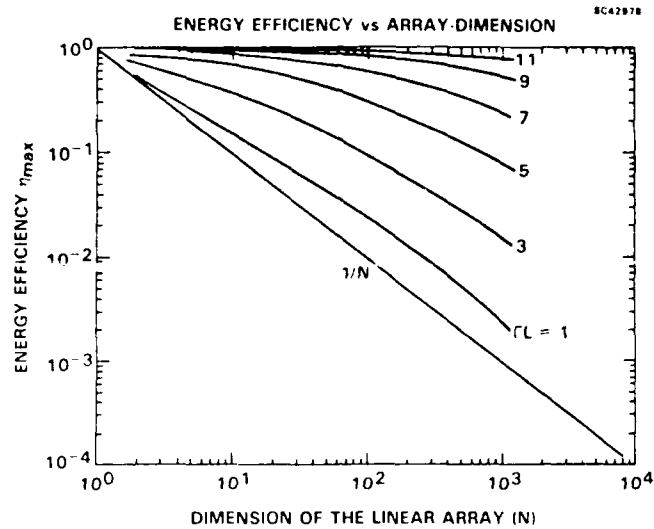


Fig. 17 The theoretical energy efficiency as a function of the dimension of the array as predicted by Eq. (8) for $t = 1$, $\alpha = 0$, and an optimum $R \sim 0$.

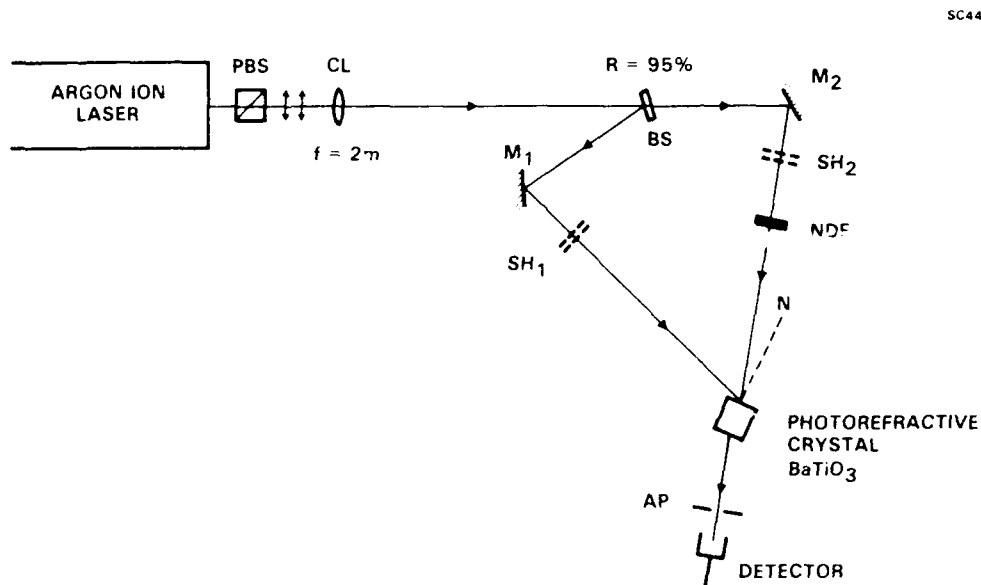


Fig. 18 A schematic diagram of the experimental configuration for measurement of the energy efficiency of photorefractive interconnection holograms in a barium titanate crystal.

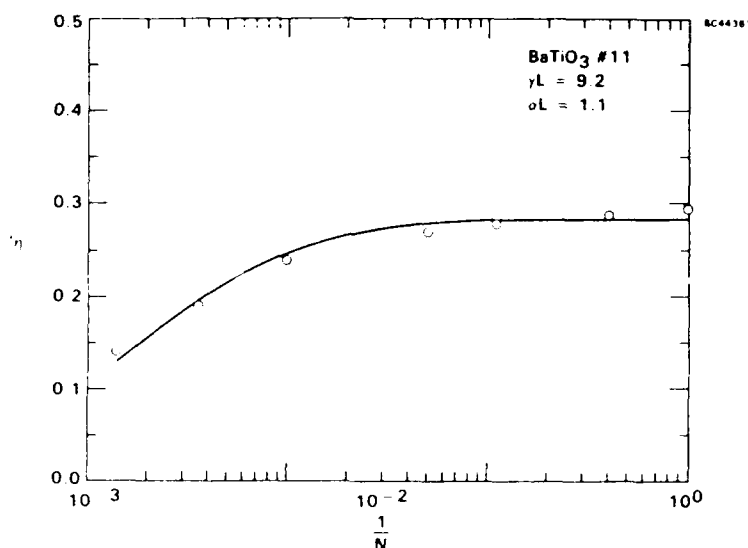


Fig. 19 Energy efficiency (η) of photorefractive two-beam coupling in a barium titanate sample as a function of the transmittance of a neutral density filter placed in the signal input arm. The transmittance is labeled $1/N$ to relate it to the fanout loss of a $N \times N$ permutation crossbar network.

are spatially modulated. The energy efficiency of the photorefractive interconnection depends on the spatial overlap of the beams. We have developed the utilization of Fourier transform to achieve maximum beam overlap and thus to achieve maximum energy efficiency.

It is important to note that although the beamlets in the signal beam and the pump beam are intrinsically different because of the interconnection pattern, the individual pixels can have identical shape (e.g., square). Complete overlap is possible in the Fourier domain, provided all the pixels are identical. Let $s(x,y)$ be the aperture of an individual pixel, and $\sigma(u,v)$ be the Fourier transform. Fourier transformation of a beamlet of the pump beam and the corresponding column of beamlets of the signal beam can be performed by a lens. The resulting amplitude distributions at the rear focal plane are given by

$$\text{Pump: } P(u,v) = \sigma(u,v) \quad (11)$$

$$\text{Signal: } S(u,v) = \sum_n \sigma(u,v) \exp [i\phi_n(u,v)] \quad (12)$$



respectively, where u, v are coordinates in the Fourier plane. The summation in Eq. (12) is over all the windows open in the column, and $\phi_n(u, v)$ is a phase which depends on the position of the window.

We note that the Fourier transform of a column of the signal beam consists of a linear superposition of identical patterns each with a different phase factor. Such phase factors ($\exp(i\phi_n)$) are due to the relative positions of the windows in each column. Although these phase factors may lead to interference structures, all the energies are confined under the same envelop $\epsilon(u, v)$. As a result of the shift invariance in Fourier transformation, each of the signal beamlets overlaps completely with the pump beam at the Fourier plane. Thus, maximum energy coupling is achieved.

The experimental configuration is illustrated in Fig. 20. The output from an argon laser (514.5 nm) is spatial-filtered and expanded to form a collimated beam with 2 cm diameter. A variable beam splitter consisting of a half-wave plate and a polarizing beam splitter cube is used to split the incoming beam into two, a pump beam and a signal beam. Another half-wave plate is used to rotate the polarization of the reflected (signal) beam by 90° from the direction perpendicular to the plane of the paper to the in-plane direction. A polarizer placed downstream further filters out the residual perpendicular component. A 10×10 binary matrix mask is used to encode a spatial pattern onto the signal beam.

To maximize the spatial overlap of the pump and the signal beams inside the crystal via the properties of Fourier transform, a pump mask with a single aperture identical to the unit cell of the signal mask is used. The two masks are placed at the front focal planes of two Fourier transform lenses FL_1 and FL_2 (of identical focal length $f = 25$ cm), respectively. The crystal is located at the common Fourier plane of the two masks (Fig. 20). The shift-invariant property of Fourier transformation ensures that, apart from a phase factor, the diffraction pattern from each signal channel overlaps with that from the pump inside the crystal. The intensity patterns of the pump and the signal at the image plane and the Fourier plane are shown in Fig. 21. Note that the two intensity distributions at the Fourier plane differ significantly in fine structures due to multiple beam interference among the various signal channels.



SC-C0310

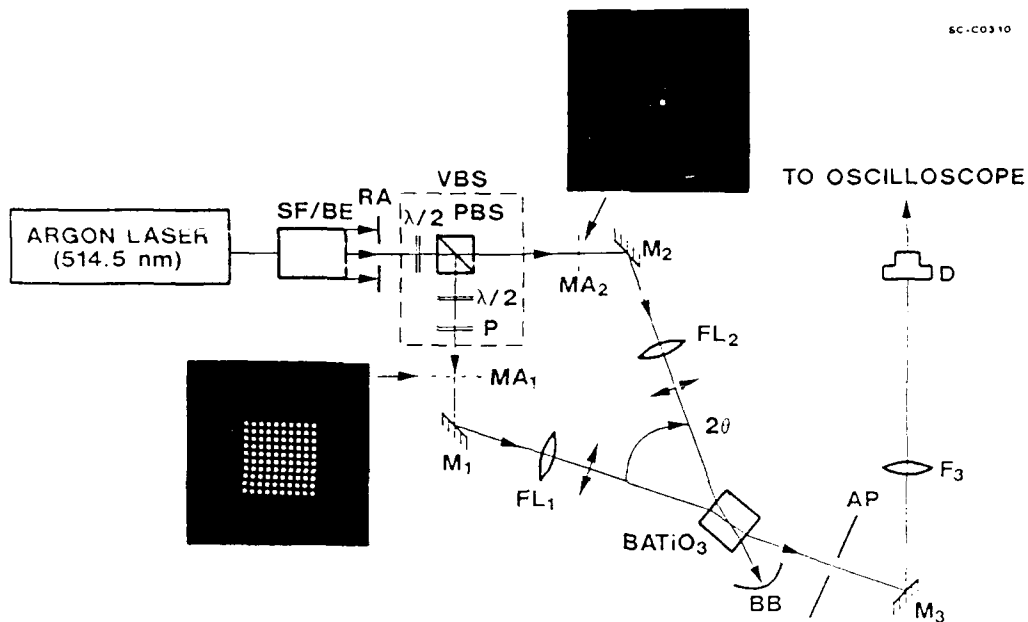


Fig. 20 An experimental configuration for a 1-to- $N \times N$ (for $N = 10$) broadcasting network using photorefractive holograms at the Fourier domain.

Intensity Patterns

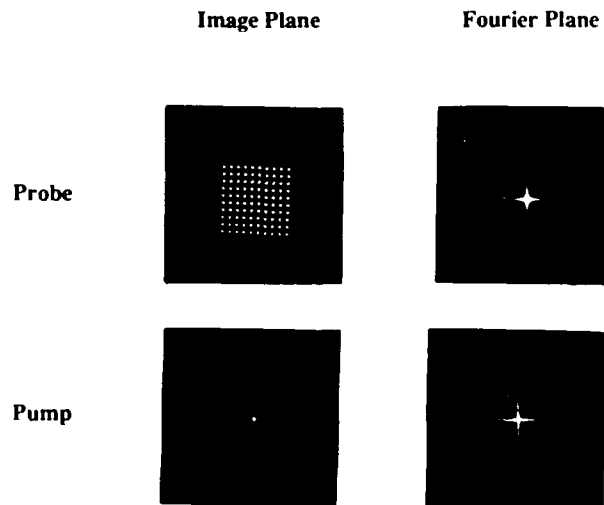


Fig. 21 The intensity patterns of the masks for the probe and the pump beams at the image plane and the Fourier plane.



To investigate how the energy efficiency depends on the number of signal channels, we used a variable rectangular aperture in front of the signal mask to vary the number of channels from 100 to 1. In each case, we also adjusted the laser power and the variable beam splitter so that both the pump power and the total signal input power are fixed at $600 \mu\text{W}$ and $6 \mu\text{W}$, respectively. Figure 22 is a plot of energy efficiency vs number of signal channels. The energy efficiency turns out to be fairly insensitive to the number of signal channels. The crystal orientation used in this particular experiment is far from optimum, and one can expect significant improvement in energy efficiency once optimized.

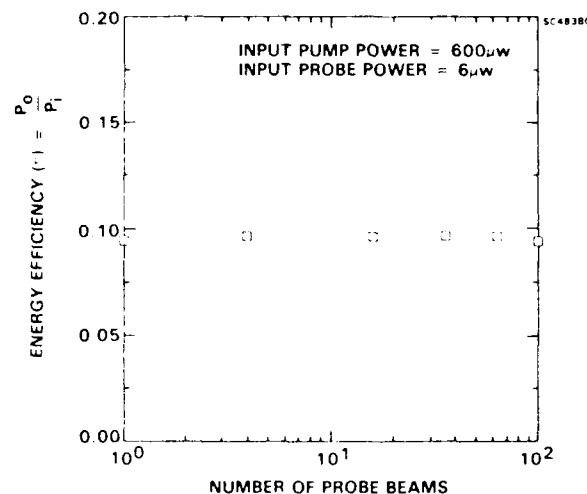


Fig. 22 Energy efficiency (η) as a function of number of signal channels (N) in a 1-to- $N \times N$ broadcasting configuration using photorefractive holograms in a barium titanate sample.

3.5.6 Contrast Enhancement by Double Passage (see Appendix 5.9)

All of our experimental results reported earlier are obtained with photographic masks replacing the SLM. To demonstrate the reconfigurability and to study the reconfiguration time, one can no longer avoid the use of SLM which, in general, have relatively poor contrast ratio (of the order 10 to 100). In the parallel matrix-vector multiplication approach, the maximum number of fan-out channels of the optical cross-bar can be limited by the finite contrast of the SLM.



As a simple example, consider a $M \times M$ permutation matrix mask with contrast ratio $C = T_1/T_0$, where T_1 and T_0 are the intensity transmittance of the "ON" state and the "OFF" state, respectively. We assume that the signal from each source is intensity modulated between zero and peak value P , the signal level received by each detector through the "ON" cell is PT_1 , whereas the noise level received through the $(M-1)$ "OFF" cell is $P(M-1)T_0$. The signal-to-noise ratio (S/N) is therefore given by $S/N = T_1/(M-1)T_0 = C/(M-1) \approx C/M$ for $M > 1$. The condition $S/N > 1$ is satisfied provided that the number of fan-out channels (M) is less than the contrast ratio (C).

A simple method to improve the contrast is by double passage through the same SLM via retroreflection or phase conjugation⁵. In principle, if the contrast ratio for signal passage is C , the contrast ratio for double passage will become C^2 . The experimental configuration used to verify this fact is shown schematically in Fig. 23. An expanded and collimated laser beam from an argon laser (514.5 nm) is transmitted through a circular aperture (diameter ≈ 14 mm) located at the input plane. Half of the aperture is masked by a NDF to form a binary amplitude mask at the input plane. The transmitted beam is collected by a lens (L) and directed into a barium titanate crystal. The crystal is oriented so that the incoming beam is phase-conjugated back via self-pumped mode. After reversing through the aperture, the phase-conjugated beam is sampled by a beam splitter through imaging optics which reimages the binary mask on the output plane. The input intensity distribution (i.e., single-passage through the mask) and the output intensity distribution (i.e., double-passage through the mask) are measured by scanning a detector with a small aperture (diameter ≈ 1 mm) across the beam diameter at the input and the output planes, respectively. The experimental results (for a mask with optical density $OD = 0.5$) are shown in Fig. 24(a) and (b). Apart from some imperfection at the edge of the output image, the output contrast ratio is approximately the square of that of the input as expected. Instead of a phase-conjugate mirror, one can also place a plane mirror at the input plane immediately after the mask to retroreflect the beam back through the binary mask. The resulting intensity distribution is shown in Fig. 24(c). The phase conjugation has the key advantage of being intrinsically self-aligned. The grating formation time for self-pumped phase conjugation using a typical barium titanate crystal at a few tens of milliwatt of optical power, is, however, relatively slow (a fraction of a second to several seconds). Note that the output obtained

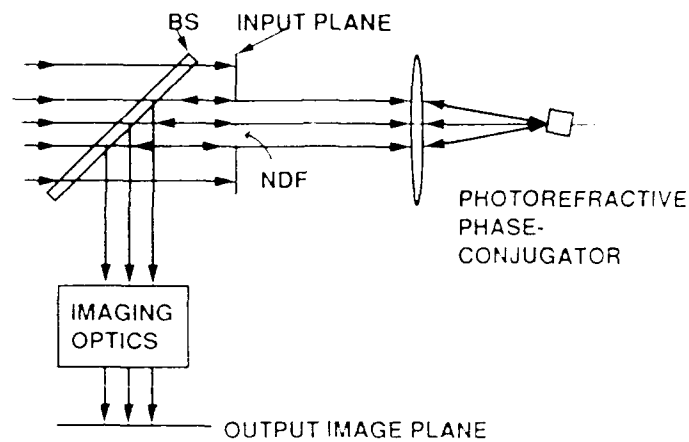


Fig. 23 An experimental configuration for contrast enhancement by double passage.

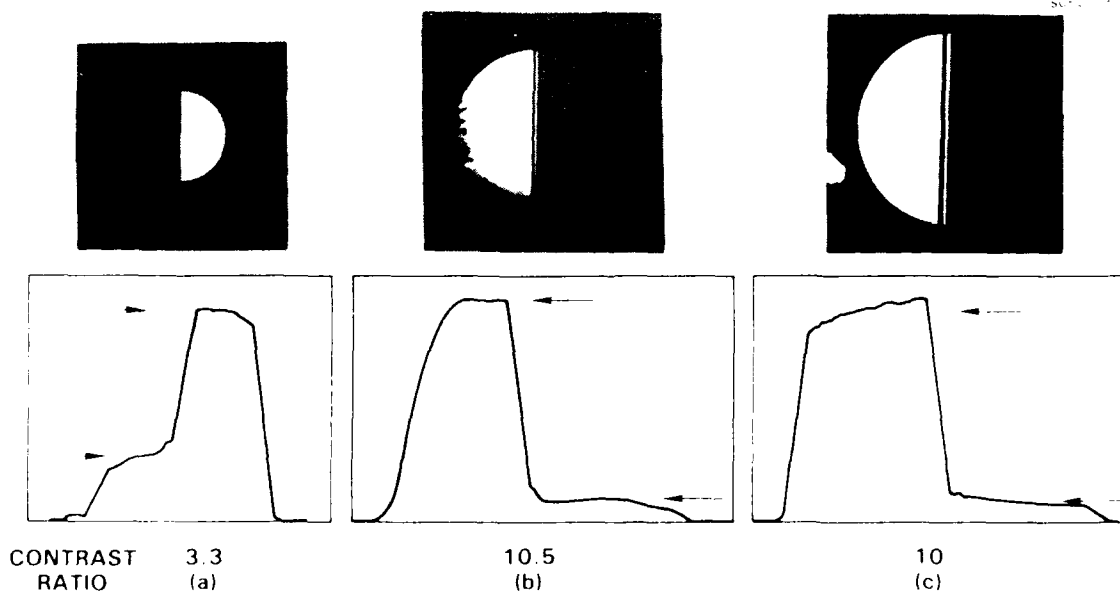


Fig. 24 Intensity profiles and contrast of a binary image: (a) at the input plane, (b) at the output plane after double passage via phase-conjugate reflection, and (c) at the output plane after double passage via mirror reflection.

by mirror reflection is fairly uniform (see Fig. 24(c)) and the reflection is practically instantaneous.



The photorefractive interconnection holograms used to diffract the pump beam into the signal channels specified by the matrix mask do not degrade the contrast provided that the photorefractive crystal is placed at the Fourier plane (see Appendix 5.8). In comparison, photorefractive image amplification via two-wave mixing in the image plane tends to decrease the contrast of the input image. An experimental result verifying this contrast preserving property is given in Fig. 25. Intensity profiles of a binary image and its amplified output are shown in Figs. 25(a) and 25(b), respectively. Note that the contrast ratio of the input and the output image are almost identical, and that the vertical scale in Fig. 25(b) is 25 times that of Fig. 25(a).

SC50017

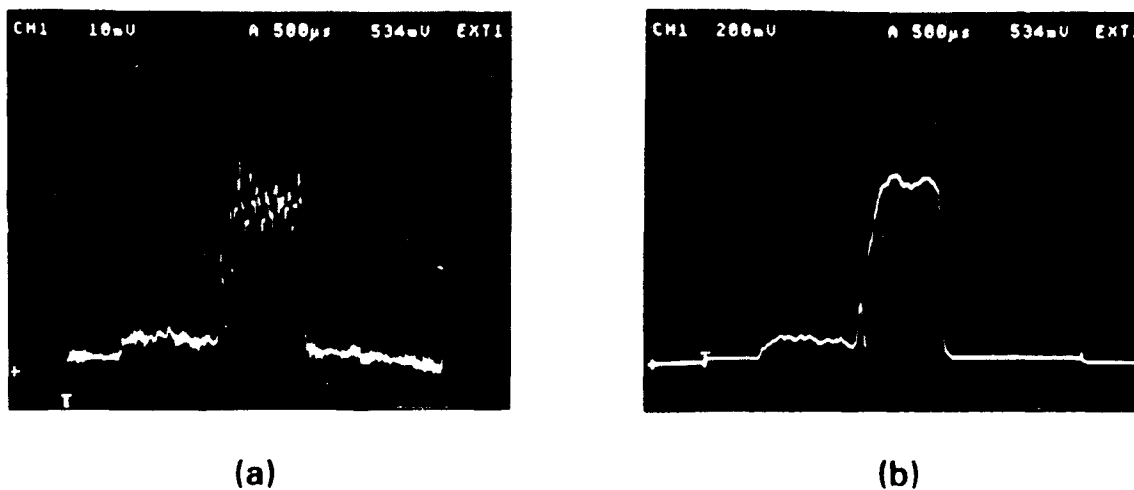


Fig. 25 Experimental results showing contrast-preserving image amplification by photorefractive two-wave mixing at the Fourier domain: (a) input intensity profile, and (b) amplified output intensity profile.

Based on the discussion given above, one can extrapolate that if an SLM with a contrast ratio of the order of 100 (for example, a ferroelectric liquid crystal SLM) is used in the time-division mode, the maximum number of channels (M) of an $M \times M$ crossbar switch limited by the contrast ratio can be as high as 10^4 .



3.5.7 Experimental Demonstration of Reconfigurability

Using an experimental configuration similar to the one illustrated in Fig. 20, with the photographic mask (transparency) replaced by an SLM, we have demonstrated the reconfigurability of the interconnection by writing new interconnection matrix pattern on the LCTV. The pattern is generated by an IBM PC and sent to the LCTV. With optical power of the order of tens of milliwatts, the frame rate is currently limited by the photorefractive response time to a few frames per second. As explained in Section 3.5.3, the data rate is not limited by the photorefractive response time and can be higher than several megahertz. To enhance the contrast of the binary pattern, the signal beam is passed through the SLM twice via a retroreflecting mirror (as described in Section 3.5.6) prior to interacting with the pump beam in a photorefractive barium titanate crystal.



4.0 REFERENCES

1. V.L. Vinetskii, N.V. Kukhtarev, S.G. Odoulov and M.S. Soskin, "Dynamic Self-Diffraction of Coherent Light Beams," *Sov. Phys. Usp.* **22**, 742 (1979).
2. N.V. Kukhtarev, V.B. Markov, S.G. Odulov, M.S. Soskin and V.L. Vinetskii, "Holographic Storage in Electro-Optic Crystals. Beam Coupling and Light Amplification," *Ferroelectrics* **22**, 949 (1979).
3. J.A. Neff, "The Role of Optics in Future Computational Systems," Topical Meeting on Optical Computing, March 18-10, Incline Village, NV, 1985.
4. J.W. Goodman, F.J. Leonberger, S-Y. Kung and R.A. Athale, "Optical Interconnections for VLSI Systems," *Proc. IEEE* **72**, 850-866 (1984).
5. See, for example, R.A. Fisher, ed., Optical Phase Conjugation, Academic Press, NY (1983).
6. A. Yariv, "Phase Conjugate Optics and Real-Time Holography," *IEEE J. Quantum Elect.* **QE14**, 650 (1978).
7. C.R. Giuliano, "Application of Optical Phase Conjugation," *Physics Today*, 27-35 (April, 1981).
8. See, for example, A. Yariv and P. Yeh, "Optical Waves in Crystals" (Wiley, 1984), Chapters 12 and 13.
9. Y.R. Shen, "Principles of Nonlinear Optics (Wiley, 1984).
10. J.O. White and A. Yariv, "Real-Time Image Processing via Four-Wave Mixing in a Photorefractive Medium," *Appl. Phys. Lett.* **37**, 5-7 (1980).
11. R.A. Athale, "Optical Matrix Algebraic Processors," in *Proc. 10th Int. Optical Computing Conf.*, IEEE, Cat. No. 83CH1880-4, April 1984, pp. 24-31.
12. R.A. Athale and W.C. Collins, "Optical Matrix-Matrix Multiplier Based on Outer Product Decomposition," *Appl. Opt.* **21**, 2089-2090 (1982), and references therein.
13. P. Yeh, A. Chiou, J. Hong, P. Beckwith, T. Chang, and M. Khoshnevisan, "Photorefractive Nonlinear Optics and Optical Computing," *Opt. Eng.* **28**(4), 328-343 (1989).
14. See also papers in the Session on Optical Matrix Processing at the Topical Meeting in Optical Computing, March 18-20, Incline Village, NV, 1985.



15. A. Chiou, M. Khoshnevisan and P. Yeh, "Optical Matrix-Matrix Multiplication Using Multi-Color Four-Wave Mixing," Proc. SPIE, Vol. 881 (1988).
16. C. Mead, "Potential and Limitations of VLSI," Topical Meeting in Optical Computing, March 18-20, Incline Village, NV, 1985.
17. B.K. Jenkins, A.A. Sawchuk, T.C. Strand, R. Forchheimer and B.H. Soffer, "Sequential Optical Logic Implementation," Appl. Opt. 23, 3455-3464 (1984).
18. B.K. Jenkins, P. Chavel, R. Forchheimer, A.A. Sawchuk and T.C. Strand, "Architecture Implementation of a Digital Optical Processor," Appl. Opt. 23, 3465-3474 (1984).
19. P. Yeh and A. Chiou, "Optical Matrix-Vector Multiplication Through Four-Wave Mixing in Photorefractive Media," Opt. Lett. 12(2), 138-140 (1987).
20. A. Chiou, M. Khoshnevisan and P. Yeh, "Optical Matrix-Matrix Multiplication using Multi-Color Four-Wave Mixing," Proc. SPIE Vol. 881, 250-257 (1988).
21. P. Yeh, "Fundamental Limit of the Speed of Photorefractive Effect and Its Impact on Device Applications and Material Research," Appl. Opt. 26, 602-604 (1987).
22. P. Yeh, A. Chiou and J. Hong, "Optical Interconnections Using Dynamic Photorefractive Holograms," Appl. Opt. 27(11), 2093-2096 (1988).
23. A.E.T. Chiou and P. Yeh, Opt. Lett. 11, 461-463 (1986).



APPENDIX 5.1

Optical Matrix-Vector Multiplication Through Four-Wave Mixing
in Photorefractive Media

Optical matrix-vector multiplication through four-wave mixing in photorefractive media

Pochi Yeh and Arthur E. T. Chiou

Rockwell International Science Center, Thousand Oaks, California 91360

Received September 3, 1986; accepted October 30, 1986

We propose and describe a new method of optical matrix-vector multiplication by using four-wave mixing in photorefractive media. Using a BaTiO₃ crystal, we have demonstrated such a parallel multiplication. The results are presented and discussed.

A large number of signal- and image-processing algorithms can be expressed in terms of matrix operations. The multiplication of two matrices is one of the most basic operations in matrix algebra. Optics, with its inherent parallelism, can offer great improvement in the speed of these operations. Optical processors for multiplying two matrices have been described in the literature.¹⁻⁵ Considerable work has also been reported on performing optical matrix-vector multiplication.⁶⁻⁹ In this Letter, we describe a new method of performing matrix-vector multiplication by using optical four-wave mixing in nonlinear media. In addition, we also report the first experimental demonstration to our knowledge of such an optical matrix processor by using a photorefractive BaTiO₃ crystal.

Optical four-wave mixing has been a subject of considerable interest during the past several years. Much attention has been focused on wave-front-correction⁶⁻⁸ and phase-conjugate interferometry.^{9,10} In the area of signal processing, optical four-wave mixing has been used to perform spatial information processing,¹¹ image subtraction,¹²⁻¹⁴ and logic operations.¹⁵ However, little attention has been paid to the use of the inherently parallel multiplication nature of four-wave mixing for optical matrix multiplication. In this Letter we describe a new method of performing matrix-vector multiplication using four-wave mixing in nonlinear media.

In what follows, we briefly describe the basic principles of real-time matrix multiplication using optical four-wave mixing in nonlinear media. For the sake of convenience, we will limit ourselves to the case of square matrices, although extension to nonsquare matrices will be straightforward.

Referring to Fig. 1, we consider a scheme that is suitable for a matrix-vector multiplication. Here, as an example, let us consider a discrete case in which we need to carry out the multiplication of an N -element vector and an $N \times N$ matrix. In this scheme, the vector is fanned out into N rows of identical vectors. These $N \times N$ beamlets are directed to a nonlinear medium. The matrix, which also contains $N \times N$ beamlets, is also directed to the medium in such a way that each beamlet of the matrix is counterpropagating in a direction relative to the corresponding beamlet of

the vector. Thus, in the medium, there are $N \times N$ spatially separated regions, each of which is pumped by a pair of counterpropagating beamlets. Now a probing beam, which consists of $N \times N$ beamlets, is directed into the medium in such a way that each probe beamlet will propagate through the corresponding intersection region, as shown in Fig. 1. The probe beam will be plane-wave beamlets propagating in parallel. All the beamlets in this probe beam are of equal intensity. As a result of the four-wave mixing, each probe beamlet will generate a phase-conjugated beamlet, which, within a proportional factor, can be written as $M(i, j)a(j)$. By using a cylindrical lens, a summation over j can be obtained. Thus we have

$$b(i) = \sum_j M(i, j) \times a(j), \quad (1)$$

where $a(j)$ is the j th element of the vector \mathbf{a} and $M(i, j)$ is the matrix element. Such a scheme for matrix-vector multiplication can also be used for matrix-matrix multiplication by decomposing a matrix into column vectors and then multiplying the matrix with each of the column vectors.

The probe beam can also simply be a uniform plane wave, without beamlets. The phase-conjugated beam will consist of $N \times N$ beamlets, because only a matrix

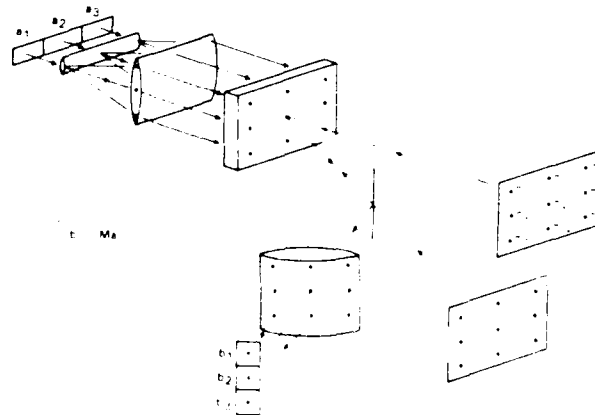


Fig. 1. Schematic drawing of the basic principle of optical matrix-vector multiplication through four-wave mixing in nonlinear media.

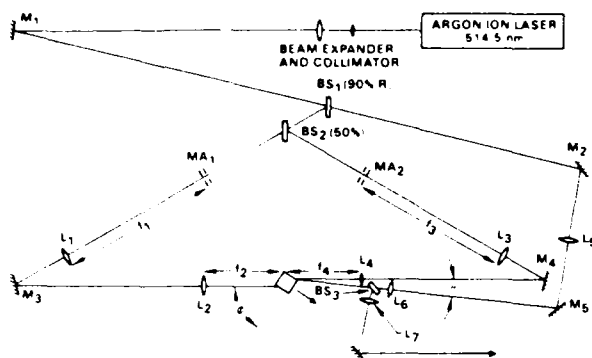


Fig. 2. Experimental setup used to demonstrate the optical matrix-vector multiplication.

of $N \times N$ regions is pumped by counterpropagating beamlets. The matrix and the vector information can actually be carried on any two of the three incident beams in the four-wave mixing process.

The summation process can also be obtained without the external cylindrical lens by using a different scheme, described as follows. Consider a probe beam that consists of a column of N equal beamlets. The probe is incident into the nonlinear medium in such a way that each of the probe beamlets is made to propagate through a row of N intersection regions. The phase-conjugation process automatically performs the summation as well as the multiplication. The phase-conjugated beam is thus the product of the matrix-vector multiplication.

As a result of the nature of the four-wave mixing process in the medium, this new matrix-vector multiplier operates on the field amplitudes and thus can be used to handle matrices and vectors with complex elements. It is a coherent device rather than an incoherent one. This aspect is distinctly different from most of the earlier approaches, which are all incoherent. When the device is operated in the coherent mode, the phase of each beamlet must be maintained uniformly over the transverse dimension of the beamlet. In addition, such phases must also be maintained fixed in the summation process. If these phases are not uniform over the beamlets, the final step becomes an incoherent summation as a result of the spatial averaging. Under such circumstances, this matrix-vector multiplier operates on the intensities and thus handles only positive numbers.

The matrix-vector multiplication is demonstrated experimentally by using four-wave mixing in a photorefractive BaTiO_3 crystal.¹⁷ The crystal is cut in such a way that the faces are all perpendicular to the principal axes. All the beams are polarized extraordinary in the xz plane and are incident onto the a faces of the crystal.

In our experiments, an Ar-ion laser beam at wavelength 514.5 nm with an output power of a few hundred milliwatts is used as the light source. The laser beam is expanded and collimated into a beam size of approximately 1 cm. Figure 2 shows our experimental setup. The expanded beam is then split into three beams by using beam splitters BS_1 and BS_2 . To dem-

onstrate the principle of operation, we chose the following matrix and vector:

$$M = \begin{bmatrix} 1 & 1 & 1 & 0 & 1 \\ 1 & 1 & 0 & 0 & 1 \\ 0 & 1 & 0 & 0 & 1 \\ 0 & 1 & 1 & 0 & 0 \\ 1 & 1 & 1 & 1 & 1 \end{bmatrix}, \quad \mathbf{a} = \begin{bmatrix} 1 \\ 0 \\ 1 \\ 1 \\ 1 \end{bmatrix}. \quad (2)$$

The matrix and the vector information is imprinted onto two of the beams by using transparencies (MA_1 and MA_2 in Fig. 2) that consist of circular dots. White circular dots represent the 1's, and the dark regions the 0's. Instead of using a cylindrical lens to fan out the vector into five identical rows as described earlier, we simply use a transparency of a matrix that consists of five identical rows of (1 0 1 1 1). The incident matrices, corresponding to the matrix M and the vector \mathbf{a} , are shown in Figs. 3(a) and 3(b). Four lenses, L_1 , L_2 , L_3 , and L_4 (with focal lengths $f_1 = f_3 = 0.5$ m and $f_2 = f_4 = 0.2$ m) are used to image the transparencies MA_1 and MA_2 onto the center of the nonlinear crystal, where the diameter of each beamlet is 0.18 mm with a center-to-center distance of 0.51 mm. The size of the whole image inside the crystal is 2.2 mm \times 2.2 mm. The uniform beam is also reduced (and collimated) to a diameter of 3.6 mm inside the crystal by lenses L_5 and L_6 (with focal lengths $f_5 = 0.6$ m and $f_6 = 0.25$ m, respectively). The angle θ between the uniform beam and one of the pump beams is 11° . The two beams that carry the matrix and the vector information, respectively, are incident onto the opposite a faces of a photorefractive BaTiO_3 crystal. The incident angle ϕ is approximately 20° with respect to the surface normal. As a result of the four-wave mixing, a phase-conjugated beam, consisting of a 5×5 beamlet pattern, is generated and is shown in Fig. 3(c). A cylindrical lens is then used to perform the summation. The resulting product vector is shown in Fig. 3(d). By

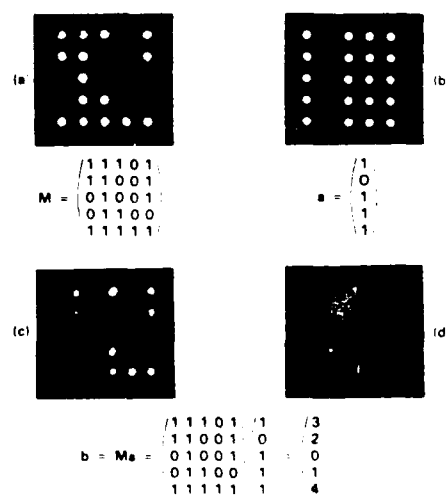


Fig. 3. Photographs showing the matrix and the vectors: (a) input matrix; (b) input vector, expanded into a matrix with five identical rows; (c) resultant phase-conjugate reflection matrix; (d) resultant vector of a matrix-vector multiplication after summation of (c) by a cylindrical lens.

measuring the intensity of the individual dots, we found that the product vector is (3 2 0 1 4), in good agreement with our prediction; in other words,

$$\mathbf{b} = \mathbf{M}\mathbf{a} = \begin{bmatrix} 1 & 1 & 1 & 0 & 1 & 1 \\ 1 & 1 & 0 & 0 & 1 & 0 \\ 0 & 1 & 0 & 0 & 1 & 1 \\ 0 & 1 & 1 & 0 & 0 & 1 \\ 1 & 1 & 1 & 1 & 1 & 1 \end{bmatrix} \begin{bmatrix} 3 \\ 2 \\ 0 \\ 1 \\ 4 \end{bmatrix} = \begin{bmatrix} 3 \\ 2 \\ 0 \\ 1 \\ 4 \end{bmatrix} \quad (3)$$

The intensities of the product vector elements are measured by integrating over the cross section of each beamlet. The experimental error is less than 5%. This small error is due to environmental perturbations and the slow response of the photorefractive crystal. Although our experiment demonstrates the operation for matrices and vectors with binary numbers (1, 0), this matrix-vector multiplier can also be operated in the analog mode to handle elements with gray levels. Such an analog operation in photorefractive crystals requires that the probe-beam intensity be weak so that the error due to the intensity denominator in the index modulation can be neglected. This material-related error disappears when the matrix and the vector contain only binary numbers (1, 0).

In conclusion, we have proposed and demonstrated a new method of matrix operation by using optical four-wave mixing in nonlinear media. In particular, we have demonstrated experimentally matrix-vector multiplication in a photorefractive BaTiO₃ crystal.

The authors acknowledge helpful discussions with M. D. Ewbank and M. Khoshnevisan (Rockwell International) and J. Neff (Defense Advanced Research Projects Agency).

References

1. R. A. Athale, in *Proceedings of the Tenth International Optical Computing Conference*, Catalog No. 83CH1880-4 (Institute of Electrical and Electronics Engineers, New York, 1983), pp. 24-31.
2. R. A. Athale and W. C. Collins, *Appl. Opt.* **21**, 2089 (1982), and references therein.
3. See also papers in the session on optical matrix processing in *Digest of Topical Meeting on Optical Computing* (Optical Society of America, Washington, D.C., 1985), pp. TuD1-TuD7.
4. M. A. Monahan, K. Bromley, and R. P. Bocker, *Proc. IEEE* **65**, 121 (1977).
5. J. W. Goodman, A. R. Dias, and L. M. Woody, *Opt. Lett.* **2**, 1 (1978).
6. B. Ya. Zel'dovich, V. I. Popovichev, V. V. Ragul'skii, and F. S. Faizullov, *Sov. Phys. JETP* **15**, 109 (1972).
7. A. Yariv, *IEEE J. Quantum Electron.* **QE14**, 650 (1978).
8. C. R. Giuliano, *Phys. Today* **34**(4), 27 (1981).
9. M. Ewbank, P. Yeh, and M. Khoshnevisan, *Proc. Soc. Photo-Opt. Instrum. Eng.* **464**, 2 (1984).
10. M. Ewbank, P. Yeh, M. Khoshnevisan, and J. Feinberg, *Opt. Lett.* **10**, 282 (1985).
11. See, e.g., J. O. White and A. Yariv, *Opt. Eng.* **21**, 224 (1982).
12. A. E. Chiou, P. Yeh, and M. Khoshnevisan, *Proc. Soc. Photo-Opt. Instrum. Eng.* **613**, 201 (1986).
13. S. Kwong, G. A. Rakuljic, V. Leyva and A. Yariv, *Proc. Soc. Photo-Opt. Instrum. Eng.* **613**, 36 (1986).
14. A. E. T. Chiou and P. Yeh, *Opt. Lett.* **11**, 306 (1986).
15. S. K. Kwong, G. A. Rakuljic, and A. Yariv, *Appl. Lett.* **48**, 201 (1986).
16. Y. Fainman, C. C. Guest and S. H. Lee, in *Digest of Topical Meeting on Optical Computing* (Optical Society of America, Washington, D.C., 1985), paper TuA5.
17. Sample of BaTiO₃ purchased from Sanders Associates, Nashua, N.H. 03061.



APPENDIX 5.2

Optical Matrix-Matrix Multiplication Using Multi-Color Four-Wave Mixing

Arthur E. Chiou, Monte Khoshnevisan, and Pochi Yeh

Rockwell International Science Center
1049 Camino Dos Rios, Thousand Oaks, CA 91360

ABSTRACT

The concept of using color-multiplexed four-wave mixing to achieve optical matrix-matrix multiplication with N^3 parallelism is described. Experimental results, for the case of 2×2 matrices, using two-color four-wave mixing in a photorefractive crystal are presented.

1. INTRODUCTION

In this paper we propose and demonstrate the concept of color-multiplexed four-wave mixing to achieve optical matrix-matrix multiplication (MMM) with N^3 parallelism. This is an extension of our earlier work on optical matrix-vector multiplication (MVM)¹ using photorefractive four-wave mixing. The additional degree of parallelism required by MMM (N^3 for MMM versus N^2 for MVM) is provided by color-multiplexing the nonlinear wave-mixing process. In Section 2 the background for optical matrix processors is briefly reviewed, and the general idea of using color-multiplexing to convert a MVM scheme into MMM is described. In Section 3 we present a specific approach to apply the color multiplexing technique to photorefractive four-wave mixing for MMM with full parallelism. The experimental details and results are discussed in Section 4. In Section 5 we summarize our results and discuss some of the practical difficulties and limitations, as well as some advantages of this approach.

2. BACKGROUND

Matrix algebra has been used extensively as a convenient mathematical language to formulate the problems frequently encountered in signal and image processing and numeric computing. Some of the more recent applications in optical computing include optical interconnections,² optical neural network processors,³ and optical artificial intelligence.^{4,5} In particular, two-dimensional format of a matrix can be conveniently represented as a spatial intensity distribution of an optical beam over a plane. In this context, a matrix can be viewed as a two-dimensional image and can be transferred to any designated plane and scaled to appropriate size by conventional optical technique. The two computational primitives involved in matrix algebra, namely multiplication and addition, can also be carried out optically using simple reflective, refractive, or diffractive optics or their combinations. Various aspects of optical matrix processors have been discussed fairly extensively in some recent review articles.⁶⁻⁹ In the following, we describe briefly only those directly relevant to this work.

A basic architecture for an incoherent optical MVM scheme for performing discrete Fourier transforms was reported by Goodman et al.¹⁰ A schematic diagram of this architecture for multiplying a 4×4 matrix and a 4×1 vector is illustrated in Fig. 1. In general, a linear array of "N" sources (light emitting diodes or semiconductor lasers, for instance) is used to represent the input vector (dimension = N); the value of each element of the input vector is encoded as the optical power of each of the source. The source array can be addressed electronically in parallel. A transparency or a spatial light modulator (SLM) is used to encode the input matrix with the value of each matrix element represented by the (local) optical intensity transmittance at the corresponding location on the matrix mask. The appropriate pixel-by-pixel multiplication as prescribed by the definition of MVM is achieved by projecting the source array to match the matrix mask, using anamorphic optics (omitted in Fig. 1 for the sake of clarity). The required summations are then carried out by another set of anamorphic optics (also omitted in Fig.1) that projects the transmitted light onto a linear detector array. The output of the detector represents the product. When the sources are addressed in parallel, the two dimensional matrix mask allows one to carry out the MVM operation with full parallelism (of order N^2).

The computational complexity for the multiplication of two $N \times N$ matrices is of the order N^3 . In other words, it requires N^3 multiplications and N^3 summations to multiply two $N \times N$ matrices. The problem can also be decomposed into N sub-problems of MVM. This is illustrated in Fig. 2 for the special case of $N = 3$. Since the columns with all the elements equal to zero can be ignored, each sub-problem essentially involves only one MVM. Using the configuration shown in Fig. 1, one can, therefore, complete the multiplication of two $N \times N$ matrices M_1 and M_2 in N clock cycles by clocking into the source array a sequence of N vectors V_i ($i = 1$ to N) which together constitute the matrix M_1 ; the other matrix M_2 is

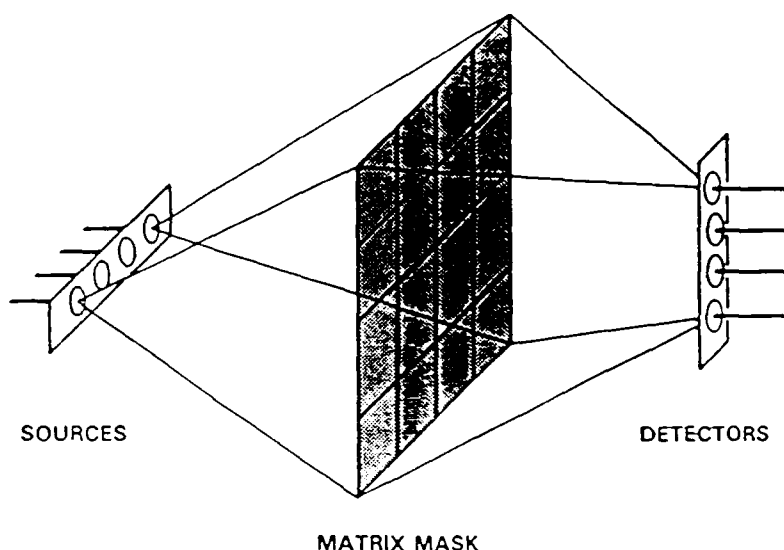


Figure 1. The incoherent matrix-vector multiplication scheme; the cylindrical optics are omitted for clarity.

$$\begin{bmatrix} m_{11} & m_{12} & m_{13} \\ m_{21} & m_{22} & m_{23} \\ m_{31} & m_{32} & m_{33} \end{bmatrix} \begin{bmatrix} a_{11} & a_{12} & a_{13} \\ a_{21} & a_{22} & a_{23} \\ a_{31} & a_{32} & a_{33} \end{bmatrix} = \begin{bmatrix} m_{11} & m_{12} & m_{13} \\ m_{21} & m_{22} & m_{23} \\ m_{31} & m_{32} & m_{33} \end{bmatrix} \begin{bmatrix} a_{11} & 0 & 0 \\ a_{21} & 0 & 0 \\ a_{31} & 0 & 0 \end{bmatrix} \\
 + \begin{bmatrix} m_{11} & m_{12} & m_{13} \\ m_{21} & m_{22} & m_{23} \\ m_{31} & m_{32} & m_{33} \end{bmatrix} \begin{bmatrix} 0 & a_{12} & 0 \\ 0 & a_{22} & 0 \\ 0 & a_{32} & 0 \end{bmatrix} \\
 + \begin{bmatrix} m_{11} & m_{12} & m_{13} \\ m_{21} & m_{22} & m_{23} \\ m_{31} & m_{32} & m_{33} \end{bmatrix} \begin{bmatrix} 0 & 0 & a_{13} \\ 0 & 0 & a_{23} \\ 0 & 0 & a_{33} \end{bmatrix}$$

Figure 2. Decomposition of a problem of matrix-matrix multiplication into the sub-problems of matrix-vector multiplication.

represented by the two-dimensional mask as described earlier. In this approach, a storage device is required at the output end since the final result, which takes the form of N column vectors, is obtained sequentially in N steps. In addition to the time-multiplexing approach with N^2 parallelism described above, one can also use a color (wavelength) multiplexing scheme to achieve MMM with full (N^3) parallelism.

A schematic diagram illustrating the basic principle of the color multiplexing MMM scheme is shown in Fig. 3. Each constituent column vector V_i of the matrix M_1 is color encoded by illuminating it with a unique color at a unique input angle. Chromatic (as well as angular) multiplexing is achieved by combining the output color beam strips into a single column with the aid of color dispersion in a prism. Multiplication in parallel of each color encoded vector V_i with matrix M_2 is accomplished as described earlier (see Fig. 1). The output, after chromatic (and angular) demultiplexing via another prism, is resolved into the product matrix which can be image onto a two-dimensional array of detectors. In practice, one may have to calibrate the output to correct for the spectral non-uniformities of the source, the matrix mask and the detectors.

The color multiplexing technique is by no mean limited to the incoherent matrix processing scheme described above. The incoherent approach is chosen as an example in this section to explain the basic idea of color multiplexed matrix processors mainly because of its

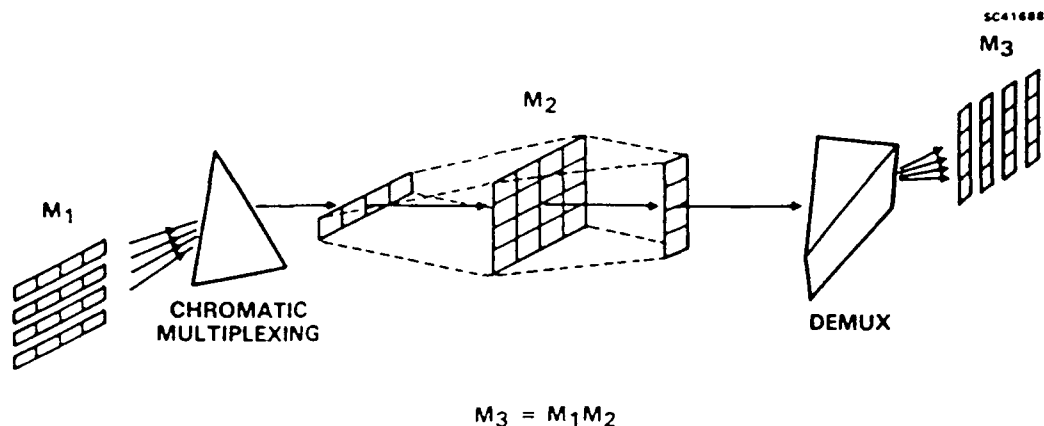


Figure 3. A color-multiplexing scheme for incoherent optical matrix-matrix multiplication.

simplicity. It also serves as a reference for comparison with the coherent processor using photorefractive four-wave mixing to be described in the next section.

3. OPTICAL MATRIX PROCESSORS BASED ON NONLINEAR FOUR-WAVE MIXING

The investigations of nonlinear optical four-wave mixing for optical phase conjugation and spatial convolution/correlation were reported^{11,12} several years ago. Recently, the applications of nonlinear four-wave mixing for other optical processings such as MVM,¹ parallel logic operations,¹³ optical pattern recognition for symbolic substitution,¹⁴ and residue-arithmetic computation¹⁵ have also been demonstrated. Most of these applications utilize the same basic multiplicative properties of four wave mixing. They differ only in the input spatial patterns and in their particular uses of lenses, some for imaging and others for spatial Fourier transform. A configuration for MVM is illustrated schematically in Fig. 4. A matrix-mask M is illuminated with a uniform coherent beam and imaged onto the nonlinear medium from one side. The mask representing the vector (a_1, a_2, a_3) is illuminated from the other side. The transmitted beams are expanded by cylindrical optics, into three identical row vectors which align pixel-by-pixel with the matrix M . In practice,

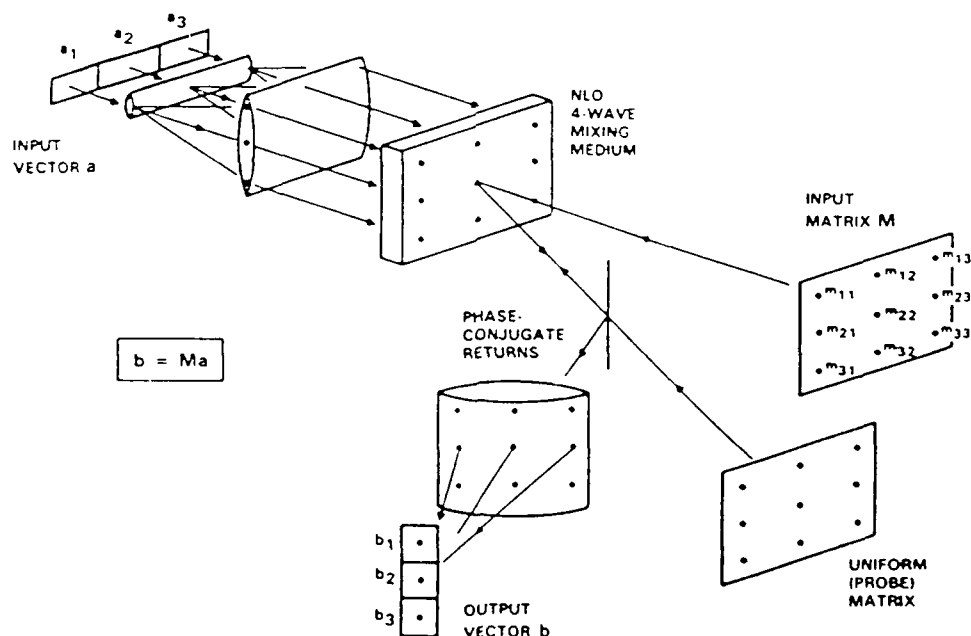


Figure 4. A schematic diagram illustrating the basic concept of optical matrix-vector multiplication using nonlinear four-wave mixing.

one can avoid the cylindrical optics by using a two-dimension mask to encode directly three (or N , in general) identical rows of the input vector. This allows one to use identical imaging optics in both input ports and thus achieve better beam-overlap. Inside the nonlinear crystal, there are nine pairs of counter-propagating beamlets, representing the elements of the matrix M and the vector a . When a uniform probe beam is injected into the nonlinear crystal, optical phase conjugation takes place via the four-wave mixing process. Under appropriate conditions, the phase-conjugate output intensity is proportional to the products of the three input intensities.¹⁶ A beam splitter is used to sample the phase-conjugate output, which consists of nine beamlets representing the pixel-by-pixel product of the matrix and the vector. A cylindrical lens is then used to perform the row-wise additions of the beamlets to obtain the product vector (b_1, b_2, b_3) at the output plane. The experimental detail and results demonstrating the multiplication of a binary matrix (5×5) and a binary vector using a photorefractive barium titanate crystal as the nonlinear medium were reported recently.¹

Experimental observation of simultaneous optical phase conjugation of several colors of input from a single barium titanate crystal has been reported by Chang et al.¹⁷ Such multi-color phase conjugation via four-wave mixing in photorefractive crystal can be employed to perform MMM. Figure 5 shows a schematic diagram of such a matrix processor. This configuration is basically the same as the one shown in Fig. 4 except for the addition of two dispersive elements, one in the input for color-multiplexing, and another in the output for color-demultiplexing. Notice that the input matrix A is decomposed into its constituent vectors encoded with different colors as described in the previous section. The beam illuminating the other matrix M and the probe beam consists of all the colors uniformly distributed over the beam profiles. As a result of four-wave mixing of each of the spectral component independently, pixel-by-pixel multiplication with N^2 parallelism is achieved. The signal to noise ratio of the output depends critically on the the pixel interaction, and hence the beam alignment of each of the spectral components inside the crystal. In the scheme that we propose (see Fig. 5), the alignment is accomplished in two steps. The input angles for each of the spectral components and the associated vector masks are first adjusted so that the output appears as a single column consisting of all the spectral components. Cylindrical optics are then used to expand this single column to coincide with the matrix inside the nonlinear medium. This procedure ensures that all the spectral components are in unison and can be aligned simultaneously in the second step. Cross-talk due to interactions among different colors does not exist, provided the frequency separation between the colors are far beyond the temporal (frequency) bandwidth of the nonlinear process. This is usually the case for most of the photorefractive materials since their response time typically ranges from micro-second to second.

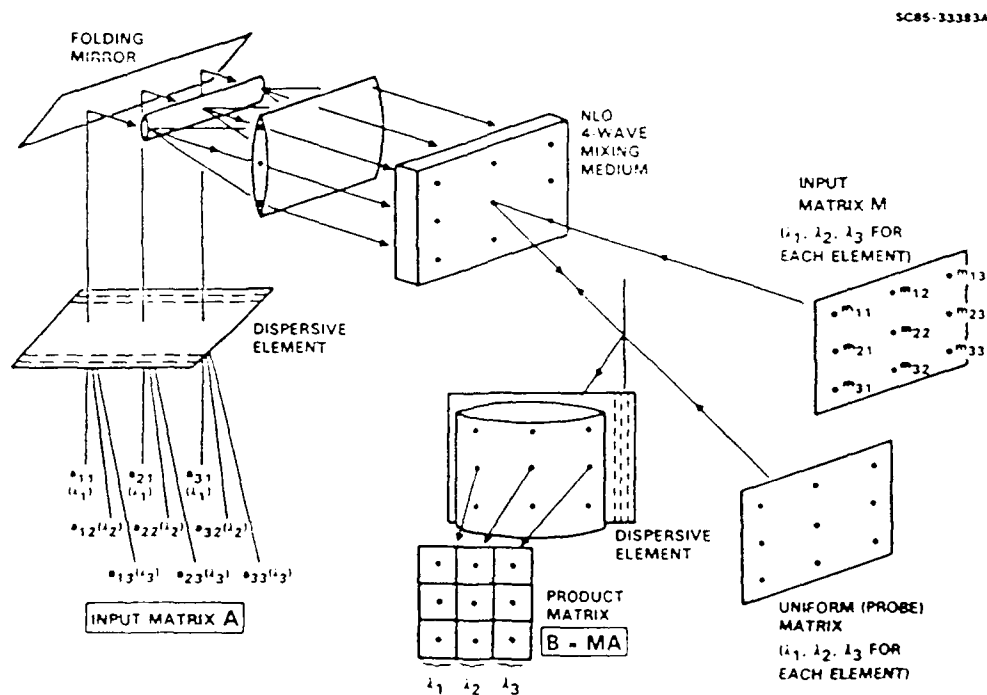


Figure 5. A schematic diagram illustrating the basic idea of optical matrix-matrix multiplication using color-multiplexed four-wave mixing.

4. EXPERIMENTAL CONFIGURATION AND RESULTS

Using a photorefractive barium titanate crystal as the nonlinear medium and an argon ion laser, we have demonstrated the multiplication of 2×2 binary matrices. The experimental configuration is shown schematically in Fig. 6. Broad band reflectors are used for the laser resonator so that it oscillates at more than one wavelength. Specifically, we operate the laser (Spectra Physics Model 171) at five wavelengths (514.5 nm, 496.5 nm, 488 nm, 476.5 nm, and 457.9 nm) in the blue-green region of the visible spectrum. The 5-color output beam is expanded to about 1 cm in diameter and collimated by the beam expander/collimator (BE). A neutral density filter (NDF) with OD = 1 is used to reduce the phase conjugate feedback into the laser, and a polarizing beam splitter cube (PBS) is used to filter out the s-polarization component. The beam splitter BS₁ (R = 50%), lens L₁ (f = 75 cm), mirror M₂ and lens L₂ (f = 33.3 cm) constitute the optics for the probe beam. A 2×2 matrix mask MM₁ is illuminated with one of the pumping beams split off from the beam splitter BS₂. The folding mirror M₂, and the two lens imaging system [lenses L₃ (f = 50 cm) and L₄ (f = 30 cm)] are used to project a reduced image of the mask MM₁ onto the crystal. The angle θ subtended by the two beams is about 7°. The beam transmitted through BS₂ is sent through a prism P₁ to angularly separate all the 5-color components two of which (476.5 nm and 514.5 nm) are selected to illuminate the masks MM₂ and MM₃, respectively. The two color-encoded patterns are combined at beam splitter BS₃ and imaged onto the crystal through the folding mirror M₇, and the two lenses L₅ (f = 50 cm) and L₆ (f = 30 cm). For proper operation, beam alignment and pixel interaction inside the crystal are critical. The barium titanate crystal (5 mm × 4 mm × 4 mm) is cut so that the angle ϕ between the c-axis and one of the input surface is about 30°. This is approximately equal to the angle between the c-axis and the grating (normal) vector when the incidence of the two writing beams are near normal (see Fig. 6). Such a configuration allows us to maximize the effective electro-optic coefficient without using oblique incidence, which reduces the useful area of the nonlinear medium. The phase conjugate beam encoded with the pixel-by-pixel multiplication of each of the colors is sampled by the beam splitter BS₄. In the output port, the folding mirror M₈ and lens L₇ (f = 80 cm) image the center of the crystal onto the screen S, the prism P₂ angularly separates the color components (color demultiplexing) of the output beam, and the cylindrical lens CL carries out the row-wise summation for each of the colors.

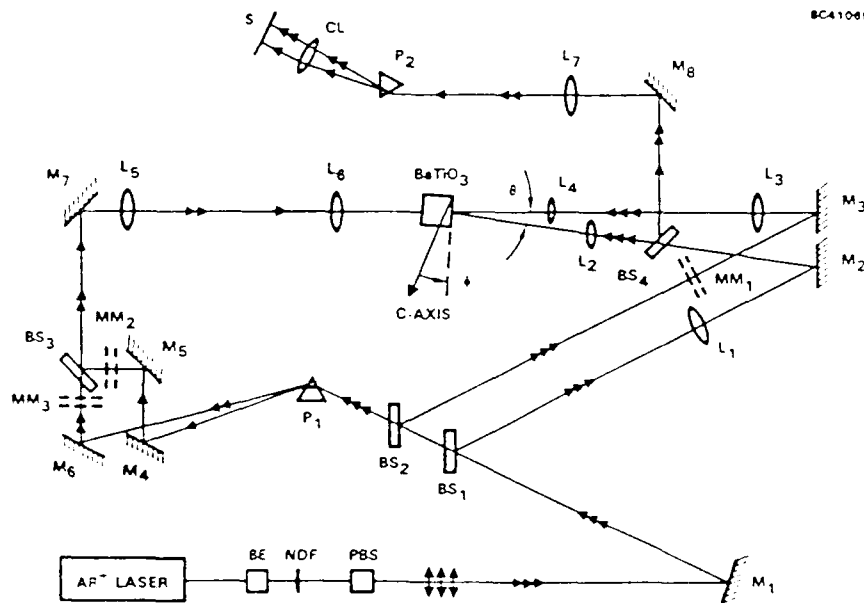


Figure 6. The layout for demonstrating the multiplication of two 2×2 matrices using color-multiplexed photorefractive four-wave mixing.

Figure 7a shows the two matrices M and A , the decomposition of matrix A into column vectors, and the color encoding scheme. The three masks MM₁, MM₃ and MM₂ (see Fig. 6) for encoding the matrix M and the first and second column of the matrix A , respectively, are shown in Fig. 7b. The experimental results are shown in Fig. 8. Figure 8a is a picture of the output pattern on the screen S when the summing cylindrical lens (CL) is removed; the relative optical power of each pixel monitored by a detector is indicated by the traces from the chart recorder. Figure 8b is the final result representing the product matrix when the cylindrical lens (CL) is in place. In practice, calibration to compensate for the spectral characteristic of the source, masks, and detector may be necessary.

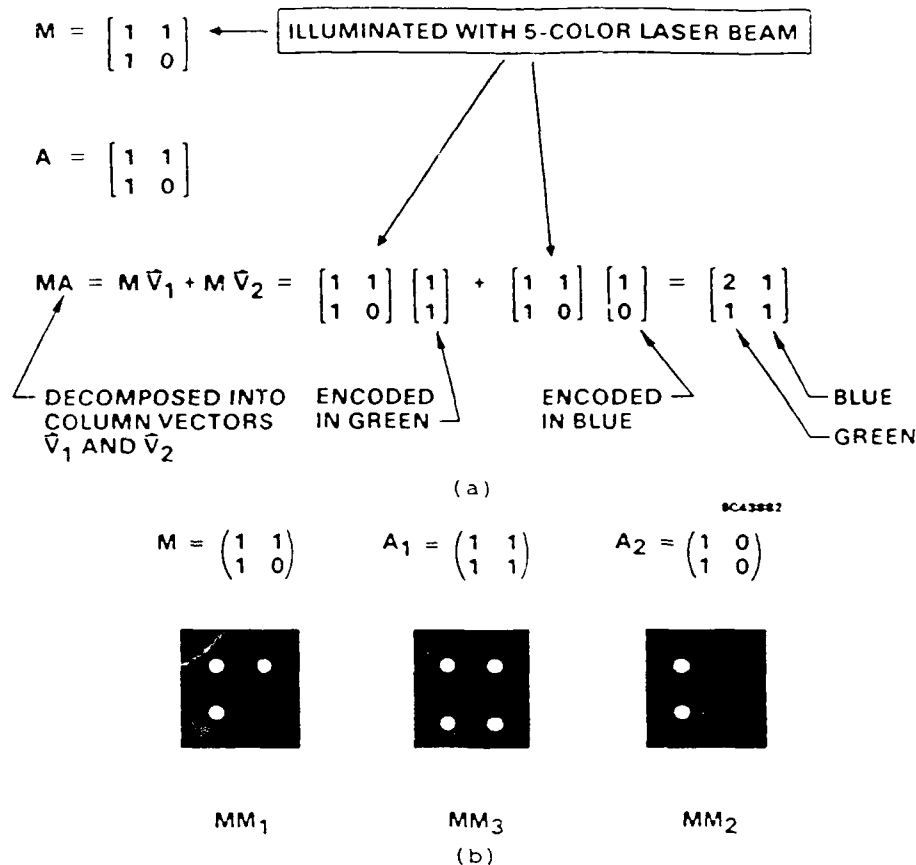


Figure 7. (a) The two matrices (M and A) chosen for our demonstration, the decomposition of A into column vectors, and the encoded colors. (b) The three matrix masks MM₁, MM₃, and MM₂ (see Fig. 6) for encoding the matrix M and the two column vectors A₁ and A₂ derived from matrix A.

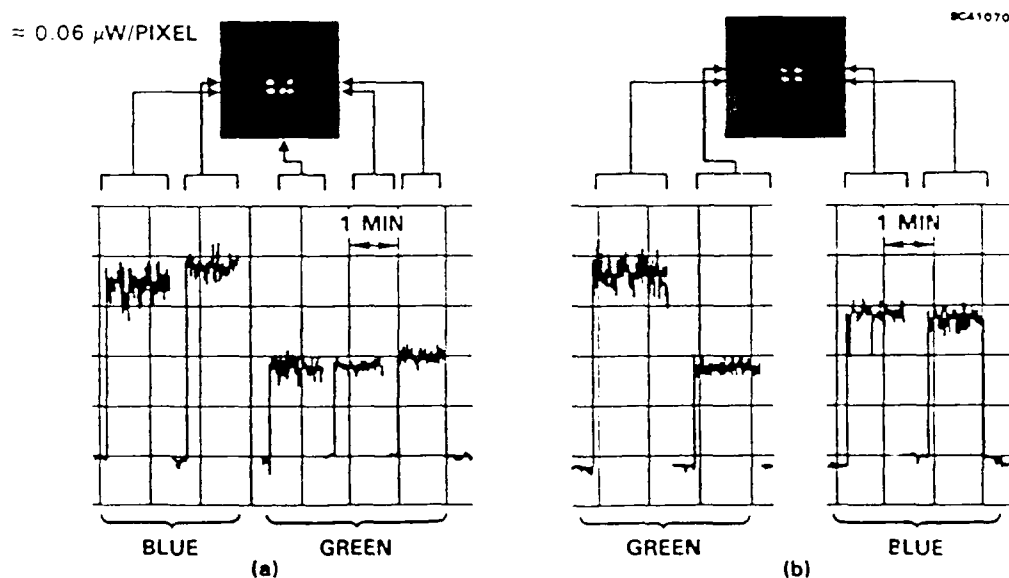


Figure 8. (a) the output pattern with the summing cylindrical lens (CL) (see Fig. 6) removed; the relative power of each pixel is indicated by the chart recorder traces and the color of the pixel is indicated below. (b) The corresponding results representing the product of M and A when the summing cylindrical lens (CL) is in place.

5. SUMMARY AND CONCLUSION

We have presented the basic concept and experimental results for optical matrix-matrix multiplication using color-multiplexed four-wave mixing in a nonlinear medium. To clarify the concept of color-multiplexing, an incoherent optical approach was also introduced. Although the latter is relatively simple and straight forward to implement, no experimental results, to the best of our knowledge, have yet been reported. For multicolor four-wave mixing, a photorefractive barium titanate crystal is chosen for our experimental demonstration because of its strong nonlinear response in the blue-green region of the visible spectrum and its availability. When the number of colors is limited to a few, no significant reduction in phase-conjugate reflectivity of each color component is observed. However, as the number of colors increases, say to 10 or 20, it is anticipated that the grating contrast, and hence the phase conjugate reflectivity for each color will be reduced because of the photo-excitation of charges by all the other colors sharing the same volume. Multiple quantum well structures with different sets of layers designed to enhance the optical nonlinearity at different wavelengths are potential candidates for color multiplexed four-wave mixing. With the current technology, the nonlinear optical approach is limited by the availability of an optical medium with sufficient nonlinearity (for four-wave mixing) over a wide spectral range and a multi-color coherent source that matches the same spectral range.

In our experimental demonstration, we chose to use binary matrices and monitored the final result in a mixed binary format. For analog operation, several important issues such as the dynamic range and pixel-to-pixel uniformity require further investigation.

One of the major advantage of the four wave mixing configuration is the availability of three input ports. As a result, the system is sufficiently flexible that it can be adapted, with little or no modification, to perform other types of processing such as parallel logic operations,¹³ pattern recognition for symbolic substitution,¹⁴ and residue arithmetic computation.¹⁵ It is quite conceivable that the incorporation of color multiplexing, which adds another dimension to this approach with even more degrees of freedom, will equip the system for other forms of image or data processings.

7. ACKNOWLEDGEMENTS

This work is supported by a DARPA/AFOSR Contract (NO.F49620-87-C-0015).

8. REFERENCES

1. P. Yeh and A. Chiou, "Optical matrix-vector multiplication through four-wave mixing in photorefractive media," *Opt. Lett.* **12**(2), 138-140 (1987).
2. J.A. Neff, "Major initiatives for optical computing," *Opt. Eng.* **26**(1), 002-009 (1987).
3. N.H. Farhat, D. Psaltis, A. Prata, and E. Paek, "Optical implementation of the Hopfield model," *Appl. Opt.* **24**(10), 1469-1475 (1985).
4. J. Jau, F. Kiamilev, Y. Fainman, S. Esener, and S. H. Lee, "Optical expert system based on matrix-algebraic formulation," *J. Opt. Soc. Am.* **A4**, (13), 57 (1987).
5. F. Kiamilev, J. Jau, Y. Fainman, S. Esener, and S.H. Lee, "Comparison of prolog and matrix-algebraic AI system," *J. Opt. Soc. Am.* **A4**, (13), 58 (1987).
6. W.T. Rhodes, "Optical matrix-vector processors: basic concepts," in *Highly Parallel Signal Processing Architectures*, Proc. SPIE **614**, 146-152 (1986).
7. P.A. Athale, "Optical matrix processors," in *Optical and Hybrid Computing*, E. H. Szu, Ed., SPIE **634**, 96-111 (1986).
8. D. Casasent and B.V.K. Vijaya Kumar, "Optical linear algebra processors," in *Optical Signal Processing*, J.L. Horner, Ed., pp. 389-407, Academic, San Diego (1987).
9. H.J. Caulfield, J.A. Neff, and W.T. Rhodes, "Optical computing: the coming revolution in optical signal processing," *Laser Focus/Electro-optics*, pp.100-110 (Nov., 1983).
10. J.W. Goodman, A.R. Dias, and L.M. Woody, "Highly parallel, high-speed incoherent optical method for performing discrete Fourier transforms," *Opt. Lett.* **2**(1), 103 (1978).
11. A. Yariv, "Phase conjugate optics and real-time holography," *IEEE J. Quantum Electron.*, **QE-14**(9), 650-660 (1978), and erratum, *IEEE J. Quantum Electron.*, **QE-15**(4), 256 (1979).
12. J.O. White and A. Yariv, "Real-time image processing via four-wave mixing in a photorefractive medium," *Appl. Phys. Lett.* **37**(1), 5-7 (1980).
13. G. Eichmann, Y. Li, and R.R. Alfano, "Parallel optical logic using optical phase conjugation," *Appl. Opt.* **26**(2), 194-196 (1987).
14. Y. Li, G. Eichmann, F. Dorsinville, and R.R. Alfano, "An AND operation-based optical symbolic substitution pattern recognizer," *Opt. Commun.* **63**(6), 375-379 (1987).

15. Y. Li, G. Eichmann, R. Worsenville, and R.R. Alfano, "Demonstration of a picosecond optical-phase-conjugation-based residue-arithmetic computation," *Opt. Lett.* 13(2), 178-180 (1988).
16. See, for example, Optical Phase Conjugation, R.A. Fisher, Ed., Academic, New York (1983).
17. T.Y. Chang, D.L. Naylor, and R.W. Hellwarth, "Continuouswave multi-color phase conjugation," *Appl. Phys.* B28, 156 (1982).



APPENDIX 5.3

Optical Matrix-Matrix Multiplication with N^3 Parallelism by Spatial Convolution via Four-Wave Mixing

Arthur E. Chiou and Khanh B. Nguyen

Rockwell International Science Center
1049 Camino Dos Rios
Thousand Oaks, CA 91360
(805) 373-4464

SUMMARY

The convolution of two (two-dimensional) spatial patterns using nonlinear optical four-wave mixing in their common Fourier plane can be devised to achieve matrix-matrix multiplication optically, in full parallelism. In principle, it can be applied to the multiplication of a matrix A (of any dimension $m \times n$) and a compatible matrix B (of dimension $n \times p$). A unique feature of this approach is that the output beamlets representing the elements of the product matrix lie on a straight line; therefore, a linear array of detectors (instead of a two-dimensional array) can be used for monitoring the result. The major advantage of this scheme is the full parallelism achieved with a relatively simple optical arrangement. The trade-off is the resulting spatial complexity.

White and Yariv¹ have demonstrated that (spatial) convolution and correlation of two (two-dimensional) patterns can be achieved in real time by four-wave mixing in the common Fourier plane of the input patterns and recording the phase-conjugated output at the corresponding object plane. A typical experimental configuration is shown schematically in Fig. 1. Specifically, if U_3 is a small aperture simulating a point source (or a delta function), a pattern representing the convolution of U_1 and U_2 ($U_1 * U_2$) is observed in the output plane. An illustrative example is given in Fig. 2. The design of U_1 and U_2 to represent two matrices so that their product is represented by $U_1 * U_2$ is explained in the following paragraphs. Explicit mathematical analysis, including the

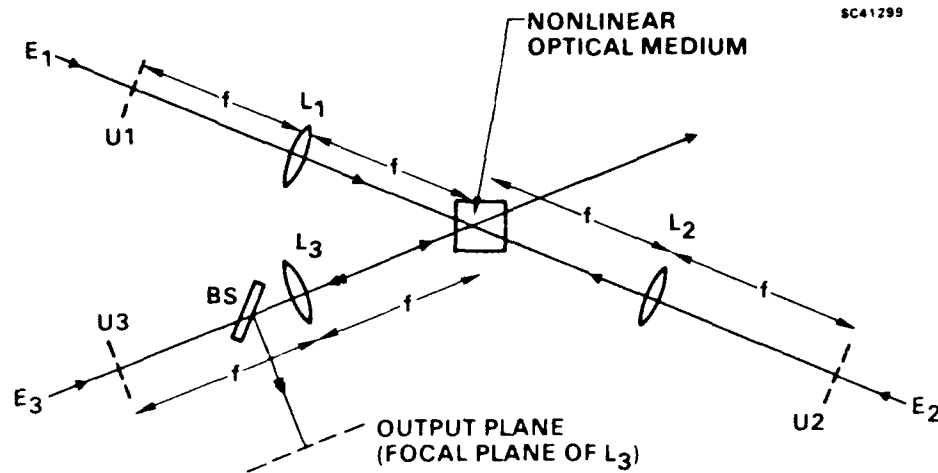


Fig. 1 A schematic diagram illustrating the basic idea of four-wave mixing in a non-linear medium located at the common Fourier plane of the input spatial pattern.

SC41298

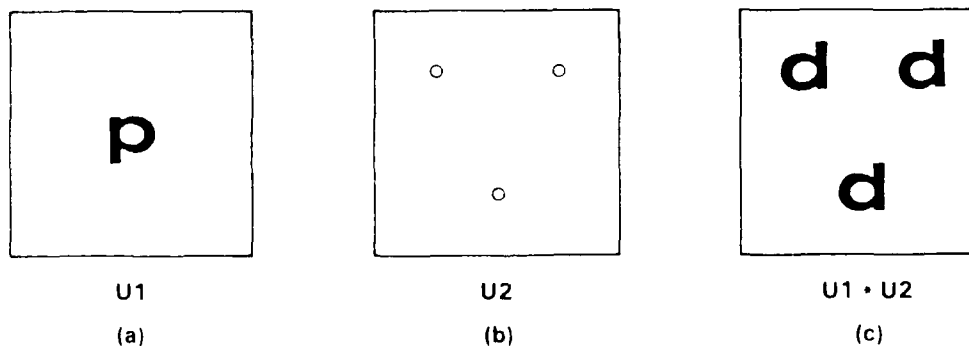


Fig. 2 A schematic illustration of convolution of two spatial patterns: (a) and (b) are the two input spatial patterns; (c) represents the resulting spatial convolution of the two inputs.

effect of finite aperture dimensions among the others, of a similar matrix multiplication concept based on spatial filtering was given by R.A. Heinz et al.²



For simplicity and clarity, let us consider the simplest cases of two matrices A and B, both of dimension 2 x 2, and their product $C = AB$ given below.

$$A = \begin{matrix} a_{11} & a_{12} \\ a_{21} & a_{22} \end{matrix}$$

$$B = \begin{matrix} b_{11} & b_{12} \\ b_{21} & b_{22} \end{matrix}$$

(7)

$$C = AB = \begin{matrix} c_{11} & c_{12} \\ c_{21} & c_{22} \end{matrix} = \begin{matrix} a_{11}b_{11} + a_{12}b_{21} & a_{11}b_{12} + a_{12}b_{22} \\ a_{21}b_{11} + a_{22}b_{21} & a_{21}b_{12} + a_{22}b_{22} \end{matrix}$$

A transparency U1 consists of four small apertures, each with its intensity transmittance proportional to each of the matrix element a_{ij} is shown in Fig. 3a. A similar transparency U2 corresponding to the transpose of B (i.e., rows and columns interchanged) is shown in Fig. 3b. Note that the vertical distance between the elements in U1 is designed so that it is considerably larger than that in U2, while the horizontal distances between the elements are identical in U1 and U2. Note also that the dashed rectangular box connecting the four elements in U2 is an artifact to facilitate the following explanation and should be ignored in the actual design. By comparing Figs. 2 and 3, it is straightforward to see how the quadruplet of the dashed rectangular box is formed at the corresponding position in Fig. 3c as a result of the two-dimensional spatial convolution. As noted before, all the dashed lines in Fig. 3c are artifacts and the actual result should show only the corners of each box, i.e., a total of 16 spots with the intensity of each proportional to the cross product of all the elements in A and those in B. The four doublets lying along the Y-axis in Fig. 3c are drawn slightly offset from the axis to expose the individual component. In practice, the two components of each doublet are spatially overlapping on the Y-axis. The intensity of the four doublets, from top to bottom, on the Y-axis are proportional to c_{12} , c_{11} , c_{22} and c_{21} , respectively. The eight cross terms that do not contribute to the matrix-matrix multiplication can be filtered out easily as they are physically separated from the Y-axis.

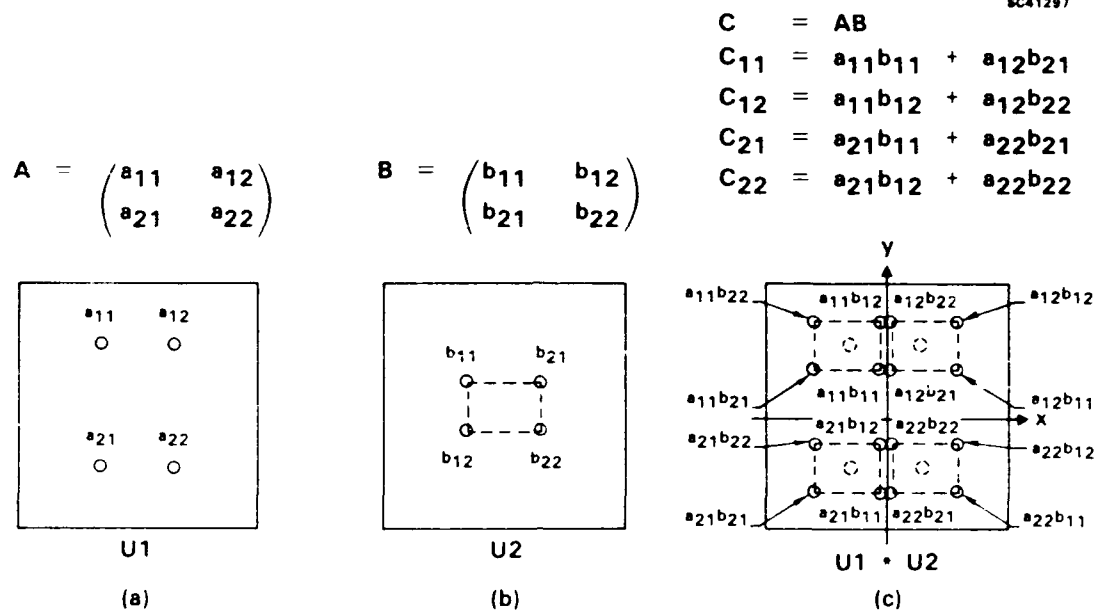


Fig. 3 A schematic diagram illustrating optical matrix-matrix multiplication by convolution for the case of 2×2 matrices: (a) matrix A and the mask U_1 to encode A; (b) matrix B and the mask U_2 to encode B; (c) the spatial pattern resulting from convolution of U_1 and U_2 .

Another example illustrating the case of multiplying a 2×3 matrix with a 3×4 matrix is shown in Fig. 4. Note that all the cross terms that do not contribute to the matrix-matrix product are omitted in Fig. 4c for the sake of clarity.

Using an argon ion laser (5145Å) and a BaTiO₃ crystal, we have experimentally demonstrated the concept described above for the case of 2×2 matrices. The images of the masks used to encode the two matrices A and B are shown in Figs. 5a and 5b, respectively. The experimental result representing the product is shown in Fig. 5c. An overexposed version of Fig. 5c is shown in Fig. 5d to reveal the noise resulting from the other cross terms that do not contribute to the matrix product.

In principle, the basic concept described above can be applied to the multiplication of a matrix (of any dimension $m \times n$) and a compatible matrix B (of dimension $n \times p$). In practice, the signal-to-noise (S/N) ratio is expected to degrade as the dimension of the matrix increases. The problem of S/N is less serious in the mixed binary mode. The major advantage of this scheme is the full parallelism achieved with relatively simple optical arrangements. From the technological point of view, the fact that all the output

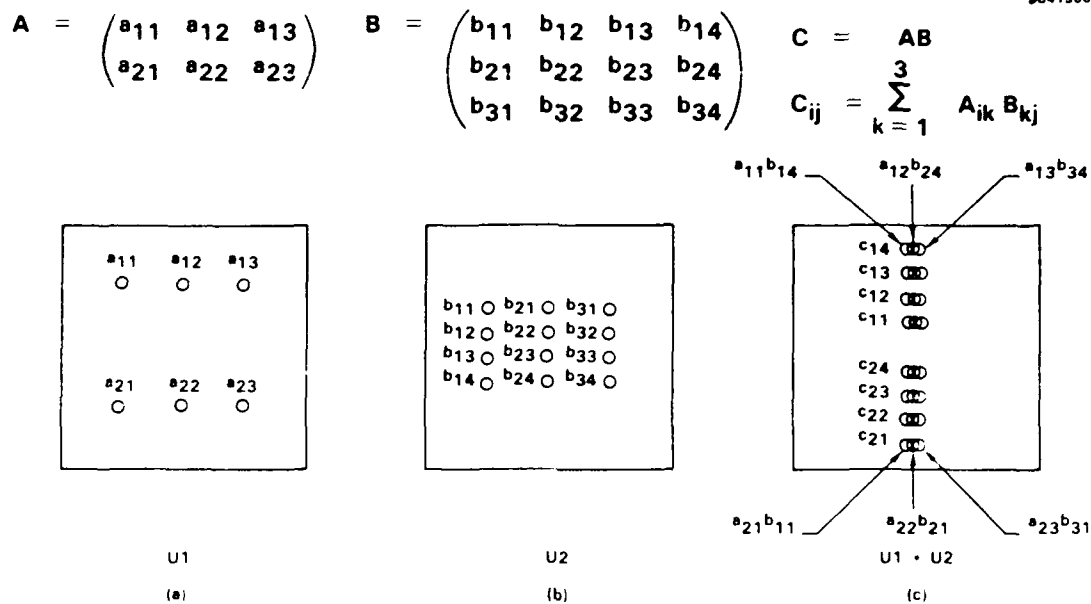


Fig. 4 An illustration similar to Fig. 3 for the case when the dimensions of the matrices A, B and C are 2×3 , 3×4 and 2×4 , respectively.

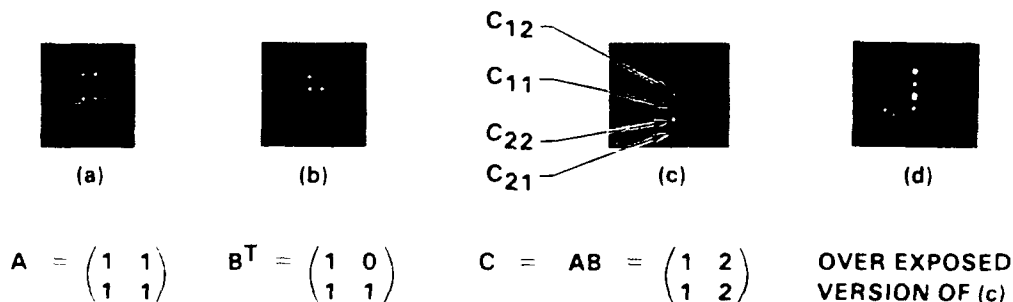


Fig. 5 Experimental results for optical matrix-matrix multiplication by convolution via four-wave mixing in the spatial frequency domain. (a) and (b) are the matrix masks used for encoding the matrices A and B^T ; (c) shows the result of their spatial convolution; (d) is an overexposed version of (c) to reveal the cross terms that do not contribute to the matrix product.

elements lie on a straight line can be significant, since this allows one to use a linear detector array instead of a 2-D array for output detection.



Rockwell International
Science Center

SC5502.FR

ACKNOWLEDGEMENT

This work is partially supported by DARPA Contract No. F49620-87-C-0015.

REFERENCES

1. J.O. White and A. Yariv, Appl. Phys. Lett. 37(1), 5 (1980).
2. R.A. Heinz, J.O. Artman, and S.H. Lee, Appl. Opt. 9(9), 2161 (1970).



Rockwell International

Science Center

SC5502.FR

APPENDIX 5.4

Optical Matrix-Vector Multiplication Using a Spatial Light Modulator and a Phase Conjugator

SPATIAL LIGHT MODULATORS AND APPLICATIONS 1988 TECHNICAL DIGEST SERIES, VOLUME 8

CONFERENCE EDITION

Summaries of papers presented at the
Spatial Light Modulators and Applications
Topical Meeting

June 15-17, 1988

South Lake Tahoe, Nevada

Sponsored by

Optical Society of America
Lasers and Electro-Optics Society of the
Institute of Electrical and Electronics Engineers
Strategic Defense Initiative Organization
Innovative Science and Technology Office
National Aeronautics and Space Administration
Office of Naval Research
Air Force Office of Scientific Research

Optical Society of America
1816 Jefferson Place, N.W.
Washington, D.C. 20036
(202) 223-8130

Optical Matrix-Vector Multiplication Using a Spatial Light Modulator and a Phase Conjugator

Arthur E. Chiou, Pochi Yeh, and Monte Khoshnevisan
Rockwell International Science Center
1049, Camino Dos Rios
Thousand Oaks, CA 91360
Tel: (805) 373-4464

SUMMARY

A variety of optical matrix processing schemes [1, 2] use two-dimensional spatial modulation of optical intensity to represent a matrix to exploit the inherent parallel nature of optics. Such an approach typically requires the projection of a spatial pattern to match another pattern to perform the element-by-element multiplication. The basic incoherent matrix-vector multiplication scheme [3], for example, requires the use of anamorphic optics to project a linear array of sources (or a one dimensional spatial light modulator) to precisely match a two dimensional matrix masks. In the matrix-vector multiplication scheme using four-wave mixing in nonlinear media [4], simultaneous alignment of all the pixels of the matrix and vector is a major task, particularly for a large number of pixels. Misalignment of the pixels may lead to severe errors. For a given size of matrix mask, the density of elements increases as the dimension (N) of the matrix increases. As a result, the requirement on alignment becomes more and more stringent. In practice, the critical alignment required is likely to impose a practical limit on the optimum dimension of the matrix (N) to be of the order of one hundred or less depending on the specific architecture.

In this paper, we report a new scheme for optical matrix-vector multiplication that uses a phase conjugator (with a finite storage time) in conjunction with a spatial light modulator (SLM) to eliminate the pixel-by-pixel alignment requirement at the cost of some reduction in parallelism ($N^2/2$ instead of N^2). Phase aberration due to imperfection in optics is also self-corrected by the phase conjugation process. The optical system involved is relatively

simple compared with the other approaches. Without any modification, such a scheme can also perform matrix-matrix multiplication with $N^2/2$ parallelism.

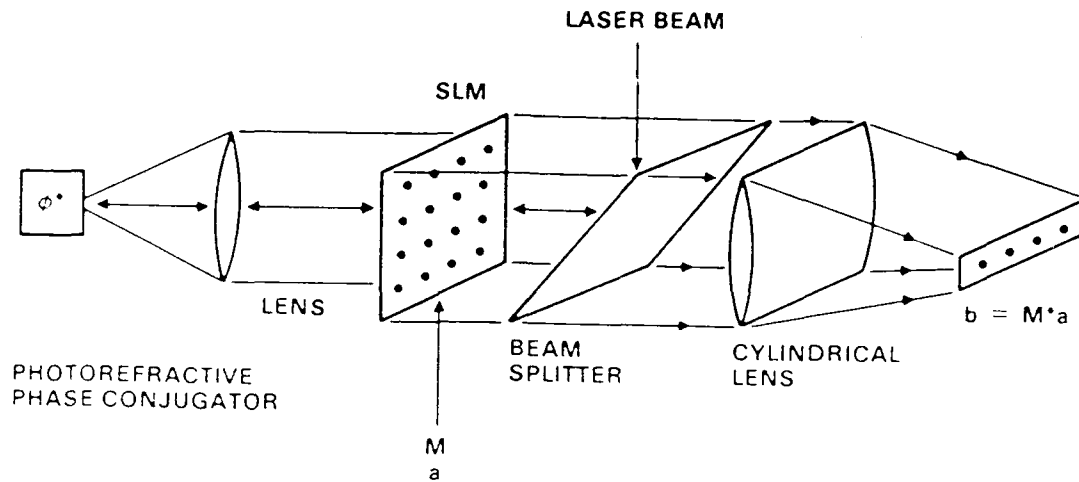


Fig.1 A schematic diagram illustrating the basic concept of optical matrix-vector multiplication using a photorefractive phase conjugator in conjunction with a spatial light modulator.

Referring to Fig.1, we use a SLM to impress the matrix and vector information in sequence to an input laser beam. This beam is directed toward a phase conjugator which has a finite storage time (a photorefractive barium titanate, for example). A cylindrical lens is inserted in the phase conjugate output beam path to perform the summation.

The principle of operation is as follows: the SLM first impresses the matrix information onto the input laser beam. This beam is then incident into a phase conjugator which stores the matrix information after a finite grating formation time. When the matrix information is removed from the SLM, say by turning all the pixels into maximum transmission condition, the phase conjugate beam which contains the reconstruction of the matrix information exists for a finite duration. This finite storage time depends on the strength of the input (read) beam. During this time, if the next frame of the SLM carries the vector information, parallel multiplication is performed as the phase conjugate beam propagates back through the SLM. Here the vector is represented as a two-dimensional array of N identical column vectors, where N is the dimension of the vector. A cylindrical lens in the output port is used to perform the

summation. The dark storage time during which the matrix information can be retrieved is determined by the photorefractive material and the pumping configuration. It ranges from seconds to microseconds.

The system can also perform matrix-matrix multiplication by time multiplexing. In this case, each column vector V_i ($i=1$ to N) which constitutes the second matrix M_2 is sequentially impressed onto the beam to multiply with the first matrix M_1 according to the matrix-vector multiplication scheme described above. To avoid the degradation of the information of M_1 stored in the photorefractive hologram during the readout, it is necessary to refresh the holographic memory with M_1 to restore its diffraction efficiency. This can be done by re-impressing M_1 onto the beam after each readout cycle. Consequently, a total of $2N$ clock cycles, consisting of N cycles of write and N cycles of read, will be required to carry out the multiplication of two $N \times N$ matrices.

Using a photorefractive barium titanate crystal as a phase conjugator in conjunction with a 48×48 magneto-optic spatial light modulator (SIGHT-MOD SMD48I from Semetex Corp.), we have demonstrated the basic principle described above. Preliminary experimental results will be discussed. Some advantages and disadvantages of this approach will be compared with those of the others.

This work is partially supported by DARPA/AFOSR contract No.F49620-87-C-0015.

REFERENCES:

- [1] R. A. Athale, "Optical matrix processors," in Optical and Hybrid Computing, H. H. Szu, Ed., SPIE Vol. 634, 96-111 (1986).
- [2] W. T. Rhodes, "Optical matrix-vector processors : basic concepts," in Highly Parallel Signal Processing Architecture, SPIE Vol. 614, 146-152 (1986).
- [3] J. W. Goodman, A.R. Dias, and L. M. Woody, "Fully parallel, high-speed incoherent optical method for performing discrete Fourier transforms," *Opt. Lett.*, **2**, 1-3 (1978).
- [4] P. Yeh and A. E. Chiou, "Optical matrix-vector multiplication through four-wave mixing in photorefractive media," *Opt. Lett.*, **12**, 138-140 (1987).



APPENDIX 5.5

Optical Interconnection Using Photorefractive Dynamic Holograms

Optical interconnection using photorefractive dynamic holograms

Pochi Yeh, Arthur E. T. Chiou, and John Hong

Rockwell International Science Center, P.O. Box 1085,
Thousand Oaks, California 91360.

Received 8 March 1988.

Sponsored by John A. Neff, Defense Advanced Research
Projects Agency.

0003-6935/88/112093-04\$02.00/0.

© 1988 Optical Society of America.

Optical interconnection linking laser arrays and detector arrays plays a key role in optical computing.^{1,2} Conceptually, such an interconnection can be achieved by using an optical matrix-vector multiplication,

$$\mathbf{v}' = \mathbf{M}\mathbf{v}, \quad (1)$$

where \mathbf{v} is the input vector representing the signals carried by an array of N lasers and \mathbf{v}' is the output vector representing the signals received by the array of N detectors. \mathbf{M} is an $N \times N$ matrix representing the interconnection pattern.

When a transparency or a spatial light modulator (SLM) is used as the interconnection mask, parallel matrix vector multiplication can be achieved. Let the interconnection

mask consist of an $N \times N$ array of transmission windows. The input vector (a row of N elements) is fanned out by using, for example, a cylindrical lens pair, so that the light from each element is broadcast over a corresponding column of the windows. After transmitting through the interconnection mask, similar optics are used to collect the light from each row of windows and to sum the output into a column vector of N elements. Such an architecture provides the N^2 -parallelism. However, a large fraction of energy is absorbed by the transparency or SLM. When used as a crossbar switch, such an architecture has an energy efficiency of only $1/N$, where N is the dimension of the array.³ This occurs because $(N-1)/N$ of the light energy from each element of the input vector does not pass through the crossbar mask. The energy loss increases as the dimension of the array increases. This is sometimes referred to as the fanout energy loss. For a 1000×1000 crossbar switch, the loss due to fanout can be as high as 99.9%. This is not acceptable in high speed computing because signals are passing through the SLM at gigabit rates and the energy loss can be enormous. In addition to the inherent fanout energy loss, all SLMs have finite insertion loss due to imperfect transmissions such as from absorption and scattering. If we include such insertion losses, the energy efficiency for a crossbar switch would become t/N , where t is the transmittance ($t < 1$) of each window.

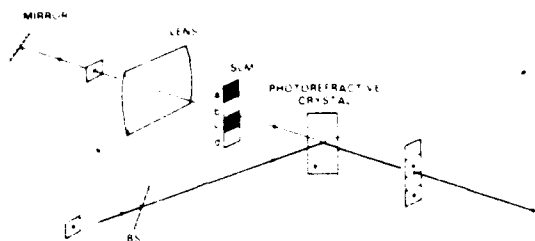


Fig. 1. Schematic drawing of an $1 \times N$ optical interconnection using dynamic photorefractive holograms with $N = 4$.

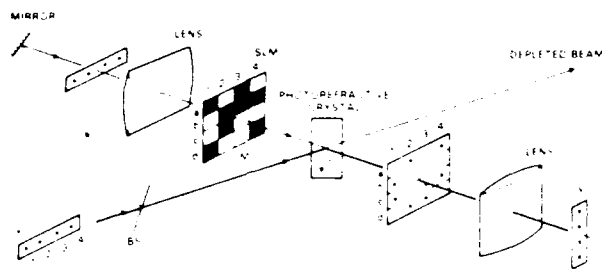


Fig. 2. Schematic drawing of an $N \times N$ optical interconnection using dynamic photorefractive holograms with $N = 4$.

It has been known for some time that a holographic optical element (HOE) can be employed for free space optical interconnection. Light from each laser source of the input array is Bragg scattered and redirected to one or more detectors of the output array. There are several specific requirements that need to be met for an HOE to be used for interconnection of VLSI circuits. These include near perfect alignment and high diffraction efficiency. In addition, a new hologram is needed for each new interconnection pattern. In view of these issues, it is desirable to use dynamic holographic media such as photorefractive crystals.¹⁻³ Photorefractive crystals such as BaTiO₃ and SBN are by far the most efficient real-time holographic media. The recording of a volume hologram inside these crystals requires a time of the order of 1 ms using light intensity of the order of 1 W/cm².

In this Communication, we propose a scheme of forming a dynamic hologram inside a photorefractive crystal so that the hologram is capable of performing reconfigurable optical interconnection with a very high energy efficiency. Such a scheme utilizes the nonreciprocal energy transfer in two-wave mixing to achieve an extremely high energy efficiency.

Referring to Figs. 1 and 2, we describe this new method of reconfigurable optical interconnection which utilizes the nonreciprocal energy transfer in photorefractive two-wave mixing to improve the energy efficiency. Figure 1 describes a 1-D case for the sake of clarity in explaining the concept. A small fraction of this incident laser beam is coupled out of the beam by using a beam splitter (BS). This small fraction (called probe beam) is then expanded by using a cylindrical lens and passes through the spatial light modulator (SLM). In the example shown, the laser beam is to be connected to detectors *b* and *a* as prescribed by the SLM. The transmitted probe beam is then recombined with the main beam inside a photorefractive crystal. As a result of nonreciprocal energy coupling, almost all the energy in the main beam is transferred to the probe beam, which carries the interconnection pattern. The result is an optical interconnection with a very high energy efficiency.

Figure 2 describes the reconfigurable interconnection for laser arrays and detector arrays. In the example (a 4×4 interconnection) shown, laser 1 is to be connected to detectors *b* and *c*, laser 2 is to be connected to detectors *a* and *d*, laser 3 is to be connected to detectors *c* and *d*, and laser 4 is to be connected to detectors *a* and *c*. In terms of the matrix-vector multiplication, such an interconnection can be written as

$$\mathbf{v}' = \begin{bmatrix} 0 & 1 & 0 & 1 \\ 1 & 0 & 0 & 0 \\ 1 & 0 & 1 & 1 \\ 0 & 1 & 1 & 0 \end{bmatrix} \begin{bmatrix} u_1 \\ u_2 \\ u_3 \\ u_4 \end{bmatrix} = \begin{bmatrix} u_2 + u_4 \\ u_1 \\ u_1 + u_3 + u_4 \\ u_2 + u_3 \end{bmatrix} \quad (2)$$

where u_1 , u_2 , u_3 , and u_4 are signals carried by the laser elements of the array u .

A cylindrical lens is used to focus the 2-D array of beams into a vector (1-D array). As a result, detector *a* receives signals from lasers 2 and 4, detector *b* receives signals from laser 1, detector *c* receives signals from lasers 1, 3, and 4, and detector *d* receives signals from lasers 2 and 3. Such a concept can be extended to interconnect N lasers with M detectors where N and M are two large numbers.

The two-wave mixing described in Figs. 1 and 2 may be viewed as a real-time holography in which the recording and readout occur simultaneously inside the photorefractive crystal. The beam splitter and the SLM are used to record a volume hologram which represents the interconnection pattern as prescribed by the SLM. The energy coupling involved in the two-wave mixing ensures that the diffraction efficiency during the readout is almost 100%. This, of course, requires a proper orientation of the crystal so that the energy of the readout beam is greatly depleted. The high energy efficiency results from the fact that most of the energy is carried by the readout beam, which does not pass through the SLM but is diffracted into the interconnection pattern by the hologram.

The energy efficiency of such an interconnection pattern can be estimated for a crossbar switch as follows. Let R be the reflectance of the beam splitter. It is legitimate to assume that the beam splitter is practically lossless. We may also assume that the surface of the photorefractive crystal is antireflection-coated so that the Fresnel reflection loss can be neglected. In these conditions, the two beams that arrive at the photorefractive crystal have energies $(1 - R)$ and R/N , respectively. Inside the crystal, these two beams undergo photorefractive coupling. As a result, most of the energy of the pump beam $(1 - R)$ is transferred to the probe beam R/N , which contains the interconnection pattern. The energy efficiency can be easily derived and is given by

$$\eta = \frac{(1 - R)}{N} \frac{1 + m}{1 + m \exp(-\gamma L)} \exp(-\alpha L) \quad (3)$$

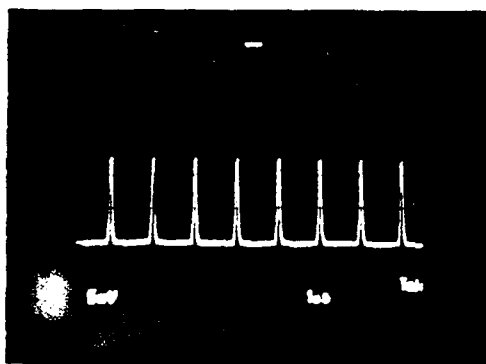
where m is the beam intensity ratio,

$$m = \frac{(1 - R)N}{(1 - R)} \quad (4)$$

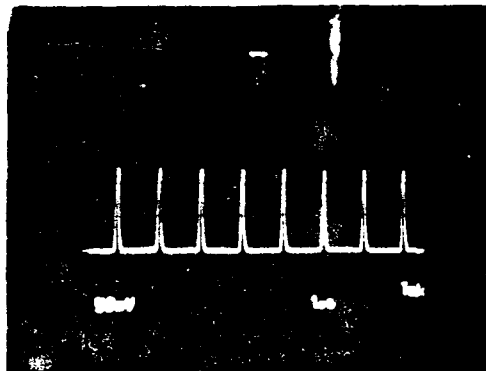
and L is the interaction length, γ is the coupling constant, and α is the bulk absorption coefficient. For photorefractive crystals such as BaTiO₃ and SBN, the coupling constant is very large (i.e., $\gamma L \gg 1$). The efficiency can be written approximately

$$\eta = \left[\frac{(1 - R)}{N} + (1 - R) \right] \exp(-\alpha L) \quad (5)$$

We notice that for large N , the energy efficiency is limited by



a) incident probe intensity (vertical scale = 5 mV/div, horizontal scale = 1 μsec/div)



b) amplified probe intensity (vertical scale = 50 mV/div, horizontal scale = 1 μsec/div)

Fig. 3. (a) Signal carried by the probe beam. Vertical scale = 5 mV/div, horizontal scale = 1 μsec/div. (b) Amplified signal carried by the probe beam, after undergoing two-wave mixing. Vertical scale = 50 mV/div, horizontal scale = 1 μsec/div.

the crystal bulk absorption $\exp(-L/\ell)$ and is maximized by using a beam splitter with a very small reflectance R (i.e., $R \sim 0$).

In our preliminary experimental work, we investigated the issue of energy efficiency and the capability of high data rate transmission. In examining the energy efficiency, we used a laser beam from an argon-ion laser operating at 514.5 nm. The laser beam is collimated into a beam of 2-mm diameter by using a lens of focal length $f = 2$ m. A beam splitter with a reflectance of $R = 0.05$ is used to redirect 5% of the energy through the spatial light modulator, establishing the probe beam. The remainder of the energy transmits through the beam splitter and constitutes the pump beam. In our preliminary experiment, the SLM was replaced with a neutral density filter with a variable optical density to simulate the fanout energy loss. The two beams intersect inside a barium titanate crystal with an interaction length of ~ 5 mm. The pump beam with an intensity of 0.1 W/cm² enters the crystal at near normal incidence. The probe beam with an intensity of 0.5 W/cm² is incident at an angle of 40°. The crystal is oriented so that the probe beam is amplified at the expense of the pump beam. After passing through the crystal, the pump beam is virtually depleted, whereas the intensity of the probe beam is elevated to 1.9 W/cm². The same experiment is repeated using neutral density with transmittance of 0.1 and 0.2. These correspond to probe beam intensities of

0.05 and 0.005 W/cm², respectively. The intensity of the amplified probe beam remains at 1.9 W/cm². This translates to an energy efficiency of $\sim 20\%$. In other words, if the fanout loss is 99% (e.g., a 100×100 crossbar), the energy efficiency of our new scheme can be at least 20 times better than that of the direct approach. Notice that our crystal is not antireflection coated, and $\sim 18\%$ of energy is lost at the front surface. Bulk absorption in this particular crystal accounts for $\sim 60\%$ of the energy loss.

Even though the reconfiguration time is limited by the photorefractive response time, which is typically of the order of milliseconds at modest intensities, the photorefractive interconnection system can accept very high data rate signals. To demonstrate this fact, temporal modulation was impressed on a laser beam (argon, $\lambda = 514.5$ nm) using an acousto-optic device to simulate a signal, which is to be inter-connected with some output. The signal used was a pulse train of frequency $f_s = 0.833$ MHz with each pulse being ~ 0.2 μs wide. This rate is clearly much higher than the reciprocal of the photorefractive response time. The modulated laser beam was then split into two beams and mixed in the crystal as described before, and the amplified probe beam was monitored with a photodetector. The upper oscilloscope trace in Fig. 3 shows the input probe signal, and the lower one shows the amplified probe signal. The results show a steady-state response in which the temporally modulated pump and probe beams interact simply by diffracting off the stationary index grating that is created in the crystal after the photorefractive response time. As this experiment was performed merely to demonstrate the high signal bandwidth of the system, optimization of the parameters was not done, and the results in Fig. 3 can clearly be improved.

Summarizing, we have described a new method of reconfigurable optical interconnection using dynamic holograms in photorefractive crystals. Such a new method provides a very high energy efficiency. The interconnection can be reconfigured by using a different SLM pattern. The hologram formation time will limit the reconfiguration time. Once the hologram which contains the interconnection pattern is formed inside the photorefractive crystal, such a scheme is capable of providing the interconnection for high data rate transmission. In such an interconnection, the output of each laser can be input to any one or all the detectors. Optical phase conjugation can also be used in conjunction with the two-wave mixing to correct for any phase aberration that may be caused by the crystal imperfections.

The authors acknowledge helpful discussions with their colleagues Monte Khoshnevisan and Derek Cheung. This research is supported in part by DARPA AFOSR under contract F49620-87-C-0015.

References

1. See, for example, J. W. Goodman, F. J. Leonberger, S.-Y. Kung, and R. A. Athale, "Optical Interconnections for VLSI Systems," *Proc. IEEE* **72**, 850 (1984).
2. See, for example, J. A. Neff, Ed., *Optical Computing*, *Proc. Soc. Photo-Opt. Instrum. Eng.* **625**, 109 (1986).
3. A. A. Sawchuk and B. K. Jenkins, "Dynamic Optical Interconnections for Parallel Processors," *Proc. Soc. Photo-Opt. Instrum. Eng.* **625**, 143 (1986).
4. V. I. Vinetski, N. V. Kukhtarov, S. G. Odulov, and M. S. Soskin, "Dynamic Self-Diffraction of Coherent Light Beams," *Sov. Phys. Usp.* **22**, 742 (1979).

5. N. V. Kukhtarev, V. B. Markov, S. G. Odulov, M. S. Soskin, and V. L. Vinetskii, "Holographic Storage in Electro-Optic Crystals. Beam Coupling and Light Amplification," *Ferroelectrics* **22**, 949 (1979).
6. See, for example, P. Yeh, "Fundamental Limit of the Speed of Photorefractive Effect," *Appl. Opt.* **26**, 602 (1987).
7. J. P. Huignard and A. Marrakchi, "Coherent Signal Beam Amplification in Two-Wave Mixing Experiments with Photorefractive B.S.O. Crystals," *Opt. Commun.* **38**, 249 (1981).
8. A. E. T. Chiou and P. Yeh, "Laser-Beam Cleanup Using Photorefractive Two-Wave Mixing and Optical Phase Conjugation," *Opt. Lett.* **11**, 461 (1986).



Rockwell International
Science Center

SC5502.FR

APPENDIX 5.6

Photorefractive Nonlinear Optics and Optical Computing

Photorefractive nonlinear optics and optical computing

Pochi Yeh

Arthur E. Chiou, MEMBER SPIE

John Hong

Paul Beckwith

Tallis Chang

Monte Khoshnevisan, MEMBER SPIE

Rockwell International Science Center

Thousand Oaks, California 91360

Abstract. This paper describes various nonlinear optical phenomena in photorefractive media and selected applications in optical computing. These phenomena include optical phase conjugation, two- and four-wave mixing, and real-time holography. The applications include image amplification and subtraction, logic and matrix operations, and optical interconnection.

Subject terms: optical computing; optical interconnections; optical image processing; nonlinear optics.

Optical Engineering 28(4), 328-343 (April 1989)

CONTENTS

1. Introduction
2. Photorefractive materials
3. Nonlinear optical phenomena
 - 3.1. Two-wave mixing
 - 3.2. Phase conjugation and real-time holography
 - 3.3. Phase-conjugate interferometry
4. Optical computing applications
 - 4.1. Image amplification
 - 4.2. Image subtraction and "exclusive OR" logic operation using phase-conjugate interferometry
 - 4.3. Matrix operations
 - 4.3.1. Optical matrix-vector multiplication using photorefractive four-wave mixing
 - 4.3.2. Matrix-matrix multiplication by means of color multiplexing
 - 4.3.3. Matrix-matrix multiplication using spatial convolution
 - 4.3.4. Optical matrix-vector multiplication using a spatial light modulator and a phase conjugator
 - 4.4. Optical interconnection
5. Conclusion
6. Acknowledgment
7. References

1. INTRODUCTION

The field of optics, specifically nonlinear optics, is emerging as an area of increasing importance for applications in optical computing because of its inherent parallelism and its extreme bandwidth of communication.¹ In addition, the nonlinear optical (NLO) response of materials allows for the possibility of manipulating

the propagation of an optical beam by another beam of light inside a nonlinear medium. These manipulations include changes of phase, polarization, intensity, direction of propagation, and even the frequency of light itself.²⁻³ In the area of optical computing, these NLO manipulations offer unique capabilities in holographic interconnection, parallel image subtraction, phase conjugation, optical data storage, spatial light modulations, and bistable optical devices.

Some of the most useful NLO phenomena include optical phase conjugation,⁴ four-wave mixing,⁵ and two-wave mixing.⁶ Traditionally, these phenomena are observed in nonlinear media that exhibit a large third-order susceptibility. Typically, these phenomena require very high optical intensities for efficient operation. Using one of the most efficient NLO materials such as carbon disulfide, an optical intensity level on the order of 1 MW cm^{-2} is still needed. These intensity levels are too high for optical computing applications. Photorefractive materials such as BaTiO_3 , SBN , BSO , and BGO are by far the most efficient media for these NLO phenomena using relatively low intensity levels (e.g., 1 W cm^{-2}). In addition, these materials are acentric and exhibit nonreciprocal energy transfer in a degenerate two-beam coupling configuration. Such optical nonreciprocity is not available in a third-order nonlinearity.

In this paper, we review some of the most useful NLO phenomena in photorefractive media. We then discuss their applications in optical computing.

2. PHOTOREFRACTIVE MATERIALS

The photorefractive effect is a phenomenon in which the local index of refraction is changed by a spatial variation of the light intensity. Such an effect was first reported in 1966.⁷ The spatial index variation leads to distortion of the wavefront, and such an

Invited Paper. OC-111 received Oct. 3, 1988; revised manuscript received Jan. 12, 1989; accepted for publication Jan. 16, 1989.

© 1989 Society of Photo-Optical Instrumentation Engineers.

effect was first referred to as "optical damage." The photorefractive effect has since been observed in many electro-optic crystals including LiNbO₃, BaTiO₃, SBN, BSO, BGO, GaAs, InP, etc. It is generally believed that the photorefractive effect arises from optically generated charge carriers that migrate when the crystal is exposed to a spatially varying pattern of illumination with photons having sufficient energy. Migration of the charge carriers due to drift or diffusion produces a space-charge separation, which then gives rise to a strong space-charge field. Such a field induces a refractive index change via the Pockels effect. This simple picture of the photorefractive effect explains several interesting steady-state optical phenomena in these media.

Although there are several models for the photorefractive effect,⁸⁻¹² the Kukhtarev Vinetskii model is the most widely accepted one.^{8,9} In this model, the photorefractive materials are assumed to contain donor and acceptor traps that arise from imperfections in the crystal. These traps create intermediate electronic energy states in the bandgap of the insulators. When photons with sufficient energy are present, electronic transitions due to photoexcitation take place. As a result of the transitions, charge carriers are excited into the conduction band and the ionized donors become empty trap sites. The rate of carrier generation is $(sI + \beta)(N_D - N_D^+)$, whereas the rate of trap capture is $\gamma_R N N_D^+$. Here, s is the cross section of photoionization, I is the light intensity, β is the rate of thermal generation, γ_R is the carrier-ionized trap recombination rate, and N and N_D^+ stand for the concentration of the carriers and ionized traps. N_D is the number density of the donor.

The space-charge field produced by the migration of the charge carriers is determined by the following set of equations^{8,9}:

$$\frac{\partial N}{\partial t} = \frac{\partial N_D^+}{\partial t} - \frac{1}{e} \nabla \cdot \mathbf{J} \quad (1)$$

$$\frac{\partial N_D^+}{\partial t} = (sI + \beta)(N_D - N_D^+) - \gamma_R N N_D^+ \quad (2)$$

$$\mathbf{J} = e\mu N \left(\mathbf{E} - \frac{kT}{e} \nabla \log N \right) + pI\hat{c} \quad (3)$$

$$\nabla \cdot (\epsilon \mathbf{E}^s) = e(N_A + N - N_D^+) \quad (4)$$

where \hat{c} is the unit vector along the c -axis of the crystal, N_A is the acceptor concentration, μ is the mobility, T is the absolute temperature, k is Boltzmann's constant, n is the index of refraction, ϵ is the dielectric tensor, pI is the photovoltaic current, e is the electronic charge, and p is the photovoltaic constant. \mathbf{E}^s stands for the space-charge field. \mathbf{E} is the total field, which includes \mathbf{E}^s and any external or internal fields (such as chemical or internal ferroelectric fields).

As a result of the presence of the space-charge field, a change in the index of refraction is induced by means of the linear electro-optic effect (Pockels effect):

$$\Delta \left(\frac{1}{n^2} \right) = r_{ijk} E_k \quad (5)$$

where r_{ijk} is the electro-optic coefficient (with $i, j, k = x, y, z$).

3. NONLINEAR OPTICAL PHENOMENA

All of the NLO phenomena mentioned earlier involve the formation of volume index gratings inside the photorefractive me-

dium. The simplest way to produce a volume index grating is to employ two-beam interference inside a nonlinear medium. This process takes advantage of the nonlinear response of the material to illumination by electromagnetic radiation. Thus, when two beams of coherent light intersect inside a photorefractive medium, they create a volume index grating. When the two beams propagate through the self-induced grating, they undergo Bragg scattering. One beam scatters into the other and vice versa in a process termed two-wave mixing. The hologram formed by the two-beam interference inside the photorefractive medium can also be erased by uniform light illumination. Thus, dynamic holography is possible by using photorefractive materials.

The Bragg scattering involved in two-wave mixing is very similar to the readout process in holography. In four-wave mixing, a third beam is used to read the hologram formed by the two-beam interference. The fourth beam is generated as a result of the Bragg scattering. To satisfy the Bragg condition, the third beam must be counterpropagating relative to one of the two beams that are involved in the formation of the index grating. In two-wave mixing, the Bragg condition is automatically satisfied. In what follows, we discuss some of the NLO phenomena in photorefractive media that are useful for optical computing applications.

3.1. Two-wave mixing

Two-wave mixing is important in practically all of the useful NLO phenomena observed in photorefractive media. The process of forming an index variation pattern inside a nonlinear medium using two-beam interference is very similar to that of hologram formation. Such an index variation is often periodic and is called a volume grating. In addition to the holographic process known traditionally, beam coupling occurs simultaneously. This is a unique property of photorefractive materials. In what follows, we briefly review the coupling and energy transfer of two beams inside a photorefractive medium.

Consider the interaction of two laser beams inside a photorefractive medium (Fig. 1). If the two beams are of the same frequency, a stationary interference pattern is formed. Let the electric field of the two waves be written

$$\mathbf{E} = A_j \exp[i(\omega t - \mathbf{k} \cdot \mathbf{r})] \quad j = 1, 2 \quad (6)$$

where A_1, A_2 are the wave amplitudes, ω is the angular frequency, and $\mathbf{k}_1, \mathbf{k}_2$ are the wave vectors. For simplicity, we assume that both beams are polarized perpendicular to the plane of incidence (i.e., s -polarized).

Within a scaling factor, the intensity can be written

$$I = |\mathbf{E}|^2 = |\mathbf{E}_1 + \mathbf{E}_2|^2 \quad (7)$$

Using Eq. (6) for the electric field, this can be written

$$I = A_1^2 + A_2^2 + A_1^* A_2 \exp(-i\mathbf{K} \cdot \mathbf{r}) + A_1 A_2^* \exp(i\mathbf{K} \cdot \mathbf{r}) \quad (8)$$

where

$$\mathbf{K} = \mathbf{k}_1 - \mathbf{k}_2 \quad (9)$$

and $\mathbf{K} = 2\pi/\Lambda$, where Λ is the period of the fringe pattern. The intensity [Eq. (8)] has a spatial variation inside the photo-

refractive medium. According to Kukhtarev's model, such an intensity pattern will generate and redistribute photocarriers, creating a space-charge field in the medium. This field induces a volume index grating due to the Pockels effect. In general, the index grating will have a spatial phase shift relative to the interference pattern.⁸ The index of refraction, including the fundamental component of the intensity-induced gratings, can be written

$$n = n_0 + \left[\frac{n_1}{2} \exp(i\phi) \frac{A_1^* A_2}{I_0} \exp(-i\mathbf{K} \cdot \mathbf{r}) + \text{c.c.} \right] \quad (10)$$

where

$$I_0 = I_1 + I_2 \equiv |A_1|^2 + |A_2|^2 \quad (11)$$

n_0 is the index of refraction when no light is present, ϕ is real, and n_1 is a real and positive number. For the sake of simplicity, we assume a scalar grating. The phase ϕ indicates the degree to which the index grating is shifted spatially relative to the intensity pattern. In photorefractive media that operate by diffusion only (i.e., no external static field), for example, BaTiO₃, the magnitude of ϕ is $\pi/2$ with its sign depending on the direction of the c -axis. \mathbf{K} is the grating wave vector given by Eq. (9). The parameter n_1 depends on the grating spacing and direction and on the material properties of the crystal, e.g., the electro-optic coefficient. Expressions for $n_1 \exp(i\phi)$ can be found in Refs. 9 through 11.

The spatial phase shift between the interference pattern and the induced volume index grating has been known for some time.^{8,13} The phase shift allows for nonreciprocal steady-state transfer of energy between the beams.^{9,14-16} To investigate the coupling, we substitute Eq. (10) for the index of refraction and $\mathbf{E} = \mathbf{E}_1 + \mathbf{E}_2$ for the electric field into the wave equation. This leads to a set of coupled equations.

The solutions for the intensities $I_1(z)$ and $I_2(z)$ are¹⁷

$$I_1(z) = I_1(0) \frac{1 + m^{-1}}{1 + m^{-1} \exp(\gamma z)} \exp(-\alpha z) \quad (12)$$

$$I_2(z) = I_2(0) \frac{1 + m}{1 + m \exp(-\gamma z)} \exp(-\alpha z) \quad (13)$$

where z is normal to the crystal surfaces and m is the input intensity ratio

$$m = \frac{I_1(0)}{I_2(0)} \quad (14)$$

In the absence of absorption ($\alpha = 0$), $I_2(z)$ is an increasing function of z and $I_1(z)$ is a decreasing function of z , provided γ is positive. The sign of γ depends on the direction of the c -axis. As the result of the coupling for $\gamma > 0$ in Fig. 1, beam 2 gains energy from beam 1. If this two-wave mixing gain is large enough to overcome the absorption loss, then beam 2 is amplified. Such an amplification is responsible for the fanning, stimulated scattering and oscillation of laser beams in photorefractive crystals.^{18,19}

We mentioned the holographic interpretation of two-wave mixing in photorefractive media earlier. Elaborating, we consider the formation of an index grating due to the presence of two coherent laser beams inside a photorefractive crystal. This

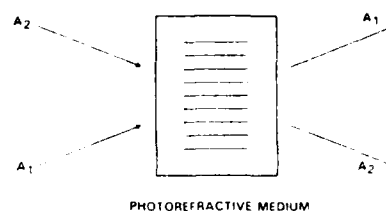


Fig. 1. Schematic diagram illustrating the basic idea of photorefractive two-wave mixing.

is formally analogous to the recording process in conventional holography. Consider Fig. 1, in which two laser beams intersect and form an induced index grating. The index grating [Eq. (10)] contains the product of the amplitudes A_1 and A_2 . This grating is a hologram formed by an "object" beam A_1 and a "reference" beam A_2 . The diffraction component of the transmission function of such a hologram [$t \approx \exp(-i\Delta n L/\lambda)$] is given approximately by

$$t \sim \Delta n \sim A_1^* A_2 \exp(-i\mathbf{K} \cdot \mathbf{r}) + A_1 A_2^* \exp(i\mathbf{K} \cdot \mathbf{r}) \quad (15)$$

where A_1 and A_2 denote the complex amplitudes of the object and reference fields, respectively. Equation (15) assumes that the modulation is weak, so the higher order terms can be neglected.

For reconstruction (see Fig. 1), the hologram is illuminated by the reference beam $A_2 \exp(-i\mathbf{k}_2 \cdot \mathbf{r})$. The diffracted beam can be written

$$\eta A_1 A_2^* A_2 \exp(-i\mathbf{k}_1 \cdot \mathbf{r}) \quad (16)$$

where η is the diffraction efficiency. Notice that the phase of A_2 cancels out and the diffracted beam is a reconstruction of the object beam $A_1 \exp(-i\mathbf{k}_1 \cdot \mathbf{r})$. Similarly, the reference beam A_2 can be reconstructed by illuminating the hologram with object beam A_1 , provided beam A_1 is a phase object (i.e., A_1 has only phase variation, with $|A_1|^2 = \text{constant}$).

In addition to holographic analogy, two-wave mixing exhibits amplification, which is a unique feature not available in conventional holography. Using these two properties, two-wave mixing can be used for beam processing. As a result of its real-time holographic nature, photorefractive two-wave mixing exhibits nonreciprocal energy transfer without any phase cross talk.¹⁹

The lack of phase cross talk can be understood in terms of the diffraction from the self-induced index grating in the photorefractive crystal. Normally, if a beam that contains phase information $\phi(\mathbf{r}, t)$ is diffracted from a fixed grating, the same phase information appears in the diffracted beam. For a self-induced index grating, the phase information $\phi(\mathbf{r}, t)$ is impressed onto the grating in such a way that diffraction will be accompanied by a phase shift $-\phi(\mathbf{r}, t)$. Such a dynamic hologram makes self-cancellation of phase information possible when the incident beam is diffracted from the grating produced by the incident and reference beams. This self-cancellation of phase information is actually equivalent to the reconstruction of the reference beam when the hologram is read out by the object beam.

Energy transfer without phase cross talk can be employed to compress both the spatial and temporal spectra of a light beam.²⁰

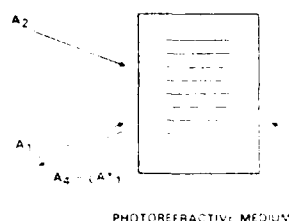


Fig. 2. Schematic diagram illustrating the basic idea of photorefractive four-wave mixing.

In other words, the energy transfer without phase cross talk can be utilized to clean up the wavefront of a laser beam. This has been demonstrated experimentally using a photorefractive SBN crystal^{19,20} to correct for the spatial-wavefront and temporal-wavefront aberrations.

3.2. Phase conjugation and real-time holography

Referring to Fig. 2, consider optical four-wave mixing in a photorefractive medium. Beams A_1 and A_2 incident from the left form a volume index grating inside the medium. If the third beam A_3 is exactly counterpropagating relative to A_2 , then a fourth beam is generated that propagates backward relative to A_1 and is a time-reversed replica of that beam. This is what happens in the readout process of conventional holography,²¹ except that in four-wave mixing the writing and readout processes occur simultaneously. For this reason, phase conjugation by means of optical four-wave mixing is often referred to as real-time holography.

If we consider the combination of the photorefractive medium and the two counterpropagating beams (A_2 and A_3) as an optical device, then such a device behaves like a retroreflective mirror. An incident beam will be phase conjugated and propagate backward, retracing its path. Such an optical device is called a phase-conjugate mirror (PCM). Reflection from a PCM exhibits many interesting properties, including wavefront aberration correction,²² polarization restoration,^{23,24} and amplification.⁵ The amplification is possible because energy can be coupled from the two counterpropagating beams.

A class of phase conjugators that have received considerable attention recently are the self-pumped phase conjugators.²⁴⁻²⁷ In these conjugators, there are no externally supplied counterpropagating pump beams. Thus, no critical alignment is required. The phase-conjugate reflectivity is relatively high at even low laser power. These devices are by far the most convenient PCMs available. Although several models have been developed for self-pumped phase conjugators,²⁷⁻³² the phenomena can be easily understood with the resonator model.³³⁻³⁵ In the two-interaction region model,²⁷ two separate four-wave mixings are responsible for the phase conjugation. In the 2-K grating model, self-pumped phase conjugation is considered as a process similar to stimulate Brillouin scattering (SBS). In the resonator model, the crystal cube is viewed as an optical cavity that supports a multitude of modes. These modes are trapped inside the crystal owing to total internal reflection at the surface.

When a laser beam enters the crystal, some of the modes may be excited as a result of the strong parametric gain due to two-wave mixing. In particular, ring oscillation can be generated according to a theory developed in Ref. 33. When the configuration of the resonance cavity relative to the incident laser beam

supports bidirectional oscillation, a phase-conjugate beam is generated by means of four-wave mixing.

According to this theory,³³ the frequency of oscillation inside the crystal can be slightly detuned from that of the pump beam. If ω is the frequency of the incident laser beam, the frequency of the internal oscillation can be written

$$\omega' = \omega + \delta, \quad (17)$$

where δ is the frequency detuning and is of the order of ± 1 Hz for BaTiO₃. This frequency detuning depends upon the path length of the ring oscillation inside the crystal. The bidirectional oscillation provides the counterpropagating pumping beams. By conservation of energy, the phase-conjugated beam has a frequency of $\omega + 2\delta$.

The resonator model presents a simple explanation of the frequency shift observed in BaTiO₃ self-pumped phase conjugators.^{28,36,37} Experimental evidence indicates that internal oscillations play a key role in the generation of phase-conjugate waves.³⁵

3.3. Phase-conjugate interferometry

A phase-conjugate interferometer is simply an interferometer that uses one or more PCMs. Several configurations of phase-conjugate interferometers have been investigated. These include a Mach-Zehnder interferometer incorporating a phase conjugator for self-referencing phase contouring based upon the interference between an incident wave and its phase-conjugate counterpart,^{38,39} a Michelson interferometer with one of the mirrors replaced by a phase conjugator,³⁹⁻⁴¹ and a Michelson interferometer with both mirrors replaced by one or two phase conjugators.⁴²⁻⁴⁹ Several optical computing applications, including coherent image subtraction,⁴⁴⁻⁴⁷ "exclusive OR" logic operation,⁴⁴⁻⁴⁷ and spatial differentiation,⁴⁷ have been demonstrated using the Michelson configuration with both mirrors replaced by a single self-pumped BaTiO₃ phase conjugator (see Sec. 3.2). A similar configuration for temporal differentiation (or novelty filtering) has also been conceived.⁴⁹ In this section, we briefly review the unique features of a phase-conjugate Michelson interferometer (PCM). Applications in optical computing are discussed in Sec. 4.2.

One of the most important and interesting phenomena associated with PCMs is *time reversal*. Referring to Fig. 3(a), consider a Michelson interferometer with PCMs. An incident laser beam (with intensity 1) is split by beamsplitter BS (assuming lossless) into two components, which are retroreflected back by the PCMs. According to Stokes' principle of time reversibility,⁵⁰ when the two phase-conjugate beams recombine at the beamsplitter, a time-reversed replica of the incident beam is generated. This beam propagates backward, retracing the original incident beam path. Thus, there is no light at the output port (port A); the total darkness is a result of time reversal. Such an optical time reversal has been observed experimentally using two coupled BaTiO₃ crystals for the PCMs.⁴³

Referring to Fig. 3(b), (ignoring transparencies $T_1(x,y)$ and $T_2(x,y)$, the effects of which will be discussed in Sec. 4.2), let t, r and t^*, r^* be the amplitude transmission and reflection coefficients of beamsplitter BS for beam entering from the right and left, respectively. The input beam with complex field amplitude E is split by the beamsplitter into a reflected component rE and a transmitted component tE . These two components are phase conjugated to give r^*E^* and t^*E^* and are further split and re-

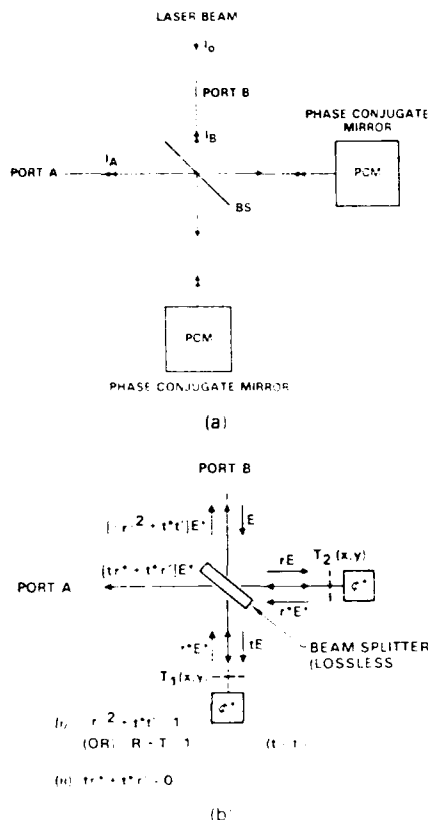


Fig. 3. (a) Time reversal for a Michelson interferometer equipped with PCMs. (b) Quantitative analysis of the time reversal of a PCMI.

combined with $r^*E^*r + t^*E^*t$ at port B and $r^*E^*t + t^*E^*r$ at port A. The principle of reversibility requires that

$$(r^2 + t^*t)E^* = E^* \quad (18)$$

$$(tr^* + t^*r)E^* = 0 \quad (19)$$

Thus, the amplitude coefficients satisfy the relations

$$r^2 + t^*t = 1 \quad (20)$$

$$tr^* + t^*r = 0 \quad (21)$$

Equation (21) establishes the condition for complete cancellation of the field at port A. These equations are known as Stokes' equations.⁵⁰

In practice, the cancellation at port A may not be complete because one cannot obtain an ideal phase conjugation. The measurement of time-reversal fidelity using a PCMI was reported recently by Ewhank and Vazquez.⁵¹ The phase instability arising from the use of two independent (not coupled) self-pumped phase conjugators is discussed in Ref. 43.

4. OPTICAL COMPUTING APPLICATIONS

The NLO phenomena, including two- and four-wave mixing, optical phase conjugation, and phase-conjugate interferometry, described in the previous section can be employed in a wide range of applications for optical computing and image processing. A few examples are given in this section to illustrate some of the merits and limitations of these NLO approaches.

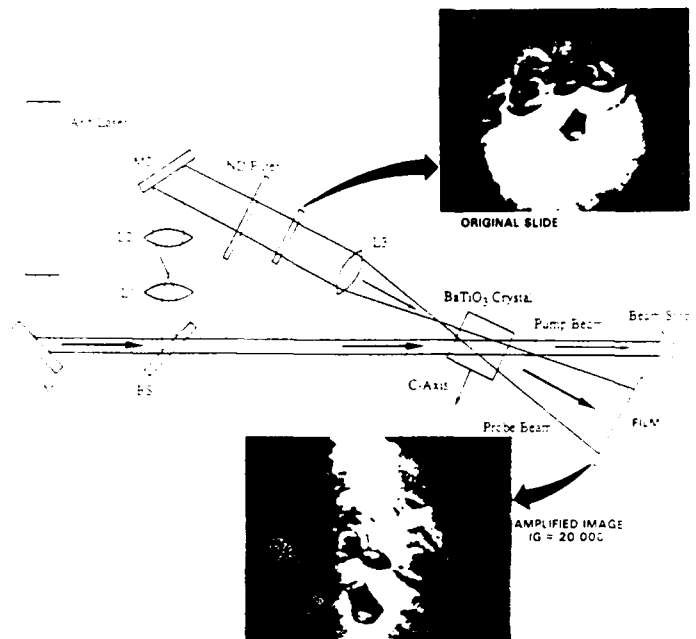


Fig. 4. Experimental configuration and results of image amplification using photorefractive two-wave mixing.

4.1. Image amplification

The energy transfer in photorefractive two-wave mixing discussed in Sec. 3.1 can be used for image amplification.⁵² Specifically, the interaction of a strong pump beam with a weak image-bearing beam inside a photorefractive medium results in an amplification of the image information. To preserve the contrast of a gray scale transparency, it is crucial that the amplification factor be uniform spatially and throughout the intensity dynamic range of the image-carrying beam. This issue has been analyzed by Fainman and Lee.⁵³ Their results indicate that a uniform intensity gain of more than 40 dB over an input dynamic range of four decades (i.e., 13 bits) is possible in photorefractive crystals such as BaTiO₃ and SBN with strong coupling ($\gamma L \sim 10$, where γ is the coupling coefficient and L is the interaction length).

The basic idea described above is illustrated in Fig. 4 along with the experimental results. Both the pump and the image-carrying beams were split off from the same laser output (514.5 nm). The signal beam was first attenuated to be about six orders of magnitude weaker than the pump and then sent through the transparency to carry the image information prior to mixing with the pump beam inside the crystal. An xyz-cut BaTiO₃ crystal was used as the nonlinear medium. The close resemblance between the amplified image (with a gain of approximately 20,000) and the original image indicates that the gain is sufficiently uniform over the dynamic range of a typical gray scale picture to preserve the contrast.

In photorefractive crystals such as BaTiO₃ and SBN, the phase shift between the interference fringes and the index grating, in the absence of an externally applied electric field, is approximately $\pi/2$ (see Sec. 3.1). As a result, the coupling constant and hence the signal gain are strongest when the optical frequencies of the pump and probe beams are identical [see, for example, Eq. (14) in Ref. 54]. The signal gain decreases drastically¹⁹ as the optical frequency difference between the

pump and probe beams exceeds the reciprocal of the photorefractive response time. Since the typical response time of a high gain photorefractive crystal (e.g., BaTiO₃ or SBN) is of the order of a fraction of a second at an intensity level of the order of 1 W/cm², the frequency difference of the two beams has to be less than 10 Hz. Practically, this requires that the two beams originate from the same laser. To overcome this limitation, there have been numerous investigations worldwide to search for alternative materials or processes with much faster time response.

Several other image processing applications employ photorefractive two-wave mixing. These include incoherent to coherent image conversion,⁵⁵ positive and negative image transfer,⁵⁶ dynamic range compression,^{57,58} NLO range imaging,⁵⁸ visualization of vibrational mode patterns,⁵² and novelty filters.⁵⁹ In Sec. 4.2 we describe a unique application in image subtraction using phase-conjugate interferometry.

4.2. Image subtraction and "exclusive OR" logic operation using phase-conjugate interferometry

The PCMI examined in Sec. 3.3 can be readily adapted to perform several mathematical operations over a (or a pair of) two-dimensional spatial pattern(s) of amplitude or phase modulation. These include parallel image subtraction and addition, negation and XOR logic operations, and spatial and temporal differentiations. We briefly review some of these applications in this section. The major advantages of the techniques using PCMIs over conventional approaches are dynamic stability and alignment insensitivity. Details are discussed in Ref. 60.

Optical image subtraction: Optical image subtraction⁶⁰⁻⁶² has been a subject of considerable interest because of its potential in many important applications. In this technique, one image is subtracted optically from another to detect the differences between them.

The PCMI described earlier can be used as a real-time image subtractor. Referring to Fig. 3(b), consider the insertion of a pair of transparencies [with intensity transmittance functions $T_1(x,y)$ and $T_2(x,y)$] in the beam path in each arm of the interferometer equidistant from beamsplitter BS. By an analysis similar to that in the previous section, it can be shown that when the two phase-conjugated beams recombine at the beamsplitter, the image intensity at output plane A is given by

$$I_A(x,y) = |E|^2 \rho^2 [r^* T_1(x,y) - r^* T_2(x,y)]^2, \quad (22)$$

where ρ is the reflection coefficient of the phase conjugators (assuming equal phase-conjugate reflectivity). Using Stokes equation [Eq. (21)], this becomes

$$I_A(x,y) = |E|^2 \rho^2 R [T_1(x,y) - T_2(x,y)]^2, \quad (23)$$

where $R \equiv |r|^2$ and $T \equiv |t|^2$ are the intensity reflectance and transmittance, respectively, for beamsplitter BS. Note that the output intensity is proportional to the square of the difference between the intensity transmittance functions.

Real-time parallel image subtraction using a PCMI that incorporates a self-pumped BaTiO₃ crystal as the PCM (at 514.5 nm) has been demonstrated.⁴⁴⁻⁴⁶ An example of the experimental results is given in Fig. 5. The horizontal and vertical bars are the images at output port A [see Fig. 3(b)] of transparencies 1 and 2, respectively, when the illuminating beam for the other arm is blocked. The right checkerboard pattern represents the coherent subtraction of the two images due to destructive inter-

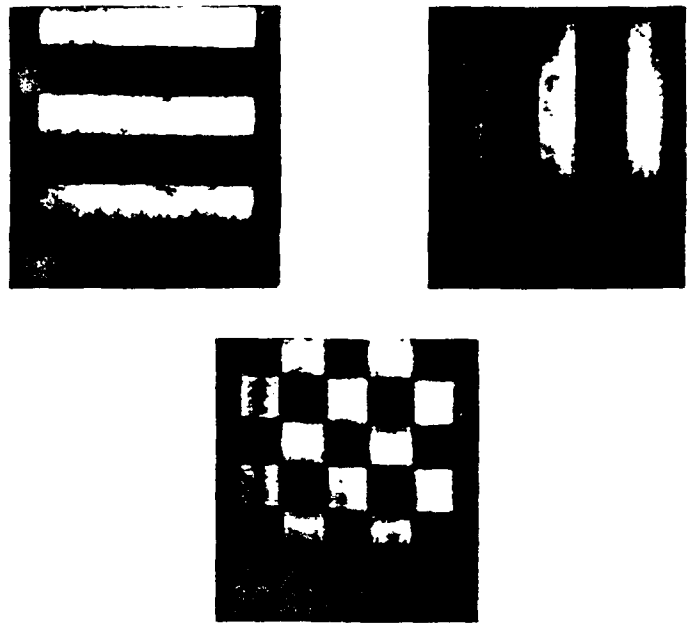


Fig. 5. Experimental results for image subtraction using a PCMI. The horizontal and vertical bars are the images of transparencies 1 and 2, respectively, when the illuminating beam for the other arm is blocked. The checkerboard pattern is the intensity distribution of the coherent subtraction of the two images.

ference when both illuminating beams are present. Note that the intensity distribution where subtraction takes place is fairly uniform and is very close to that of the true dark background (i.e., dark squares where the dark regions of the bars overlap).

"Exclusive OR" logic operation: The image subtractor can also perform logic operation. Consider the case in which both transparencies are either 1 or 0. According to Eq. (23), a complete cancellation would require that the two transparencies be identical. An output intensity of 1 will appear at port A when only one of the transparencies transmits. Thus, such an image subtractor can act as an XOR gate. When the transparencies are encoded with matrices of binary data, such an image subtractor acts as a two-dimensional array of XOR gates.

Intensity inversion: A special case of image subtraction is intensity inversion, which is obtained by removing one of the transparencies such that the transmittance becomes unity in one arm. Experimental results are shown in Fig. 6.

Amplitude image subtraction: The image subtraction methods described thus far result in subtraction of two intensity patterns due to double passes of light through each transparency. A new method that provides parallel and real-time amplitude subtraction of two images by using holographic interference in photorefractive media has recently been demonstrated.⁶³ This method uses a double Mach-Zehnder interferometer with a BaTiO₃ PCM and requires only a single pass of light through the transparencies.

Spatial differentiation: A PCMI with a pair of identical spatial patterns (one in each arm) can be used to perform spatial differentiation. Referring to Fig. 3(b), if one of the transparencies is displaced relative to the other along any direction x perpendicular to the optical axis by an amount Δx , Eq. (23) becomes

$$I_A(x,y) = |E|^2 \rho^2 R [T(x + \Delta x, y) - T(x, y)]^2. \quad (24)$$

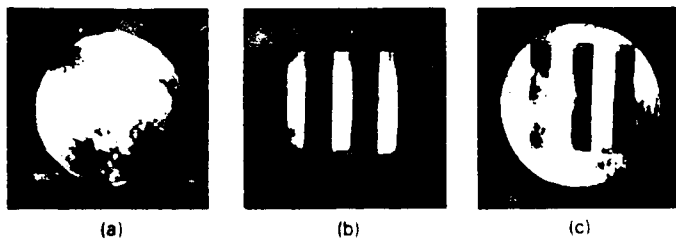


Fig. 6. Experimental results for the intensity inversion. (a) Intensity distribution of the phase-conjugate beam in the first arm with the transparency removed [$I_1 \propto T_1(x,y)^2 = 1$], (b) image of the transparency in the second arm [$I_2 \propto T_2(x,y)^2$], and (c) the intensity inversion of (b) [$I \propto T_1(x,y) - T_2(x,y)^2 = 1 - T_2(x,y)^2$].

where T_0 is the transparency intensity transmittance. This equation can be interpreted as the discrete version of spatial differentiation with respect to the x coordinate. Note that such an operation leads to edge enhancement. Using a slightly different experimental configuration, Kwong et al.⁴ demonstrated both first- and second-order spatial differentiation of a two-dimensional transmission pattern.

Temporal differentiation: An architecture that uses a two-dimensional spatial phase modulator in one arm of a PCMI for the temporal differentiation of a scene has been proposed⁴⁹ and demonstrated.⁶²

4.3. Matrix operations

In this section, we review the use of four-wave mixing in nonlinear media to perform matrix-vector and matrix-matrix multiplications. It was pointed out in Sec. 3.3 that four-wave mixing is an NLO process in which three input waves mix to yield a fourth wave. In phase-matched four-wave mixing, the three input waves consist of two counterpropagating pump waves E_1 and E_2 and an arbitrary probe wave E_3 . These three waves are coupled through the third-order susceptibility $\chi^{(3)}$ of the medium. A fourth wave E_4 is generated that can be written as³

$$E_4 \propto \chi^{(3)} E_1 E_2 E_3^* \quad (25)$$

This indicates that four-wave mixing can be used for the multiplication of signals. In addition, if we use the parallel nature of optical waves, each wave can carry spatial information for the purpose of image processing,⁶⁶ logic operations,^{44,66,67} numeric processing,⁶⁸ and matrix operations.^{66,67} In what follows, we describe some unique concepts that use the two transverse dimensions to carry matrix information for the purpose of matrix multiplication.

Matrix multiplication between two $N \times N$ matrices can be written as

$$C = AB \quad (26)$$

where

$$C = \sum_j A_j B_j \quad (27)$$

Note that matrix multiplication consists of two main operations: a parallel multiplication and a summation.

Referring to Fig. 7(a), consider a four-wave mixing configuration suitable for matrix multiplication. Beams 1 and 2 contain the information about the two matrices $A(x,z)$ and $B(z,y)$, re-

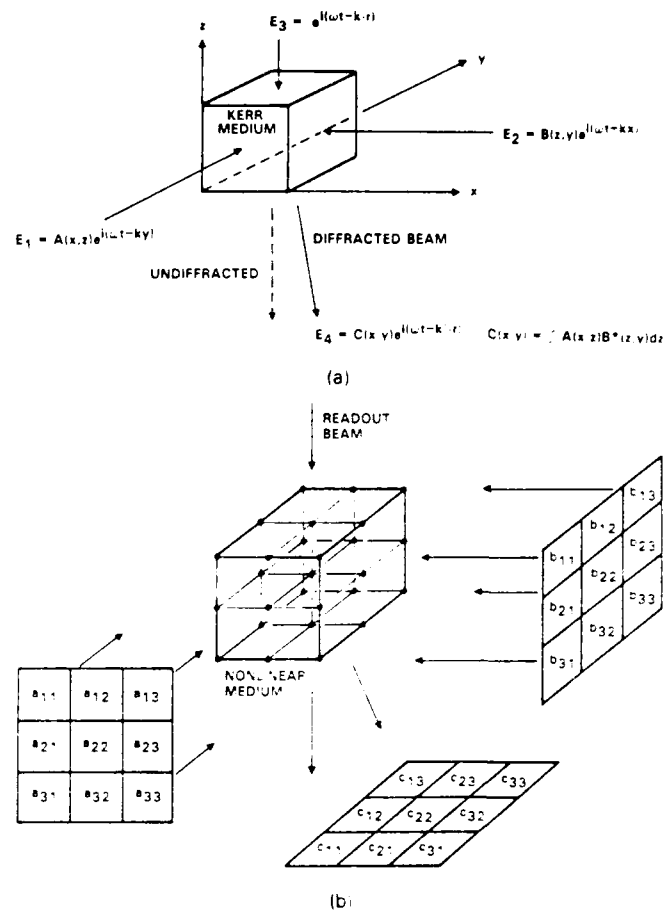


Fig. 7. Schematic diagram illustrating the basic idea of optical matrix-matrix multiplication using nonlinear four-wave mixing.

spectively. Beam 1 is chosen to propagate along the y -axis and beam 2 along the x -axis. The matrices can be either continuous or discrete. In the discrete case, each beam consists of a matrix of beamlets, as shown in Fig. 7(b).

In the nonlinear medium, the two matrix-carrying beams form an interference pattern, and a volume grating is formed. This grating contains information about the product of the matrix elements of the two matrices and can be written as

$$\Delta n = n_2 A(x,z) B^*(z,y) \exp(i\mathbf{K} \cdot \mathbf{r}) + \text{c.c.} \quad (28)$$

where \mathbf{K} is the difference of the wave vectors of the matrix-carrying beams. The parameter n_2 is the Kerr coefficient and is proportional to the third-order susceptibility $\chi^{(3)}$ of the medium. Note that the nonlinear response of the medium performs the function of parallel multiplication.

The volume grating is read out by a third beam, which can simply be a plane wave. The diffracted beam consists of the integrated contribution from each part of the grating along the beam path and can be written

$$C(x,y) \propto \int A(x,z) B^*(z,y) dz \quad (29)$$

where the integration is carried out along the beam path. Note that the integration completes the operation of matrix multiplication. The information about the product of these two matrices

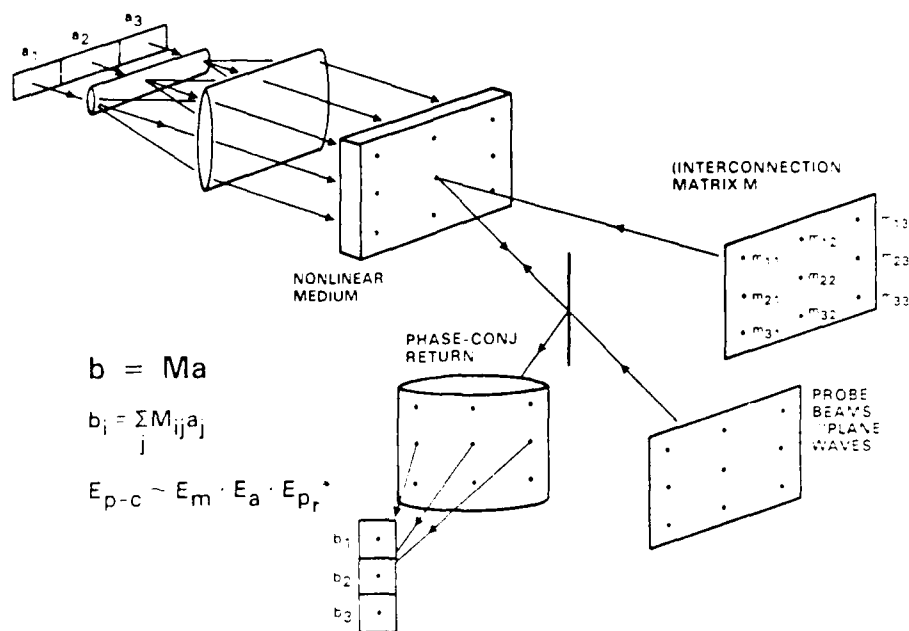


Fig. 8 Schematic diagram illustrating the basic idea of optical matrix-vector multiplication using nonlinear four-wave mixing.

is now impressed on the transverse spatial distribution of the diffracted beam. In practice, the dimensions of the matrices may be limited by cross talk between various channels due to diffraction and/or imperfection in the optics.

Owing to the phase-matching requirement, the readout beam must be incident along a direction that satisfies the Bragg diffraction condition to achieve high efficiency. In anisotropic nonlinear media, the polarization states, as well as the direction of propagation, can be chosen such that the largest of the nonlinear susceptibilities is fully utilized.

Four-wave mixing can be either degenerate or nondegenerate. In the degenerate case, all of the beams have the same frequency. In the nondegenerate case, the frequencies of the beams can be slightly different. This may be useful for the purpose of separating the diffracted beam from the undiffracted portion.

Another scheme, shown in Fig. 8, is suitable for matrix-vector multiplication. Here, as an example, consider a discrete case in which we need to carry out the multiplication of an N -element vector and an $N \times N$ matrix. The vector is fanned out into N rows of identical vectors. These $N \times N$ beamlets are directed to a nonlinear medium. The matrix, which also contains $N \times N$ beamlets, is also directed to the medium in such a way that each beam of the matrix is counterpropagating relative to the corresponding beam of the vector. Thus, in the medium there are $N \times N$ spatially separated regions, pumped by a pair of counterpropagating beams. Now, $N \times N$ probe beams are directed into the medium in such a way that each probe beam can propagate through an intersection region. The probe beams will be "plane wave" beamlets propagating in parallel. As a result of the four-wave mixing, each probe beam generates a phase-conjugated beam that, within a proportionality factor, can be written

Multiplication. By using a cylindrical lens, we obtain a summation over j . Thus, we have

$$b_i = \sum_j M_{ij} a_j \quad (30)$$

where $a(j)$ is the j th element of the vector a and $M(i,j)$ is the matrix element. Such a scheme for matrix-vector multiplication can also be used for matrix-matrix multiplication by decomposing a matrix into column vectors and then multiplying the matrix with each of the column vectors.

As a result of the nature of the four-wave mixing process in the medium, this matrix-vector multiplier operates on the field amplitudes and thus can be used to handle matrices and vectors with complex elements. It is a coherent device rather than an incoherent one. This aspect is distinctly different from most of the earlier approaches, which are all incoherent. When the device is operated in the coherent mode, the phase of each beamlet must be maintained uniformly over the transverse dimension of the beamlet. In addition, such phases must also be maintained fixed in the summation process. If these phases are not uniform over the beamlets, the final step becomes an incoherent summation as a result of the spatial averaging. Under such circumstances, this matrix-vector multiplier operates on the intensities and thus handles only positive numbers.

We now describe a few specific examples of optical matrix-vector multiplication and optical matrix-matrix multiplication using various architectures based on four-wave mixing and phase conjugation. Other approaches to optical matrix processors are discussed in several review articles.

4.3.1. Optical matrix-vector multiplication using photorefractive four-wave mixing

In the first experimental demonstration of optical matrix-vector multiplication using four-wave mixing,⁶⁰ phase conjugation in a photorefractive BaTiO₃ crystal was used to perform pixel-by-pixel multiplication. The summation required to obtain matrix-vector products was performed subsequently by a cylindrical lens external to the crystal.

A schematic diagram of the experimental configuration and the result is shown in Fig. 9. Mask M imprints the matrix

$$\mathbf{M} = \begin{bmatrix} 1 & 1 & 1 & 0 & 1 \\ 1 & 1 & 0 & 0 & 1 \\ 0 & 1 & 0 & 0 & 0 \\ 0 & 1 & 1 & 0 & 0 \\ 1 & 1 & 1 & 1 & 1 \end{bmatrix} \quad (31)$$

and mask M_2 imprints the vector (repeated on the mask instead of using a cylindrical lens to fan out the vector)

$$\mathbf{v} = \begin{bmatrix} 1 \\ 0 \\ 1 \\ 1 \\ 1 \end{bmatrix} \quad (32)$$

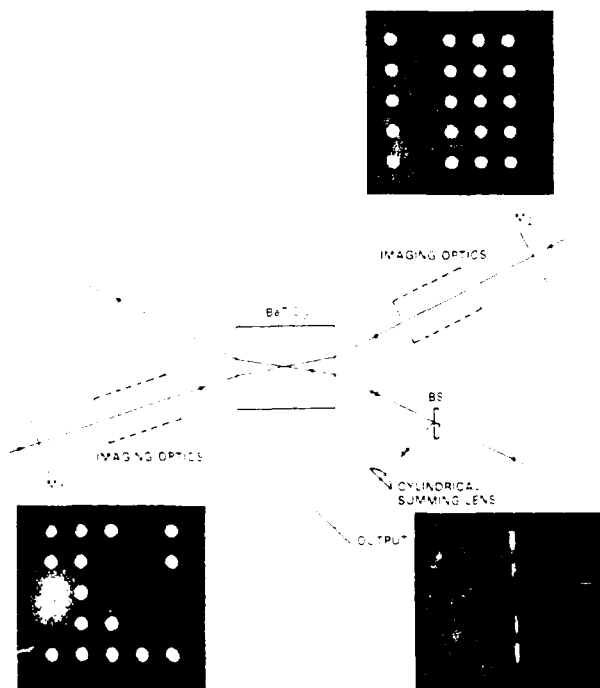


Fig. 9. Experimental configuration and the result of optical matrix-vector multiplication using photorefractive four-wave mixing.

into the two counterpropagating pumping beams. A collimated uniform beam is used as the probe. The phase-conjugate output at the focal plane of the summing cylindrical lens is shown in the lower right. The intensity of the output spatial pattern is proportional to the product vector \mathbf{v}' , given by

$$\mathbf{v}' = \mathbf{M}\mathbf{v} = \begin{bmatrix} 1 & 1 & 1 & 0 & 1 \\ 1 & 1 & 0 & 0 & 1 \\ 0 & 1 & 0 & 0 & 0 \\ 0 & 1 & 1 & 0 & 0 \\ 1 & 1 & 1 & 1 & 1 \end{bmatrix} \begin{bmatrix} 1 \\ 0 \\ 1 \\ 1 \\ 1 \end{bmatrix} = \begin{bmatrix} 3 \\ 2 \\ 0 \\ 1 \\ 4 \end{bmatrix} \quad (33)$$

With a slight modification of the experimental geometry, it has been successfully demonstrated⁷⁰ that both the pixel-by-pixel product and the summation can be done inside the nonlinear medium to achieve the desired matrix-vector product without use of an external cylindrical lens.

The experimental geometry is illustrated schematically in Fig. 10. The readout vector, which consists of a vertical column of beamlets of equal intensity, enters the crystal at an oblique angle such that each beamlet traverses all of the counterpropagating pumping beamlets in the same horizontal plane inside the crystal. Since the proper elements of the matrix and vector are encoded in the two counterpropagating beams via the appropriate masks, the phase-conjugate output of each beamlet consists of the sum of the product resulting from each individual encounter.

An experimental result for multiplication of a 4×4 binary matrix and a 4×1 binary vector is shown in Fig. 11. The magnified images of the masks used to encode the matrix, vector, and probe are shown in Figs. 11(a) through 11(c), respectively. The image representing the final matrix-vector product is shown in Fig. 11(d).

4.3.2. Matrix-matrix multiplication by means of color multiplexing

It has been experimentally demonstrated that matrix-vector multiplication using photorefractive four-wave mixing can be extended to matrix-matrix multiplication by color multiplexing.⁷¹ The basic idea is to decompose the problem into matrix-vector multiplications and carry out all of these multiplications simultaneously in parallel by using color multiplexing. This idea of encoding the component vectors with different colors is illustrated in Fig. 12 for the case of 4×4 matrices. Each row vector

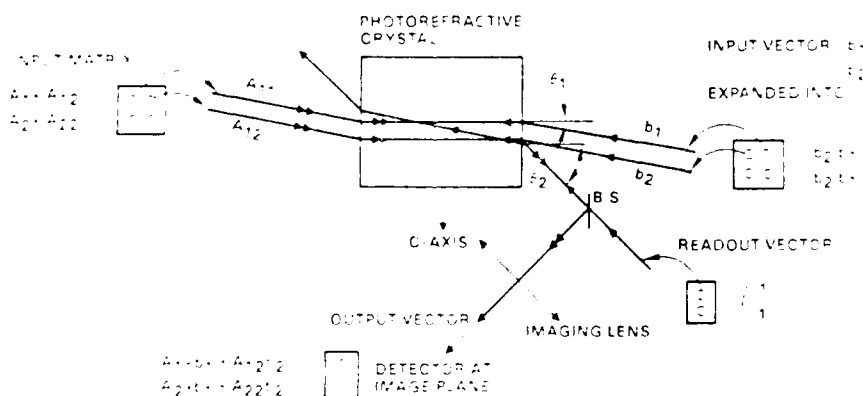


Fig. 10. Modified configuration for optical matrix-vector multiplication using photorefractive four-wave mixing. In this approach, both the multiplication and summation are carried out inside the nonlinear crystal.

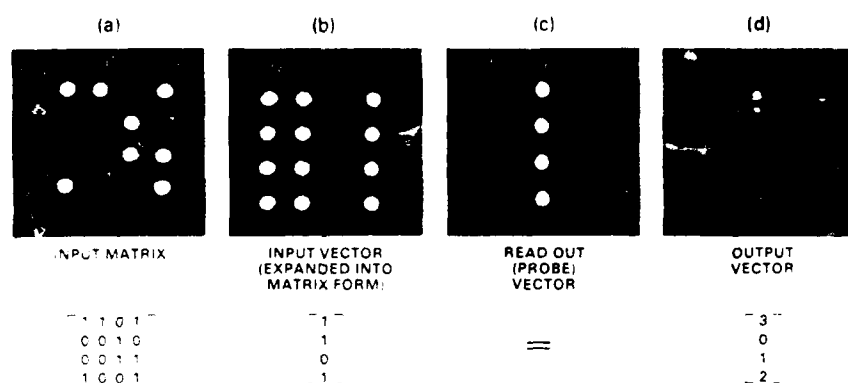


Fig. 11. Experimental results of optical matrix-vector multiplication using the approach illustrated in Fig. 10.



Fig. 12. Schematic diagram illustrating the basic idea of optical matrix-matrix multiplication using color multiplexing.

of the matrix M_1 is illuminated by one color, and all of the color components are then combined by the prism (angular multiplexing) into a single row prior to further expansion by anamorphic optics (not shown) to match the mask representing the second matrix. After proper element-by-element multiplications and summation (summing optics omitted) into the column, the resulting multicolor output is demultiplexed into different color components that together represent the final product.

4.3.3. Matrix-matrix multiplication using spatial convolution

In addition to the above scheme, another method for matrix-matrix multiplication that uses spatial convolution by means of four-wave mixing has been successfully demonstrated.²² The key difference between this approach and those described above is that the nonlinear crystal is located at the common Fourier plane, rather than at the common image plane, of the input matrix masks. The encoding scheme is also different from those used in the earlier approaches. Matrix-matrix multiplication in full parallelism is achieved by space-multiplexing by means of spatial convolution using degenerate four-wave mixing.

White and Yariv²² have demonstrated that (spatial) convolution and correlation of two (two-dimensional) patterns can be achieved in real time by four-wave mixing in the common Fourier plane of the input patterns and recording the phase-conjugated output at the corresponding object plane. A typical experimental configuration is shown schematically in Fig. 13. If U_3 is a small aperture simulating a point source (delta function), a pattern representing the convolution of U_1 and U_2 ($U_1 * U_2$) is observed in the output plane. The design of U_1 and U_2 to represent two matrices so that their product is represented by $U_1 * U_2$ is now explained.

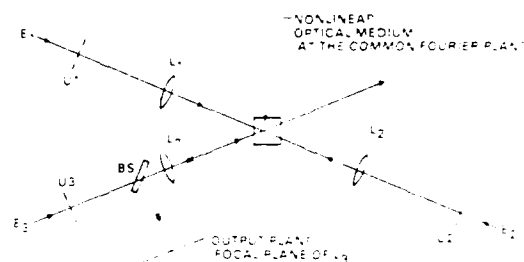


Fig. 13. Schematic diagram illustrating the basic idea of four-wave mixing in a nonlinear medium located at the common Fourier plane of the input spatial pattern.

For simplicity, consider the simplest case of two matrices A and B with dimensions 2×2 and the product $C = AB$ given below:

$$A = \begin{bmatrix} a_{11} & a_{12} \\ a_{21} & a_{22} \end{bmatrix} \quad (34)$$

$$B = \begin{bmatrix} b_{11} & b_{12} \\ b_{21} & b_{22} \end{bmatrix} \quad (35)$$

$$C = AB = \begin{bmatrix} c_{11} & c_{12} \\ c_{21} & c_{22} \end{bmatrix} \quad (36)$$

$$= \begin{bmatrix} a_{11}b_{11} + a_{12}b_{21} & a_{11}b_{12} + a_{12}b_{22} \\ a_{21}b_{11} + a_{22}b_{21} & a_{21}b_{12} + a_{22}b_{22} \end{bmatrix}$$

Transparency U_1 consists of four small apertures, each with an intensity transmittance proportional to each matrix element a_i [see Fig. 14(a)]. A similar transparency U_2 corresponding to the transpose of B (i.e., rows and columns interchanged) is shown in Fig. 14(b). Note that the vertical separation in U_1 is considerably larger than that in U_2 , while the horizontal element separations are identical in U_1 and U_2 . The two-dimensional spatial convolution of U_1 and U_2 is shown in Fig. 14(c). It consists of a total of 16 spots with the intensity of each proportional to the cross product of all of the elements in A and B . The four doublets lying along the y -axis in Fig. 14(c) are drawn slightly offset from the axis to expose the individual component

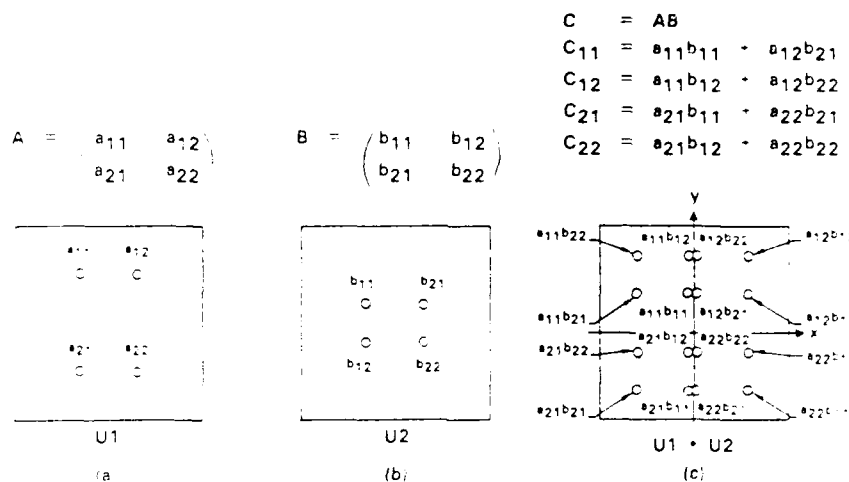


Fig. 14. Schematic diagram illustrating optical matrix-matrix multiplication by convolution for 2×2 matrices. (a) Matrix A and mask U1 to encode A, (b) matrix B and mask U2 to encode B^T , and (c) spatial pattern resulting from convolution of U1 and U2

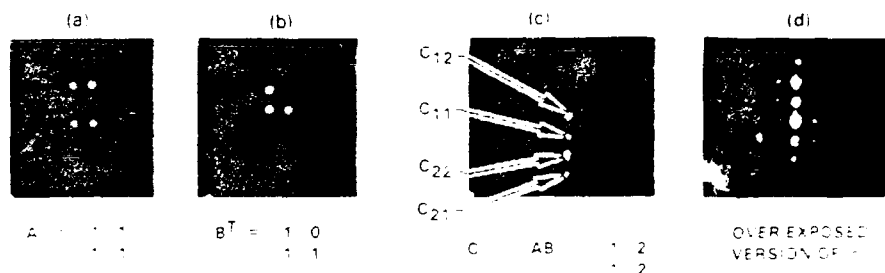


Fig. 15 Experimental results for optical matrix-matrix multiplication by convolution by means of four-wave mixing in the spatial frequency domain. (a) and (b) are the matrix masks used for encoding the matrices A and B^T , (c) shows the result of their spatial convolution, and (d) is an overexposed version of (c) to reveal the cross terms that do not contribute to the matrix product.

In practice, these two components spatially overlap on the y -axis. The intensities of the four doublets, from top to bottom on the y -axis, are proportional to c_{11} , c_{12} , c_{22} , and c_{21} , respectively. The eight cross terms that do not contribute to matrix-matrix multiplication can be filtered out easily, since they are physically separated from the y -axis.

Using an argon ion laser at 514.5 nm and a BaTiO₃ crystal, the concept described above has been demonstrated for 2 × 2 matrices (see Fig. 15). The images of the masks used to encode **A** and **B** are shown in Figs. 15(a) and 15(b). The result representing the product is shown in Fig. 15(c). An overexposed version of Fig. 15(c) is shown in Fig. 15(d) to reveal the noise resulting from the cross-term, that do not contribute to the matrix product.

4.3.4 Optical matrix-vector multiplication using a spatial light modulator and a phase conjugator

In the matrix-vector multiplication as is described above, similar row and column pairs of the matrix and vector are taken into consideration for the calculation of each M_{ij} . As a result, the time complexity of the algorithm is $O(N^2)$. For a given size matrix, the time complexity of the algorithm in the distributed system is $O(N^2)$ as well. In the distributed system, the time complexity of the algorithm is $O(N^2)$ as well. In the distributed system, the time complexity of the algorithm is $O(N^2)$ as well.

Another scheme for optical matrix-vector (and matrix-matrix) multiplications that uses a phase conjugator (with a finite storage time) in conjunction with a spatial light modulator (SLM) to eliminate the pixel-by-pixel alignment requirement at the cost of some reduction in parallelism ($N^2/2$ instead of N^2) has been reported.⁷⁶ Phase aberration due to imperfection in the optics is self-corrected by the phase-conjugation process. The optical system involved is relatively simple compared with the other approaches. Figure 16 is a schematic diagram illustrating the basic concept. An SLM is used to impress the matrix and vector information in sequence on an input laser beam. This beam is directed toward a self-pumped PCM, which has a finite time response (e.g., BaTiO₃). A cylindrical lens is used in the phase-conjugate output beam path to perform the summation.

The principle of operation is as follows. The SLM first impresses the matrix information onto the input laser beam. This beam is then incident into a self-pumped PCM, which stores the matrix information after a finite grating formation time. When the matrix information is removed from the SLM and all of the pixels are turned into maximum transmission condition, the phase-conjugate beam that contains the reconstruction of the matrix information exists for a finite duration, which depends on the strength of the input read beam. During this time, if the next frame of the SLM carries the vector information, parallel multiplication is performed as the phase-conjugate beam propagates back through the SLM. Here, the vector is represented as a two-dimensional matrix of N subpixels, each of which is \sqrt{N} pixels. N is the

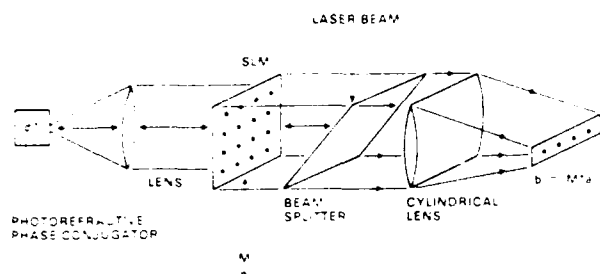


Fig. 16. Schematic diagram illustrating the concept of optical matrix-vector multiplication using a photorefractive phase conjugator in conjunction with an SLM.

dimension of the vector. A cylindrical lens in the output port performs the summation. The dark storage time during which the matrix information can be retrieved is determined by the photorefractive material and the pumping configuration. It ranges from seconds to microseconds. In this architecture, the same input beam is used for alternately writing and reading the hologram.

This system can also perform matrix-matrix multiplication by time multiplexing. In this case, each column vector V_i ($i = 1$ to N) constituting the second matrix M_2 is sequentially impressed onto the beam to multiply with the first matrix M_1 according to the matrix-vector multiplication scheme described above. To avoid degradation of the information of M_1 stored in the photorefractive hologram during the readout, it is necessary to refresh the holographic memory with M_1 to restore its diffraction efficiency. This can be done by reimpressing M_1 onto the beam after each readout cycle. Consequently, a total of $2N$ clock cycles, consisting of N cycles of write and N cycles of read, will be required to carry out the multiplication of two $N \times N$ matrices.

4.4. Optical interconnection

Optical interconnection linking laser arrays and detector arrays plays a key role in optical computing.^{1,2,3,4} Conceptually, such an interconnection can be achieved by using optical matrix-vector multiplication,

$$v = Mx \quad (37)$$

where x is the input vector representing the signals carried by an array of N lasers and v is the output vector representing the signals received by the array of N detectors. M is an $N \times N$ binary matrix representing the interconnection pattern.

When an SLM is used as the matrix mask, the interconnection is reconfigurable. Suppose the interconnection mask consists of an $N \times N$ array of transmission windows. The input vector (a row of N elements) is fanned out using astigmatic optics so that the light from each element is broadcast over a corresponding column of windows. After transmission through the interconnection mask, similar optics are used to collect the light from each row of the windows and to sum the output into a column vector of N elements. Such an architecture provides the necessary N^2 parallelism. However, a large fraction of energy is absorbed by the transparency of SLM. When used as a crossbar switch, such an architecture has an energy efficiency of only $1/N$, where N is the dimension of the array.^{5,6} This occurs because $(N-1)/N$ of the light energy from each element of the input

vector does not pass through the crossbar mask. The energy loss increases as the dimension of the array increases and is referred to as the "fan-out energy loss." For a 1000×1000 crossbar switch, the loss due to fan-out can be as high as 99.9%. This is not acceptable in high speed computing because signals are passing through the SLM at gigabit rates and the energy loss can be enormous. In addition to the inherent fan-out energy loss, all SLMs have finite insertion loss due to imperfect transmissions such as those that occur from absorption and scattering. Including such insertion losses, the energy efficiency for a crossbar switch would become t/N , where t is the transmittance ($t < 1$) of each of the windows.

Recently, a scheme has been developed^{80,81} to form a dynamic hologram inside a photorefractive crystal such that the hologram will be capable of performing reconfigurable optical interconnection. Such a scheme utilizes nonreciprocal energy transfer in two-wave mixing to achieve an extremely high energy efficiency.

Referring to Fig. 17, we describe this new method of reconfigurable optical interconnection. Figure 17(a) describes a one-dimensional case to explain the concept. A small fraction of the incident beam is split off using beamsplitter BS. The reflected beam (probe beam) is then expanded by using a cylindrical lens before entering the SLM. In this example, the input beam is to be connected to detectors b and d as prescribed by the SLM. The transmitted probe beam is then recombined with the main beam inside a photorefractive crystal. As a result of nonreciprocal energy coupling, almost all of the energy in the main beam is transferred to the probe beam, which carries the interconnection pattern. The result is an optical interconnection with a very high energy efficiency.

Figure 17(b) shows the reconfigurable interconnection for laser arrays and detector arrays. In this example (4×4 interconnection), laser 1 is to be connected with detectors b and c, laser 2 with detectors a and d, laser 3 with detectors c and d, and laser 4 with detectors a and c. In terms of matrix-vector multiplication, such an interconnection can be written as

$$v = \begin{bmatrix} 0 & 1 & 0 & 1 \\ 1 & 0 & 0 & 0 \\ 1 & 0 & 1 & 1 \\ 0 & 1 & 1 & 0 \end{bmatrix} \begin{bmatrix} v_1 \\ v_2 \\ v_3 \\ v_4 \end{bmatrix} = \begin{bmatrix} v_2 + v_4 \\ v_1 \\ v_1 + v_3 + v_4 \\ v_2 + v_3 \end{bmatrix} \quad (38)$$

where v_1 , v_2 , v_3 , and v_4 are signals carried by the laser elements of the array x .

A cylindrical lens is used to focus the two-dimensional array of beams into a vector. Thus, as a result, detector a receives signals from lasers 2 and 4, detector b receives signals from laser 1, detector c receives signals from lasers 1, 3, and 4, and detector d receives signals from lasers 2 and 3. This concept can be extended to interconnect N lasers with M detectors, where N and M are two large numbers.

The two-wave mixing described above may be viewed as a real-time holography in which the recording and readout occur simultaneously inside the photorefractive crystal. The beamsplitter and the SLM are used to generate the reference and object beams to record a volume hologram that represents the interconnection pattern as prescribed by the SLM. The energy coupling involved in two-wave mixing ensures that the diffraction efficiency during the readout is almost 100%. This requires a proper orientation of the crystal so that the energy of the readout beam is greatly depleted. The high energy efficiency results from

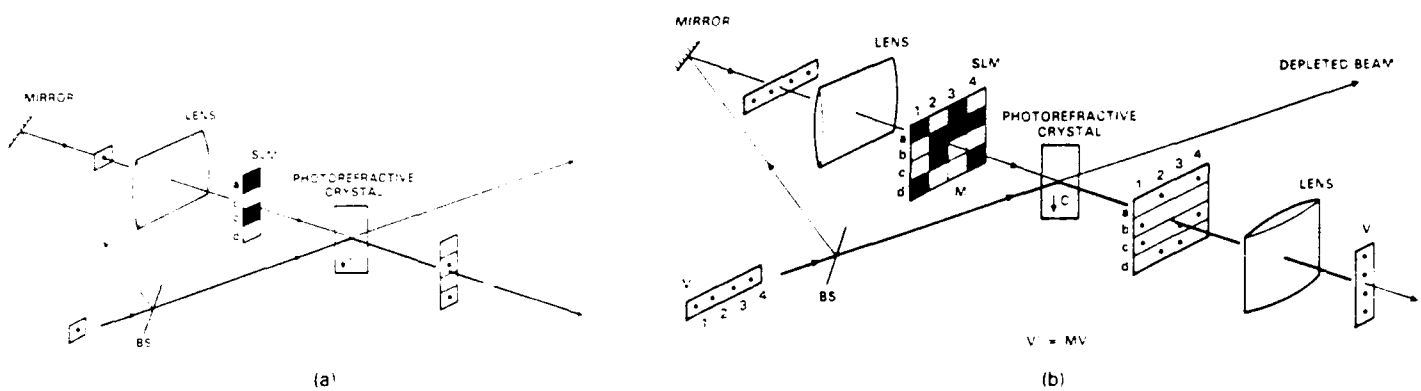


Fig. 17. Schematic drawings of optical interconnections using dynamic photorefractive holograms with $N = 4$. (a) $1 \times N$ optical interconnection and (b) $N \times N$ optical interconnection.

the fact that most of the energy is carried by the readout beam, which does not pass through the SLM but is diffracted into the interconnection pattern by the hologram.

The energy efficiency of such an interconnection pattern can be estimated for a crossbar switch as follows: Let R be the reflectance of the beamsplitter. It is legitimate to assume that the beamsplitter is practically lossless, and we may assume that the surface of the photorefractive crystal is antireflection-coated so that the Fresnel reflection loss can be neglected. Under these conditions, the two beams that arrive at the photorefractive crystal have energies $(1 - R)$ and R/N , respectively. Inside the crystal, these two beams undergo photorefractive coupling. As a result, most of the energy of the pump beam $(1 - R)$ is transferred to the probe beam R/N , which contains the interconnection pattern. The energy efficiency can be easily derived and is given by⁸

$$\eta = \frac{(1-R)}{N} \frac{1+m}{1+m \exp(-\gamma L)} \exp(-\alpha L) \quad (39)$$

where m is the beam intensity ratio,

$$m = \frac{(1-R)N}{R} \quad (40)$$

L is the interaction length, γ is the coupling constant, and α is the bulk absorption coefficient. For photorefractive crystals such as BaTiO_3 and SBN , the coupling constant is very large (i.e., $\gamma L \gg 1$). The efficiency can be written approximately as

$$\eta = \left[\frac{R}{N} + (1-R) \right] \exp(-\alpha L) \quad (41)$$

Notice that for large N , the energy efficiency is limited by the crystal bulk absorption $\exp(-\alpha L)$ and is maximized by using a beamsplitter with a very small reflectance R (i.e., $R \rightarrow 0$).

In examining the energy efficiency, we collimate an argon ion laser beam at 514.5 nm into 2 mm diameter by using a lens of focal length $f = 2$ m. A beamsplitter is used to redirect 5% of the energy through the SLM, establishing the probe beam. The remainder of the energy transmits through the beamsplitter and constitutes the pump beam. In our preliminary experiment, the SLM was replaced with a neutral density filter with a variable optical density to simulate the fan-out energy loss. The two beams of interest pass to a BaTiO_3 crystal with an interaction length

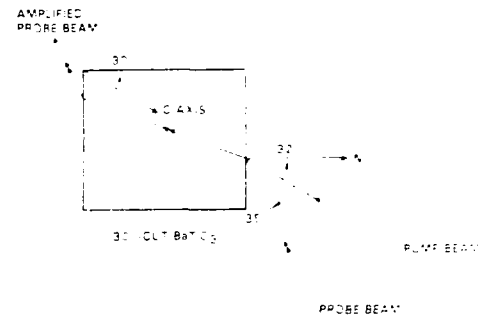


Fig. 18. Schematic diagram illustrating the relative orientation of the pump beam, probe beam, and c-axis of a 30°-cut BaTiO_3 crystal for the measurement of energy efficiency. The depleted (transmitted) pump beam is omitted for clarity.

of approximately 5 mm (see Fig. 18). The intensity of the pump beam is approximately 3.2 W/cm^2 , whereas the intensity of the probe beam varies from 0.16 W/cm^2 to 0.16 mW/cm^2 . The amplified output intensity is monitored and the result is shown in Fig. 19, where the energy efficiency (defined as the ratio of the amplified output intensity to the total input intensity) is plotted as a function of $1/N$ (where N is the number of fan-out channels). The solid line represents the theoretical fit using Eq. (39) with αL and γL as the fitting parameters. The results ($\alpha L = 9.2$ and $\gamma L = 1.1$) agree with those obtained from other independent measurements to within 10%. Note that the energy efficiency is better than 24% for $N = 1$ through 100. In other words, if the fan-out loss is 99% (e.g., a 100×100 crossbar), the energy efficiency of this new scheme can be 24 times better than that of the direct approach. Bulk absorption in this particular crystal accounts for approximately 65% of the energy loss.

Even though the reconfiguration time is limited by the photorefractive response time, which is typically on the order of milliseconds at modest intensities, the photorefractive interconnection system can accept very high data rate signals. To demonstrate this fact, we frequency modulate a laser beam (argon, $\lambda = 514.5 \text{ nm}$) using an acousto-optic device to simulate a signal that is to be interconnected with some output. The signal used had a pulse train of frequency $f_m = 0.833 \text{ MHz}$ with each pulse being approximately $0.2 \mu\text{s}$ wide. This rate is clearly much higher than the reciprocal of the photorefractive response time. The modulated laser beam was then split into two beams and mixed in the crystal as described before, and the amplified probe beam was monitored with a photodetector. The oscilloscope

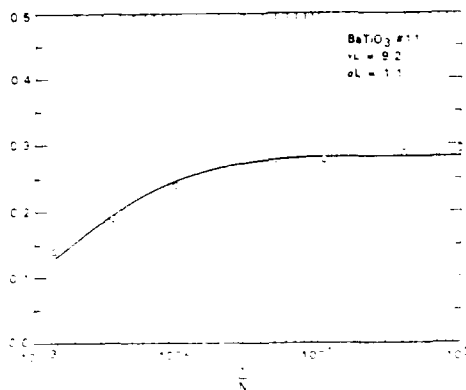


Fig. 19. The energy efficiency as a function of $1/N$, where N is the equivalent number of fan-out channels. Open circles represent the experimental results, and the solid line is a theoretical fit [using Eq. (39)] with α_L and γ_L as the fitting parameters.

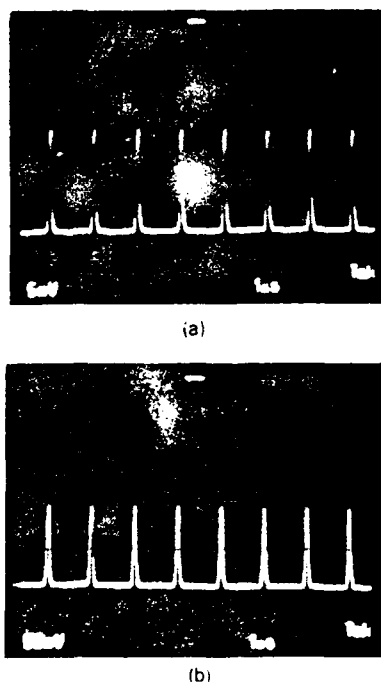


Fig. 20. (a) Signal carried by the probe beam and (b) amplified signal carried by the probe beam after undergoing two-wave mixing.

trace in Fig. 20(a) shows the input probe signal, and the trace in Fig. 20(b) shows the amplified probe signal. The results show steady-state response in which the temporally modulated pump and probe beams interact simply by diffracting off the stationary index grating that is created in the crystal after the beams interact for a time on the order of the photorefractive response time. This experiment was performed merely to demonstrate the high signal bandwidth of the system. Optimization of the parameters was not done, so the results shown in Fig. 20 can clearly be improved.

5. CONCLUSION

We have described some of the interesting and important phenomena in photorefractive media. Photorefractive materials such as BaTiO_3 , SGN , and BSO are by far the most efficient media

for the generation of holograms and phase-conjugate waves using relatively low optical intensities. In addition, two-wave mixing in these media exhibits nonreciprocal energy transfer. As a result of the strong energy coupling, several unique photorefractive phenomena occur in these media. These include self-pumped phase conjugation, nonreciprocal energy transfer without phase cross talk, phase-conjugate interferometry, etc. These unique phenomena play an important role in many of the applications in optical computing including matrix-vector multiplication, parallel subtraction, reconfigurable interconnections, etc. Some of these applications were presented and discussed.

6. ACKNOWLEDGMENT

This work is supported in part by the Defense Advanced Research Projects Agency/Air Force Office of Scientific Research under contract No. F49620-87-C-0015.

7. REFERENCES

1. J. A. Neft, "The role of optics in future computational systems," Technical Digest of OSA Topical Meeting on Optical Computing (Incline Village, Nev.), March 18-20, 1985.
2. See, for example, A. Yariv and P. Yeh, *Optical Waves in Crystals*, Wiley (1984).
3. See, for example, Y. R. Shen, *Principles of Nonlinear Optics*, Wiley (1985).
4. See, for example, D. Pepper, "Applications of optical phase conjugation," *Sci. Am.* 254, 74 (1986).
5. A. Yariv, "Phase conjugate optics and real-time holography," *IEEE J. Quantum Electron.* QE-14, 650-660 (1978).
6. See, for example, P. Yeh, "Two-wave mixing in nonlinear media," *IEEE J. Quantum Electron.* (March 1989).
7. A. Ashkin, G. D. Boyd, J. M. Dziedzic, R. G. Smith, A. A. Ballman, J. J. Levinstein, and K. Nassau, "Optically induced refractive index inhomogeneities in LiNbO_3 and LiTaO_3 ," *Appl. Phys. Lett.* 9, 72-74 (1966).
8. V. L. Vinetski, N. V. Kukhtarev, S. G. Odulov, and M. S. Soskin, "Dynamic self-diffraction of coherent light beams," *Sov. Phys. Usp.* 22, 742-756 (1979).
9. N. V. Kukhtarev, V. B. Markov, S. G. Odulov, M. S. Soskin, and V. L. Vinetski, "Holographic storage in electro-optic crystals. Beam coupling and light amplification," *Ferroelectrics* 22, 961-964 (1979).
10. J. Feinberg, D. Heiman, A. R. Tanguay, Jr., and R. Hellwarth, "Photorefractive effects and light-induced charge migration in barium titanate," *J. Appl. Phys.* 51, 1297 (1980); 52, 537 (1981).
11. S. Ducharme and J. Feinberg, "Speed of the photorefractive effect in a BaTiO_3 crystal," *J. Appl. Phys.* 56, 839 (1984).
12. R. A. Mullen and R. W. Hellwarth, "Optical measurements of the photorefractive parameters of BSO ," *J. Appl. Phys.* 58, 40 (1985).
13. D. L. Staebler and J. J. Amodi, "Coupled wave analysis of holographic storage in LiNbO_3 ," *J. Appl. Phys.* 34, 1042 (1972).
14. V. Markov, S. Odulov, and M. Soskin, "Dynamic holography and optical image processing," *Opt. Laser Technol.* 11, 95 (1979).
15. A. Marrakchi, J. P. Huignard, and P. Guenier, "Diffraction efficiency and energy transfer in two-wave mixing experiments with Ba_2SiO_4 crystals," *Appl. Phys.* 24, 131 (1981).
16. J. Feinberg and R. W. Hellwarth, "Phase conjugating mirror with continuous wave gain," *Opt. Lett.* 5, 519-521 (1980).
17. D. W. Vahey, "A nonlinear coupled-wave theory of holographic storage in ferroelectric materials," *J. Appl. Phys.* 46, 3510 (1975).
18. J. Feinberg, "Asymmetric self-defocusing of an optical beam from the photorefractive effect," *J. Opt. Soc. Am.* 72, 46 (1982).
19. A. E. T. Chou and P. Yeh, "Beam cleanup using photorefractive two-wave mixing," *Opt. Lett.* 10, 621-623 (1985).
20. P. Yeh, "Spectral compression of holographic two-wave mixing," in *Digest of Conf. on Lasers and Optics* (Baltimore, Md.), May 21-24, 1985, p. 274, OSA.
21. See, for example, W. T. Tjelt, *Optical Information Processing and Holography*, Chap. 3, Wiley (1974).
22. P. Yeh, "Scalar phase conjugators for polarization correction," *Opt. Commun.* 51, 195-197 (1984).
23. I. M. Michael, P. Beckwith, and P. Yeh, "Correction of polarization and modal scrambling in multimode fibers by phase conjugation," *Opt. Lett.* 12, 507 (1987).
24. J. Feinberg, "Self-imposed continuous wave phase conjugator using internal reflection," *Opt. Lett.* 7, 486-490 (1982).
25. J. Feinberg, "Continuous wave self-pumped phase conjugator with a wide field of view," *Opt. Lett.* 8, 480 (1983).
26. J. G. White, M. Cronin-Golomb, R. Fischer, and A. Yariv, "Coherent oscillation in self-faceted gratings in photorefractive crystals," *Appl. Phys. Lett.* 40, 450-452 (1982).

27. T. Y. Chang and R. W. Hellwarth, "Optical phase conjugation by backscattering in the photorefractive crystal barium titanate," *Opt. Lett.* 10, 408-410 (1985).
28. J. F. Lam, "Origins of phase conjugate waves in self-pumped photorefractive mirrors," *Appl. Phys. Lett.* 46, 909-911 (1985).
29. K. R. MacDonald and J. Feinberg, "Theory of a self-pumped phase conjugator with two coupled interaction regions," *J. Opt. Soc. Am.* 73, 548-553 (1983).
30. K. R. MacDonald and J. Feinberg, "Enhanced four-wave mixing by use of frequency-shifted optical waves in photorefractive BaTiO₃," *Phys. Rev. Lett.* 55, 821-822 (1985).
31. D. J. Gauthier, P. Narum, and R. W. Boyd, "Observation of deterministic chaos in a phase-conjugate mirror," *Phys. Rev. Lett.* 58, 1644-1647 (1987).
32. M. C. Gower, "Photoinduced voltages and frequency shifts in a self-pumped phase-conjugating BaTiO₃ crystal," *Opt. Lett.* 11, 458-460 (1986).
33. P. Yeh, "Theory of unidirectional photorefractive resonators," *J. Opt. Soc. Am. JOSA B* 2, 1924-1928 (1985).
34. M. D. Ewbank and P. Yeh, "Frequency shifted cavity length in photorefractive resonators," *Opt. Lett.* 10, 496-498 (1985).
35. M. D. Ewbank and P. Yeh, "Frequency shifts of self-pumped phase conjugators," in *Nonlinear Optics and Applications*, P. Yeh, ed., Proc. SPIE 613, 59-69 (1986).
36. W. B. Whitten and J. M. Ramsey, "Self-scanning of a dye laser due to feedback from a BaTiO₃ phase-conjugate reflector," *Opt. Lett.* 9, 44-46 (1984).
37. K. R. MacDonald and J. Feinberg, "Anomalous frequency and phase shifts in self-pumped phase conjugators," *J. Opt. Soc. Am. JOSA A* 1, 1213(A), (1984).
38. E. A. Hopf, "Interferometry using conjugate-wave generation," *J. Opt. Soc. Am.* 70(11), 1320-1323 (1980).
39. I. Bar-Joseph, A. Handy, Y. Katzir, and Y. Silberberg, "Low-power phase-conjugate interferometry," *Opt. Lett.* 6(9), 414-416 (1981).
40. J. Feinberg, "Interferometer with a self-pumped phase-conjugating mirror," *Opt. Lett.* 8(11), 569-571 (1983).
41. M. D. Ewbank, M. Khoshnevisan, and P. Yeh, "Phase-conjugate interferometry," in *Solid State Optical Control Devices*, P. Yeh, ed., Proc. SPIE 464, 2-6 (1984).
42. N. G. Basov, I. G. Zubarev, A. B. Mironov, S. I. Mikhailov, and A. Yu. Okulov, "Laser interferometer with wavefront-reversing mirrors," *Sov. Phys. JETP* 52(5), 847-851 (1980).
43. M. D. Ewbank, P. Yeh, M. Khoshnevisan, and J. Feinberg, "Time reversal by an interferometer with coupled phase conjugators," *Opt. Lett.* 10, 282-284 (1985).
44. A. E. Chiou and P. Yeh, "Parallel image subtraction using a phase-conjugate Michelson interferometer," *Opt. Lett.* 11(5), 306-308 (1986).
45. A. E. Chiou, P. Yeh, and M. Khoshnevisan, "Coherent image subtraction using phase conjugate interferometry," in *Nonlinear Optics and Applications*, P. Yeh, ed., Proc. SPIE 613, 201-206 (1986).
46. S. K. Kwong, G. A. Rakulic, and A. Yariv, "Real-time image subtraction and exclusive OR operation using a self-pumped phase-conjugate mirror," *Appl. Phys.* 48(3), 201-202 (1986).
47. S. K. Kwong, G. A. Rakulic, V. Leyva, and A. Yariv, "Real-time image processing using a self-pumped phase-conjugate mirror," in *Nonlinear Optics and Applications*, P. Yeh, ed., Proc. SPIE 613, 36-42 (1986).
48. W. H. Chen, P. J. Wang, P. C. San, and P. Yeh, "Phase conjugate interferometry," in *Phase Conjugation and Beam Combining and Diagnostics*, R. A. Fisher and I. Abramowitz, eds., Proc. SPIE 739, 165-108 (1987).
49. D. Z. Anderson, D. M. Lininger, and J. Feinberg, "Optical tracking novelty filter," *Opt. Lett.* 12(2), 123-125 (1987).
50. G. G. Stokes, "On the perfect blackness of the central spot in Newton's rings, and on the verification of Fresnel's formulae for the intensities of reflected and refracted rays," *Camb. Dubl. Math. J.* 4, 1 (1849).
51. M. D. Ewbank and R. A. Vazquez, "Time-reversal fidelity," *J. Opt. Soc. Am. JOSA A* 4(13), P12 (1987).
52. J. P. Hugonard and A. Marrakchi, "Two-wave mixing and energy transfer in Ba:SiO₃ crystal: application to image amplification and vibration analysis," *Opt. Lett.* 6(12), 622-624 (1981).
53. Y. Fainman and S. H. Lee, "Applications of photorefractive crystals to optical signal processing," in *Optical and Hybrid Computing*, H. H. Szu, ed., Proc. SPIE 634, 380-392 (1987).
54. J. P. Hugonard and A. Marrakchi, "Coherent signal beam amplification in two-wave mixing experiments with photorefractive Ba:SiO₃ crystals," *Opt. Commun.* 38, 249 (1981).
55. Y. Shi, D. Psaltis, A. Marrakchi, and A. R. Tanguay, Jr., "Photorefractive incoherent-to-coherent optical converter," *Appl. Opt.* 22(23), 3665 (1983).
56. L. J. Cheng, G. Ghees, M. F. Rau, and F. C. Wang, "Image transfer in photorefractive GaAs," *J. Appl. Phys.* 62(9), 3991-3993 (1987).
57. H. K. Liu and L. J. Cheng, "Infrared predetection dynamic range compression in photorefractive crystals," *Appl. Opt.* 27(5), 1006-1007 (1988).
58. I. M. Michael, M. Khoshnevisan, and P. H. Beckwith, "Nonlinear optical range imaging," in *Conf. on Lasers and Electro-Optics Tech. Digest Series 1988*, Vol. 7, p. 218, OSA (1988).
59. M. Cheng, G. Ghees, et al., "Photorefractive time differentiation of coherent optical images," in *Conf. on Lasers and Electro-Optics Tech. Digest Series 1988*, Vol. 7, p. 194, OSA (1988).
60. A. E. Chiou, P. Yeh, and M. Khoshnevisan, "Nonlinear optical image subtraction for potential industrial applications," *Opt. Eng.* 27(5), 385-392 (1988).
61. J. F. Ebersole, "Optical image subtraction," *Opt. Eng.* 14(5), 436-447 (1975).
62. H. K. Liu and T. H. Chao, "Optical image subtraction techniques, 1975-1985," in *Hybrid Image Processing*, D. P. Casasent and A. Tescher, eds., Proc. SPIE 638, 55-65 (1986).
63. P. Yeh, T. Y. Chang, and P. H. Beckwith, "Real-time optical image subtraction using dynamic holographic interference in photorefractive media," *Opt. Lett.* 13(7), 586-588 (1988).
64. J. Feinberg and D. Anderson, "Optical novelty filters," *IEEE J. Quantum Electron.* QE-25 (1989).
65. J. O. White and A. Yariv, "Real-time image processing via four-wave mixing in a photorefractive medium," *Appl. Phys. Lett.* 37(1), 5-7 (1980).
66. G. Eichmann, Y. Li, and R. R. Alfano, "Parallel optical logic using optical phase conjugation," *Appl. Opt.* 26(2), 194-196 (1987).
67. Y. Li, G. Eichmann, R. Dorsinville, and R. R. Alfano, "An operation-based optical symbolic substitution pattern recognizer," *Opt. Commun.* 63(6), 375-379 (1987).
68. Y. Li, G. Eichmann, R. Dorsinville, and R. R. Alfano, "Demonstration of a picosecond optical phase-conjugation-based residue-arithmetic computation," *Opt. Lett.* 13(2), 178-180 (1988).
69. P. Yeh and A. E. Chiou, "Optical matrix-vector multiplication through four-wave mixing in photorefractive media," *Opt. Lett.* 12(2), 138-140 (1987).
70. A. E. Chiou and P. Yeh, "Optical matrix-vector multiplication using four-wave mixing," in *Tech. Digest of OSA 1986 Annual Meeting* (Seattle, Wash., Oct. 20-24), Paper MM5 (1986).
71. A. E. Chiou, M. Khoshnevisan, and P. Yeh, "Optical matrix-matrix multiplication using multi-color four-wave mixing," in *Optical Computing and Nonlinear Materials*, N. Peyghambarian, ed., Proc. SPIE 881, 250-257 (1988).
72. A. E. Chiou and K. Nguyen, "Optical matrix-matrix multiplication by spatial convolution via four-wave mixing," (private communication).
73. R. A. Athale, "Optical matrix processors," in *Optical and Hybrid Computing*, H. H. Szu, ed., Proc. SPIE 634, 96-111 (1987).
74. W. T. Rhodes, "Optical matrix-vector processors: basic concepts," in *Highly Parallel Signal Processing Architectures*, K. Bromley, ed., Proc. SPIE 614, 146-152 (1986).
75. D. Casasent and B. V. K. Vijaya Kumar, "Optical linear algebra processors," in *Optical Signal Processing*, J. Hornet, ed., pp. 389-407, Academic Press, San Diego (1987).
76. A. E. Chiou, P. Yeh, and M. Khoshnevisan, "Optical matrix-vector multiplication using a spatial light modulator and a phase conjugator," in *Spatial Light Modulators and Applications Tech. Digest Series 1988*, Vol. 8, pp. FA1-1, OSA (1988).
77. See, for example, J. W. Goodman, F. J. Leonberger, S.-Y. Kung, and R. A. Athale, "Optical interconnections for VLSI systems," *Proc. IEEE* 72, 850-866 (1984).
78. See, for example, "Interconnections," Sec. 3 in *Optical Computing*, J. A. Neff, ed., Proc. SPIE 625, 109-172 (1986).
79. A. A. Sawchuk and B. K. Jenkins, "Dynamic optical interconnections for parallel processors," in *Optical Computing*, J. A. Neff, ed., Proc. SPIE 625, 143-153 (1986).
80. P. Yeh, A. E. Chiou, and J. Hong, "Optical interconnection using dynamic photorefractive holograms," *Appl. Opt.* 27, 2093 (1988).
81. A. Chiou, P. Yeh, and J. Hong, "Energy-efficient optical interconnection using dynamic holograms in photorefractive media," in *OSA Annual Meeting Tech. Digest Series 1988*, Vol. 2, p. 179 (1988).



Pochi Yeh obtained his undergraduate education at the National Taiwan University, receiving a BS degree in physics in 1971. He came to the United States in 1973 to continue his education at the California Institute of Technology, where he earned his MS and Ph.D. degrees in physics in 1975 and 1977, respectively. Dr. Yeh joined Rockwell International Science Center in 1977 as a member of the technical staff and currently holds the position of principal scientist. He has made

significant contributions to the discovery of several optical phenomena in superlattice structures, to the theoretical formulation of wave coupling in nonlinear media and layered media, and to the proposals and demonstration of a number of new concepts in optical phase conjugation and photorefractive phenomena. His recent research efforts are in the areas of nonlinear optics, phase conjugation, image processing

optical computing, photorefractive phenomena, etc. Dr. Yeh is the author or coauthor of more than 100 papers, 12 U.S. patents, and two textbooks on advanced optics. Dr. Yeh is a Fellow of the OSA and a senior member of the IEEE. He was the recipient of the "Engineer of the Year" award at Rockwell International Science Center in 1985.



Arthur E. Chiou received his B.Sc. degree in physics from Rangoon Arts and Science University, Burma (1969), his MS degree in physics from National Taiwan University (1972), and his Ph.D. degree in applied physics from the California Institute of Technology (1983). Dr. Chiou's graduate research at Caltech involved theoretical investigation in multilayer dielectric waveguides and experimental parametric study of optically pumped far-infrared waveguide lasers. After working as a postdoctoral

research fellow for two years (Oct. 1982 to Sept. 1984) at IBM Research Laboratory at San Jose, where his work involved design and implementation of interferometric monitoring of head-disk interface in magnetic recording and experimental investigation of photoacoustic and photothermal spectroscopy and nondestructive material inspections, he joined Rockwell International Science Center in Sept. 1984. His current research interests are in the fields of optical computing, optical information processing, laser beam cleanup, and laser beam combining using photorefractive wave mixing. Dr. Chiou has more than 20 publications and presentations to his credit. He is a member of OSA, the IEEE Laser and Electro-Optics Society, the IEEE Professional Communication Society, SPIE, the Chinese Engineer and Scientist Association of Southern California, and the National Management Association.



John Hong received the BS degree in 1982 from the Massachusetts Institute of Technology. He received the MS degree in 1983 and the Ph.D. degree in 1989, both in electrical engineering from the California Institute of Technology. Dr. Hong joined the Rockwell International Science Center in 1987 as a member of the technical staff.

Paul Beckwith and **Tallis Chang**: Biographies and photographs unavailable



Monte Khoshnevisan is the director of the Optics Function, Rockwell International Science Center. Dr. Khoshnevisan received his BS in physics and mathematics from San Jose State University in 1958 and his Ph.D. in solid state physics from Michigan State University in 1973. He was an assistant professor and vice-chairman of the Physics Department at Arya-Mehr University of Technology, Tehran, Iran (1973-1977), and a visiting research assistant professor at Michigan State University for nine months. He joined the Rockwell Science Center in 1978, carrying out research in acousto-optics and optics. He became a group leader in the area of infrared devices in 1981, doing research in infrared materials, detectors, and solid state nuclear detectors. From 1983 to 1988, he headed the Applied Optics Department, carrying out research in nonlinear optics and advanced optical devices for sensors or information processing. He has coauthored over 70 scientific papers and presentations in a number of scientific areas and holds two U.S. patents. Dr. Khoshnevisan is a member of the American Physical Society, OSA, and SPIE.



Rockwell International
Science Center

SC5502.FR

APPENDIX 5.7

Energy Efficiency of Optical Interconnection Using Photorefractive Holograms

**Energy Efficiency of Optical Interconnections
Using Photorefractive Holograms**

Arthur Chiou and Pochi Yeh
Rockwell International Science Center
1049 Camino Dos Rios
Thousand Oaks, CA 91360

ABSTRACT

We propose and demonstrate the use of Fourier transform to achieve maximum energy efficiency in a photorefractive optical interconnection. The results of experimental investigations on reconfigurable optical interconnections using photorefractive holograms in a barium titanate crystal are presented and discussed. High energy efficiency is achieved by matched amplification at the Fourier plane.

Energy Efficiency of Optical Interconnections Using Photorefractive Holograms

Arthur Chiou and Pochi Yeh
Rockwell International Science Center
1049 Camino Dos Rios
Thousand Oaks, CA 91360

1. Introduction

Optical interconnection between VLSI circuits, computing chips or boards plays an important role in optical computing [1,2]. Such a scheme of computing provides the potential of achieving extremely high speed because it utilizes the fast switching of electronics and the wide bandwidth of optics for communication [3]. A generalized optical crossbar switch can provide a reconfigurable arbitrary interconnection [4,5] between an array of N lasers and an array of N detectors. Such a crossbar can be implemented using parallel matrix-vector multiplication

which provides N^2 parallelism [5-8].

It is known that the N^2 parallelism is accompanied with an intrinsic fan-out energy loss [4,9]. The fan-out leads to an energy efficiency of $1/N$. We recently proposed and demonstrated a novel concept of reconfigurable optical interconnection [9-11] which can provide high energy efficiency. Using the beam coupling in photorefractive crystals [12,15], such a scheme of interconnection is capable of minimizing the fan-out energy loss and thus achieves extremely high energy efficiency. Although the basic concept has been validated and some of the preliminary results have been reported [9,11], the issue of energy efficiency remains a subject of experimental investigation. This paper reports the results of an extensive investigation on the energy efficiency of reconfigurable optical interconnection using photorefractive holograms.

In what follows, we will briefly review the basic principle of operation of the photorefractive interconnection. We will point out the use of Fourier transform to achieve maximum beam overlap in the photorefractive medium. We then discuss the results of our experimental investigations.

2. Principle of Operation

Figure 1 shows the basic idea of reconfigurable interconnection using photorefractive holograms. A beam splitter is used to split off a small portion of the beam which consists of beamlets each carrying information from one of the sources. This small portion of the beam will be called the signal beam. The beam splitter allows the majority of the energy to pass through. This major portion of the beam is called the pump beam. The signal beam is fanned by the cylindrical lens and then passes through the spatial light modulator (SLM) which contains the interconnection pattern. After passing through the SLM, the signal beam is imprinted spatially with the interconnection pattern. The pump beam does not pass through the spatial light modulator and thus suffers no energy loss due to the fan-out and all the other loss mechanisms associated with the SLM.

The signal beam which contains the interconnection information is then recombined with the pump beam in a photorefractive crystal. Under the appropriate conditions, the signal beam can be amplified at the expense of the pump beam. Most of the energy of the pump beam will be transferred to the signal beam provided the length of

interaction is large enough [14,15]. It is known that photorefractive two-wave mixing exhibits energy transfer without phase crosstalk [16]. Thus the amplified signal beam will also bear the interconnection pattern. The net result is an optical interconnection with high energy efficiency.

Although photorefractive two-wave mixing is involved, such a scheme can also be considered as a real-time holographic interconnection with a very high diffraction efficiency. The combination of the beam splitter and the SLM in conjunction with the pump beam is used to record a hologram inside the photorefractive crystal. Such a hologram contains the interconnection as prescribed by the SLM. Once the hologram is formed, the pump beam can be diffracted off the hologram and be redirected into the array of detectors. The advantage here is that the recording and the readout occur simultaneously. This offers the possibility of reconfigurable interconnection by controlling the SLM.

To achieve maximum energy efficiency, it is important that the signal beam and the pump beam overlap completely. Specifically, beamlet 1 of the pump beam in Fig. 1 must overlap completely with column 1 of the signal beam. And similarly, beamlets 2, 3, and 4 must also overlap completely

with their corresponding columns in the signal beam. It is important to note that although the beamlets in the signal beam and the pump beam are intrinsically different because of the interconnection pattern, the individual pixels can have identical shape (e.g., square). Complete overlap is possible in the Fourier domain, provided all the pixels are identical. Let $s(x,y)$ be the aperture of an individual pixel, and $\sigma(u,v)$ be the Fourier transform. Fourier transformation of a beamlet of the pump beam and the corresponding column of beamlets of the signal beam can be performed by a lens (see Fig.2). The resulting amplitude distributions at the rear focal plane are given by

$$\text{Pump: } P(u,v) = \sigma(u,v) \text{ ----- (1)}$$

$$\text{Signal: } S(u,v) = \sum_n \sigma(u,v) \exp [i \phi_n(u,v)] \text{ ---- (2)}$$

respectively, where u,v are coordinates in the Fourier plane. The summation in equation (2) is over all the windows open in the column, and $\phi_n(u,v)$ is a phase which depends on the position of the window.

We note that the Fourier transform of a column of the signal beam consists of a linear superposition of identical patterns each with a different phase factor. Such phase factors $\exp(i\phi_n)$ are due to the relative positions of the windows in each column. Although these phase factors may lead to interference structures, all the energies are confined under the same envelop $\sigma(u,v)$. As a result of the shift invariance in Fourier transformation, each of the signal beamlets overlaps completely with the pump beam at the Fourier plane. Thus maximum energy coupling is achieved.

3. Experimental Investigations

The energy efficiency of photorefractive interconnection depends on several parameters. In addition to the beam overlap mentioned earlier, it depends on crystal orientation, coupling constant, length of interaction, beam intensity ratio, insertion loss at SLM [17,18], and other loss

mechanisms such as Fresnel reflection, beam fanning [19] and scattering, etc. We have carried out a series of experiments to investigate the energy efficiency of photorefractive interconnection. These experiments are designed to study the dependence on those physical parameters mentioned above.

Referring to Fig. 3, we consider the efficiency of energy transfer in photorefractive two-beam coupling. An input beam of power P_i is split by a beam splitter BS into a pump beam with power P_p and a signal beam with power P_s ($P_s = P_i - P_p$). These two beams are recombined in a photorefractive BaTiO_3 crystal. The crystal is oriented such that the signal beam is amplified. Let P_o be the power of the amplified signal beam. The energy efficiency η of photorefractive two-beam coupling is defined as $\eta = P_o / P_i$. A theoretical expression of such an energy efficiency was

derived earlier in reference 9. In our experiment, we examine the dependence of η on the pump-to-signal intensity ratio m , defined as $m = P_p / P_s$. Such a parameter can be changed by using a variable beam splitter.

Using argon ion laser as the source, and a $5 \times 7 \times 7$ mm³ BaTiO₃ crystal as the photorefractive medium, we have measured the energy efficiency (η) as a function of the intensity ratio m . The maximum efficiency is approximately 10 % when the beam intensity ratio is $m = 20$. In addition to these measurements, we also repeat the experiment by inserting a neutral density filter (NDF) in the optical path of the signal beam. This neutral density filter is used to simulate the fanout energy loss. The idea here is to show that the amplified signal beam power does not decrease significantly as the input signal beam is attenuated. The experimental results are shown in Fig.4. We notice that an energy efficiency of 1.5% is obtained when the simulated

fanout loss is 99.9%. This is an improvement in energy efficiency by more than a factor of 15. As discussed earlier in reference 9, the optimum beam splitting ratio m (i.e. the pump-to-signal intensity ratio measured immediately after the beam splitter, and before the signal beam is attenuated by the NDF) depends, in general, on the photorefractive coupling constant γL and the fanout loss of the signal beam. In this particular experiment, the crystal is oriented such that both beams enter the crystal symmetrically at an angle of incidence of 20° as shown in the inset in Figure 4. This configuration is, however, not optimized for maximum energy efficiency because it only provides a coupling constant γL of approximately 4.5.

The coupling constant γL depends on the crystal orientation relative to the beams. In another experiment, the same crystal is oriented such that the signal beam enter the crystal at an angle of approximately 67° which is near

Brewster's angle. This incidence configuration minimizes the Fresnel reflection loss. The pump beam enters the crystal at an angle of incidence of 32° such that the grating induced in the photorefractive crystal provides a coupling constant γL of approximately 9.2. Again, an argon ion laser is used as the light source. The beam splitter has a reflectance of 95% which provides a beam splitting ratio of $m = 10$. Under these conditions, the energy efficiency is improved significantly. Figure 5 shows the experimental results along with a theoretical fit (the solid line) using equation (3) in reference 9. The energy efficiency is plotted as a function of $(1/N)$ which is the transmittance of the neutral density filter. We recall that $(1/N)$ represents the maximum energy efficiency achievable by a conventional $N \times N$ crossbar as a result of fanout loss. The orientation of the crystal relative to the incoming beam is shown in the inset of Figure 5. We notice that an improvement by a factor of 100 is achieved in energy efficiency when $(1/N)$ is of the order of 1×10^{-3} . Further

improvement in energy efficiency can be achieved by coating the crystal surfaces with anti-reflection dielectric films and by using crystals with higher coupling constants.

In the experiments discussed above, both signal and pump beams are Gaussian beams with no spatial intensity pattern. In the interconnection applications, these beams are spatially modulated. As we mentioned earlier, the energy efficiency of the photorefractive interconnection as depicted in Fig. 1 depends on the spatial overlap of the beams. We now discuss our experimental investigations on the utilization of Fourier transform to achieve maximum beam overlap and thus to achieve maximum energy efficiency.

The experimental configuration is illustrated in Fig.6. The output from an argon laser (514.5nm) is spatial-filtered and expanded to form a collimated beam with 2cm diameter. A variable beam splitter consisting of a half-wave plate and

a polarizing beam splitter cube is used to split the incoming beam into two, a pump beam and a signal beam. Another half-wave plate is used to rotate the polarization of the reflected (signal) beam by 90° from the direction perpendicular to the plane of the paper to the in plane direction. A polarizer placed downstream further filters out the residual perpendicular component. A 10×10 binary matrix mask is used to encode a spatial pattern onto the signal beam. The objective here is to efficiently transfer energy, via photorefractive two-wave mixing, from the pump beam to the signal beam which is encoded with the interconnection pattern. Any one or more (up to 100) of the 10×10 channels can be selected by using an appropriate mask.

To maximize the spatial overlap of the pump and the signal beams inside the crystal via the properties of Fourier transform [see equations (1) and (2)] described in Section 2.

a pump mask with a single aperture identical to the unit cell of the signal mask is used. The two masks are placed at the front focal planes of two Fourier transform lenses FL_1 and FL_2 , (of identical focal length $f = 25\text{cm}$) respectively. Here we use two lenses of identical focal length because optimum beam coupling occurs at an angle of 40° between the beams which are beyond the numerical aperture of a single lens. The crystal is located at the common Fourier plane of the two masks (see Fig.6). The shift-invariant property of Fourier transformation ensures that, apart from a phase factor, the diffraction pattern from each signal channel overlaps with that from the pump inside the crystal. The intensity patterns of the pump and the signal at the image plane and the Fourier plane are shown in Fig.7. Note that the two intensity distributions at the Fourier plane differ significantly in fine structures due to multiple beam interference among the various signal channels. A magnified version that reveals these fine structures can be found in Reference [20].

The key questions we address in this section are the following: (1) How efficiently can we transfer energy from a single channel to multiple channels ? (2) How does the energy efficiency depend on the number of signal channels ? and (3) How is the energy distributed among the signal channels ?

To investigate how the energy efficiency depends on the number of signal channels, we used a variable rectangular aperture in front of the signal mask to vary the number of channels from 100 to 1. In each case, we also adjusted the laser power and the variable beam splitter so that both the pump power and the total signal input power are fixed at 600 μ W and 6 μ W, respectively, regardless of the number of signal channels. Figure 8 is a plot of energy efficiency vs. number of signal channels. The energy efficiency turns out to be fairly insensitive to the number of signal channels. These data were taken with the geometry

shown in the inset of Figure 4. As mentioned before, this particular geometry is far from optimum, and one can expect an energy efficiency of 30 to 40% or higher once optimized.

With all the 10x10 signal channels on, the intensity pattern at the output (image) plane is shown in Figure 9. The original output pattern with the photorefractive crystal removed is shown in Fig.9 (a). When the crystal is in place, the output pattern is slightly degraded as shown in Fig.9 (b). The degradation is due mainly to beam-fanning [17]. This can be verified by observing the output pattern using a signal beam which is ordinarily polarized (o-polarized) or much lower in power. The results are shown in Fig.9 (c) and (d). In both cases the original intensity pattern is restored as the beam fanning effect diminished. In Fig.9 (c), significant reduction of beam fanning is a consequence of the much smaller electro-optic coefficients associate with the o-polarized beam. In Fig.9 (d), it is a consequence of longer

time required for the fanning grating to build up when the beam intensity is weaker. The bottom picture in Fig.9(e) shows the amplified signal output when the pump beam is turned on. The presence of the pump beam not only increases the output energy but also significantly reduces the signal degradation. To monitor the energy distribution quantitatively, a linear detector array is placed along one row of the signal channels at the image plane. The oscillograms representing the energy distribution among the 10 channels are given in Fig.10 for the following three cases: (a) with the crystal removed; (b) with the crystal in place and the pump beam off; (c) with the crystal in place and the pump beam on. In all cases, the Gaussian "top-hat" profile originated from the expanded laser beam is more or less preserved, and the energy distribution is sufficiently uniform. Note that the vertical scale of the oscillogram in Fig.10(b) is 10mV/division versus the 100mV/division scale in Fig.10(c). The signal gain, in this case is approximately 20.

Using an experimental configuration similar to the one shown in Fig.6, with all the Fourier transform lenses replaced by astigmatic optics (which image along the x-axis and Fourier transform along the y-axis in the input arms, and vice versa in the output arms), we also demonstrated a 6x6 generalized crossbar-switch. An appropriate pump mask and a signal mask for a specific interconnection pattern are shown in the left hand side of Fig.11. The corresponding intensity patterns inside the crystal at the Fourier plane are shown on the right. Ideally, we want each pump channel to interact only with the corresponding signal column. Because of the beam crossing inside the crystal, and because the laser beams in all the channels are mutually coherent, we found significant cross-talk among neighboring channels. This cross-talk can be eliminated by replacing the single laser with a linear array of mutually incoherent laser sources.

4. Summary

In summary, we have proposed and demonstrated the use of Fourier transform to achieve maximum energy efficiency in a photorefractive optical interconnection. We have shown that the energy efficiency of photorefractive dynamic holograms can be of the order of 30% to 40%. In addition, we have also verified that the energy efficiency is insensitive to the number of signal channels, and that the energy distribution among the signal channels is sufficiently uniform. Finally we have described a 6x6 crossbar-switch using this approach.

All the experiments described in this paper were carried out with photographic masks replacing the SLMs. To demonstrate the reconfigurability and to study the reconfiguration time, one can no longer avoid the use of SLMs which, in general, have relatively poor contrast ratio (of the

order of 10 to 30) relative to the photographic masks. We are currently investigating the effect of limited contrast ratio of SLMs on the operation and the reconfiguration time. The results will be the subject of future publications.

5. Acknowledgement

We thank J. Hong and F. Vachss for helpful technical discussion. This work is supported by DARPA/AFOSR under Contract No.F49620-87-C-0015.

REFERENCES

1. See, for example, J. W. Goodman, F.I. Leonberger, S.Y. Kung, and R.A. Athale, "Optical Interconnections for VLSI Systems," Proc. IEEE **72**, 850 (1984).
2. See, for example, J. A. Neff, Ed., Optical Computing, Proc. SPIE **625**, 109 (1986).
3. C. Mead, "Potential and Limitation of VLSI," Topical Meeting on Optical Computing, Technical Digest 1985, (Optical Society of America, Washington, D.C. 1985) MA2-1.
4. A. A. Sawchuk, and B. K. Jenkins, "Dynamic Optical Interconnections for Parallel Processors," Proc. SPIE **625**, 143 (1986).
5. A. A. Sawchuk, B. K. Jenkins, C. S. Raghavendra, and A. Varma, "Optical Crossbar Networks," IEEE Computer **20**, No. 6, 50 (1987).
6. J. W. Goodman, A. R. Dias, and L. M. Woody, "Fully Parallel, High-speed Incoherent Optical Method for

Performing Discrete Fourier Transforms," *Opt. Lett.* **2**, 1 (1978).

7. W. T. Rhodes, "Optical Matrix-Vector Processors: Basic Concepts," *Proc. SPIE* **614**, 146 (1986).

8. R. A. Athale, "Optical Matrix Processors," *Proc. SPIE* **634**, 96 (1986).

9. P. Yeh, A. E. T. Chiou, and J. Hong, "Optical Interconnection Using Photorefractive Dynamic Holograms," *Appl. Opt.* **27**, 2093 (1988).

10. A. E. Chiou, P. Yeh, and J. Hong, "Energy Efficient Optical Interconnection using Dynamic Holograms in Photorefractive Media," *OSA Annual Meeting, 1988 Technical Digest Series, Vol. 11*, (Optical Society of America, Washington, D.C. 1988), pp.178.

11. A. E. Chiou, and P. Yeh, "Energy Efficiency of Optical Interconnection Using Photorefractive Dynamic Holograms," *Optical Computing, 1989 Technical Digest Series, Vol. 9*, (Optical Society of America, Washington, D.C. 1989), pp.128.

12. N. V. Kukhtarev, et al., "Holographic Storage in Electrooptic Crystal. I. Steady State, Ferroelectrics," **22**, 949 (1979).
13. P. Gunter, "Holography, Coherent Light Amplification and Optical Phase Conjugation with Photorefractive Materials," Physics Report, **93**, 199 (1982).
14. N. V. Kukhtarev, et al., "Holographic Storage in Electrooptic Crystal. II. Beam Coupling - Light Amplification," Ferroelectrics, **22**, 961 (1979).
15. J. P. Huignard, and A. Marrakchi, "Coherent Signal Beam Amplification in Two-Wave Mixing Experiments with Photorefractive $\text{Bi}_{12}\text{SiO}_{20}$ Crystals," Opt. Commun. **38**, 249 (1981).
16. A. E. Chiou and P. Yeh "Beam Cleanup Using Photorefractive Two-wave Mixing," Opt. Lett. **10**, 621 (1985).
17. A. D. Fisher, and J. N. Lee, "The current Status of Two-Dimensional Spatial Light Modulator Technology," Proc. SPIE **634**, 352 (1986).

18. C. Warde, and A.D. Fisher, "Spatial Light Modulators: Applications and Functional Capabilities," in Optical Signal Processing, J. Horner, Ed., Academic Press (1987).
19. J. Feinberg, "Asymmetric Self-Defocusing of an Optical Beam from the Photorefractive Effect," J. Opt. Soc. Am. **72**, 46 (1982).
20. D. Malacara, "Diffraction and Scattering," in Physical Optics and Light Measurement, D. Malacara, Ed., Method of Experimental Physics, Vol. 26, Academic Press (1988).

FIGURE CAPTIONS

- Fig.1 A schematic diagram illustrating the basic idea of a reconfigurable optical interconnection using a photorefractive crystal in conjunction with a spatial light modulator.
- Fig.2 A schematic diagram illustrating the basic idea of using Fourier transform to achieve the spatial overlap of the pump beam and the signal beam.
- Fig.3 An experimental configuration for measuring the energy efficiency in photorefractive two-beam coupling.
- Fig.4 The energy efficiency (η) of two-beam coupling in a photorefractive barium titanate crystal as a function of pump-to-signal power ratio (m). The symbols " \square ", " \diamond ", " \circ ", and " Δ ", represent the cases without any neutral density filter, with neutral density filters NDF1, NDF2, and NDF3, respectively, in the signal input arm. The percentage transmittance of the three neutral density filters are 12.2%, 0.74%, and 0.12%, respectively. The orientation of the crystal relative to the beam is given in the inset.
- Fig.5 Energy efficiency (η) of photorefractive two-beam coupling in a barium titanate sample as a function of the transmittance of a neutral density filter placed in the signal input arm. The transmittance is labeled $1/N$ to relate it to the fanout loss of a $N \times N$ permutation crossbar network. The

orientation of the crystal relative to the beam is given in the inset.

Fig.6 An experimental configuration for a 1-to- $N \times N$ (for $N=10$) broadcasting network using photorefractive holograms at the Fourier domain.

Fig.7 The intensity patterns of the masks for the probe and the pump beams at the image plane and the Fourier plane.

Fig.8 Energy efficiency (η) as a function of number of signal channels (N) in a 1-to- $N \times N$ broadcasting configuration using photorefractive holograms in a barium titanate sample.

Fig.9 A 10×10 intensity pattern at the output image plane under various conditions: (a) with the crystal removed, (b) with the crystal in place and pump beam off, total power = $400 \mu\text{W}$, e-polarization, (c) same as in (b) but with o-polarization, (d) same as in (b) but with total power = $3 \mu\text{W}$, (e) amplified output signal, total signal input = $3 \mu\text{W}$, pump input = $600 \mu\text{W}$.

Fig.10 The intensity distribution of a selected row of 10 out of the 10×10 channels shown in Fig.9. (a) with the crystal removed, (b) with the crystal in place and pump beam off, total input power = $10 \mu\text{W}$, (c) with the crystal in place and pump beam on, input pump power = $400 \mu\text{W}$. The vertical scale (per division) in the pictures are 50mV, 10mV, and 100mV, respectively.

Fig.11 The intensity patterns of the masks for the probe and the pump beams at the image plane and the crystal plane for a 6x6 generalized crossbar network.

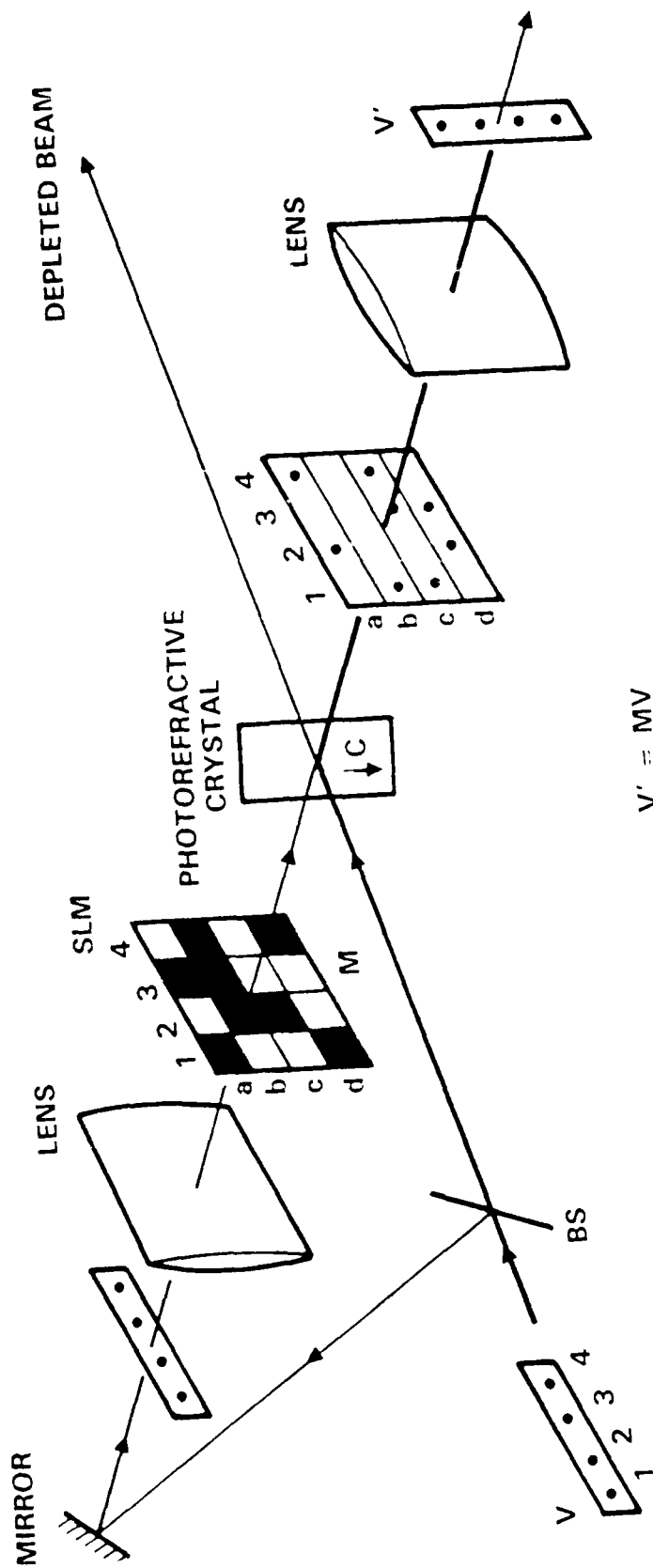


Fig. 1

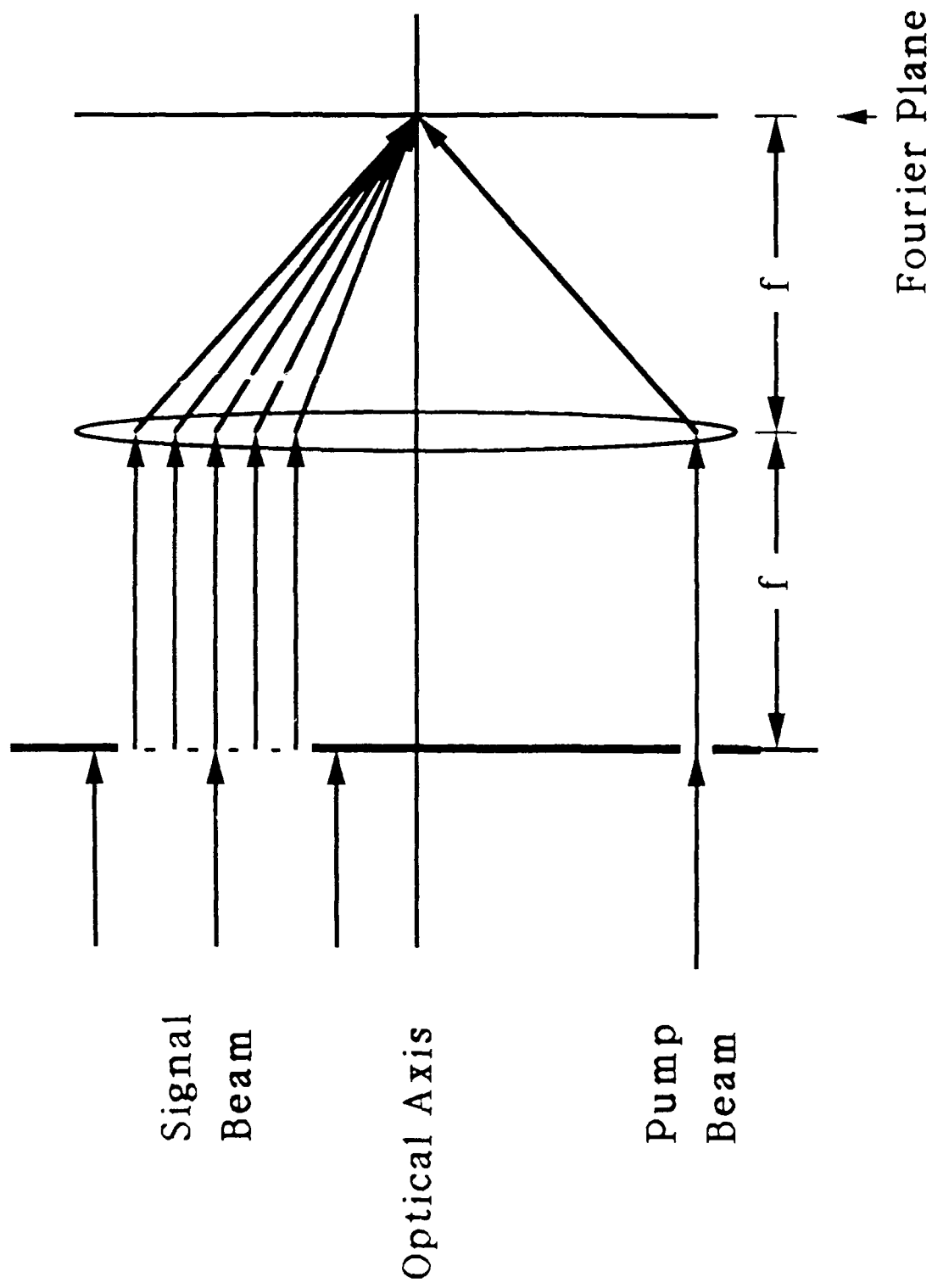


Fig. 2

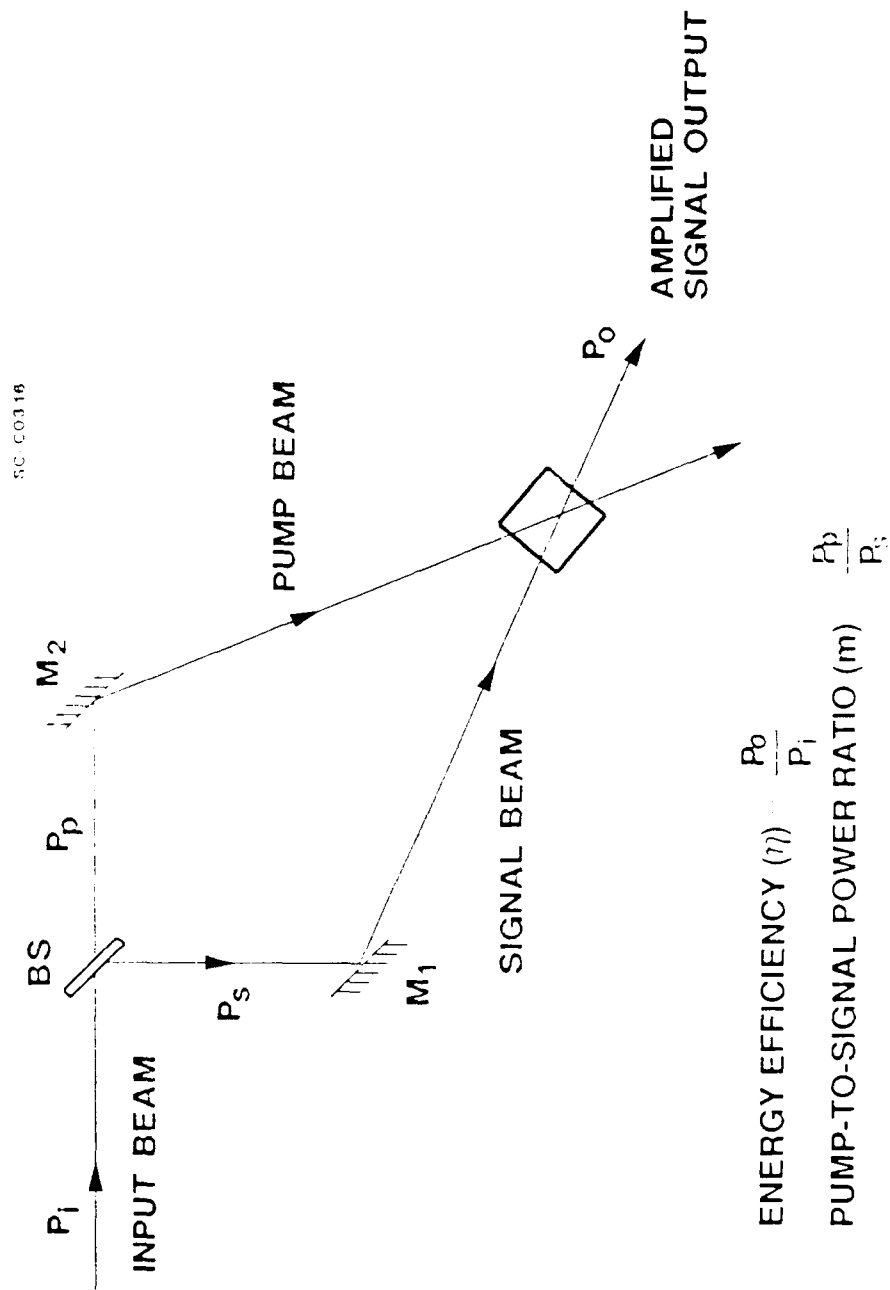


Fig. 3

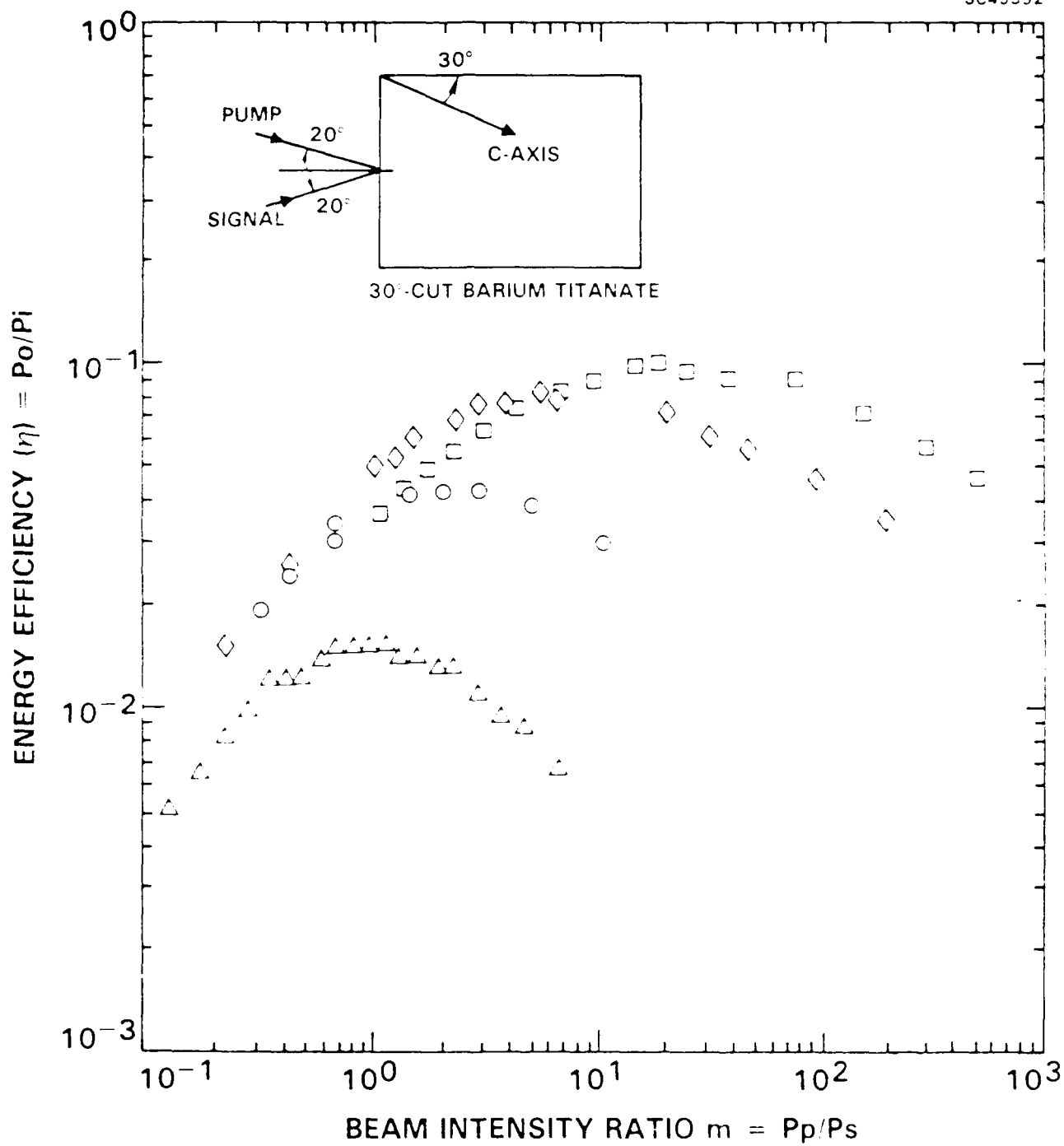


Fig. 1

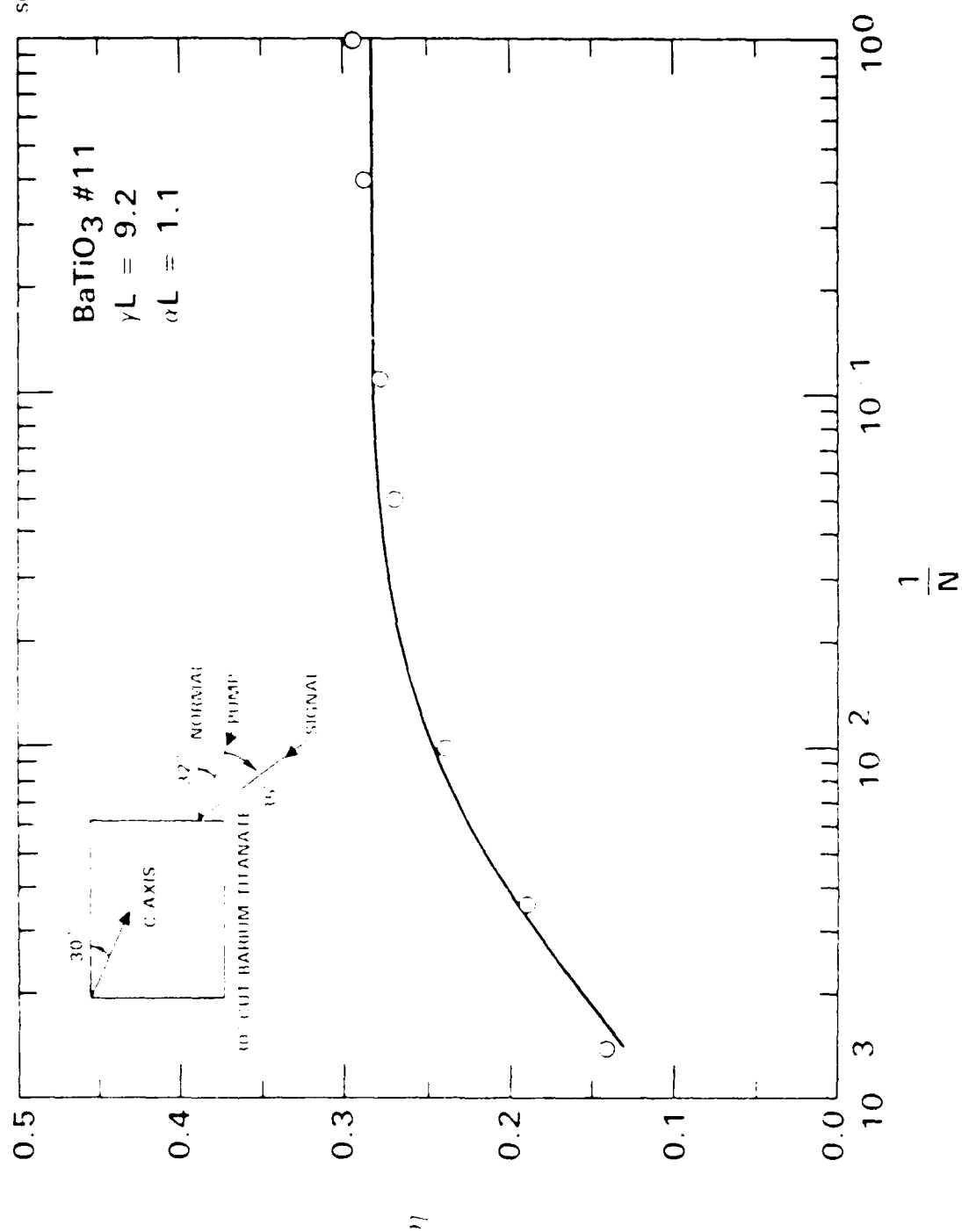


Fig. 6

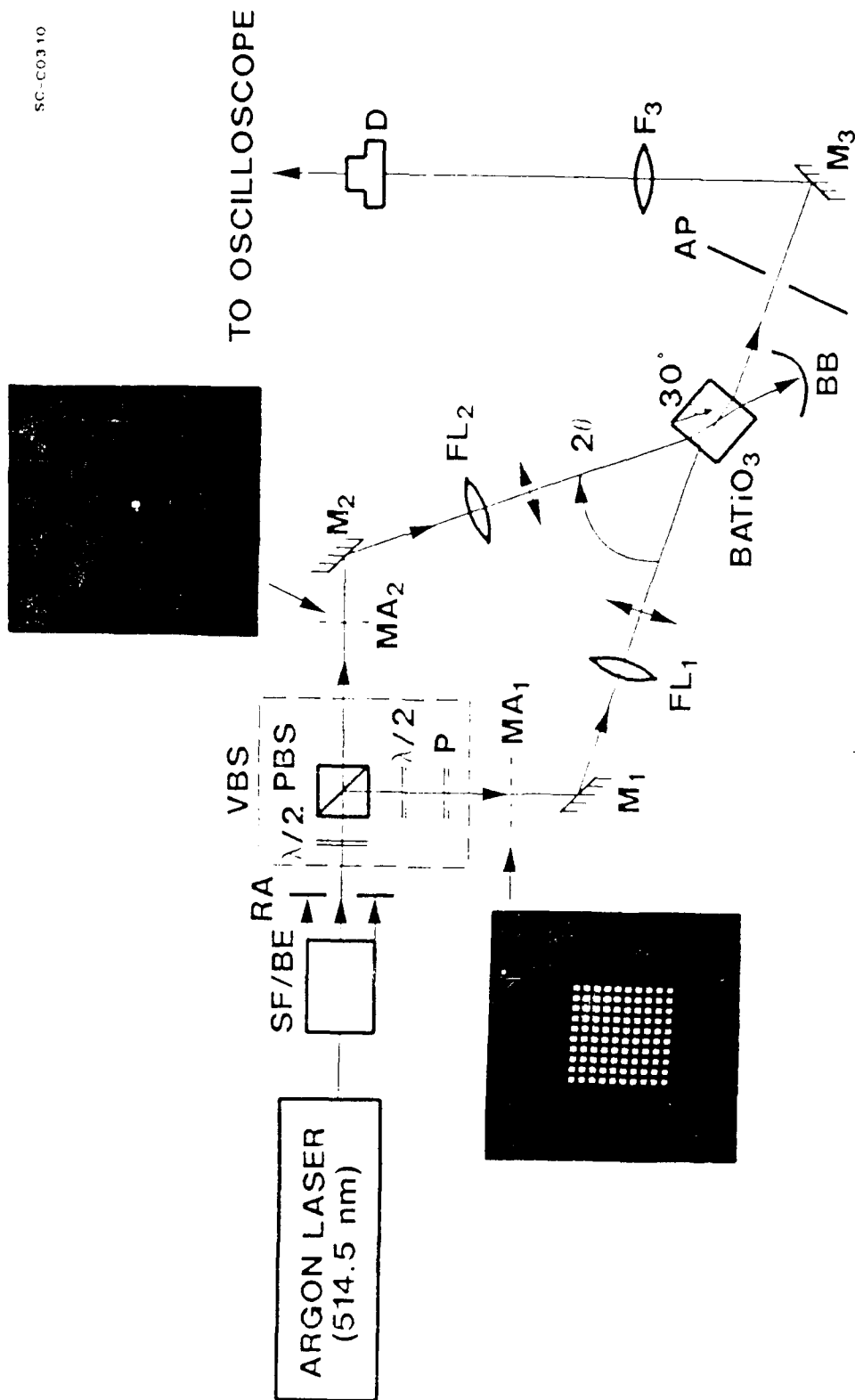


Fig. 6

SC49393

INTENSITY PATTERNS

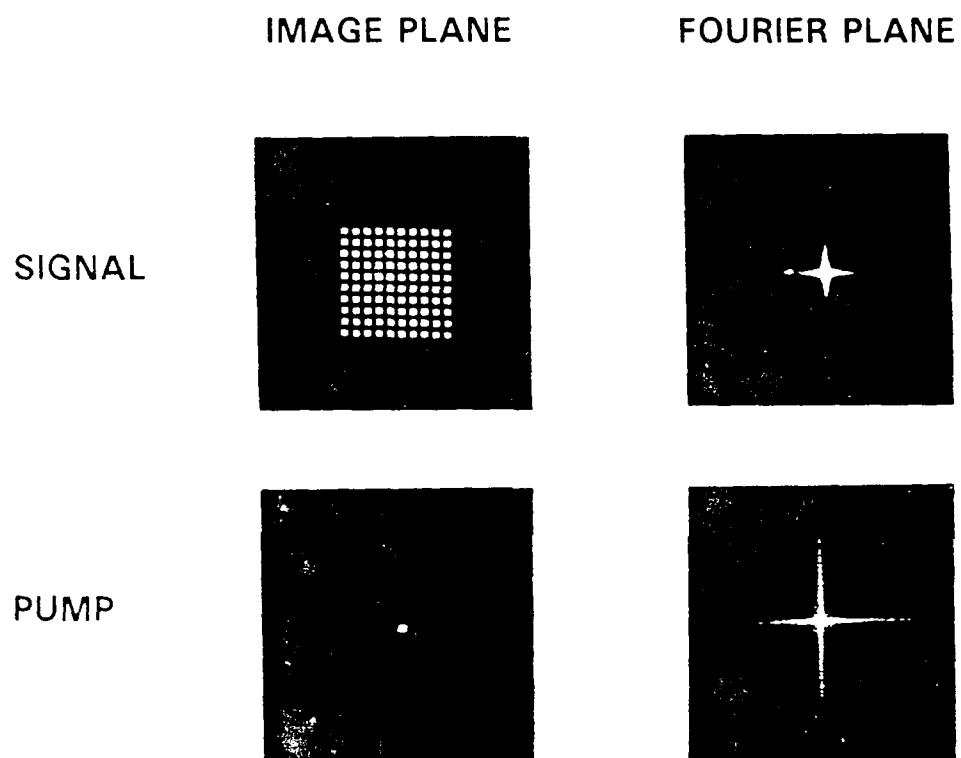


Fig. 7

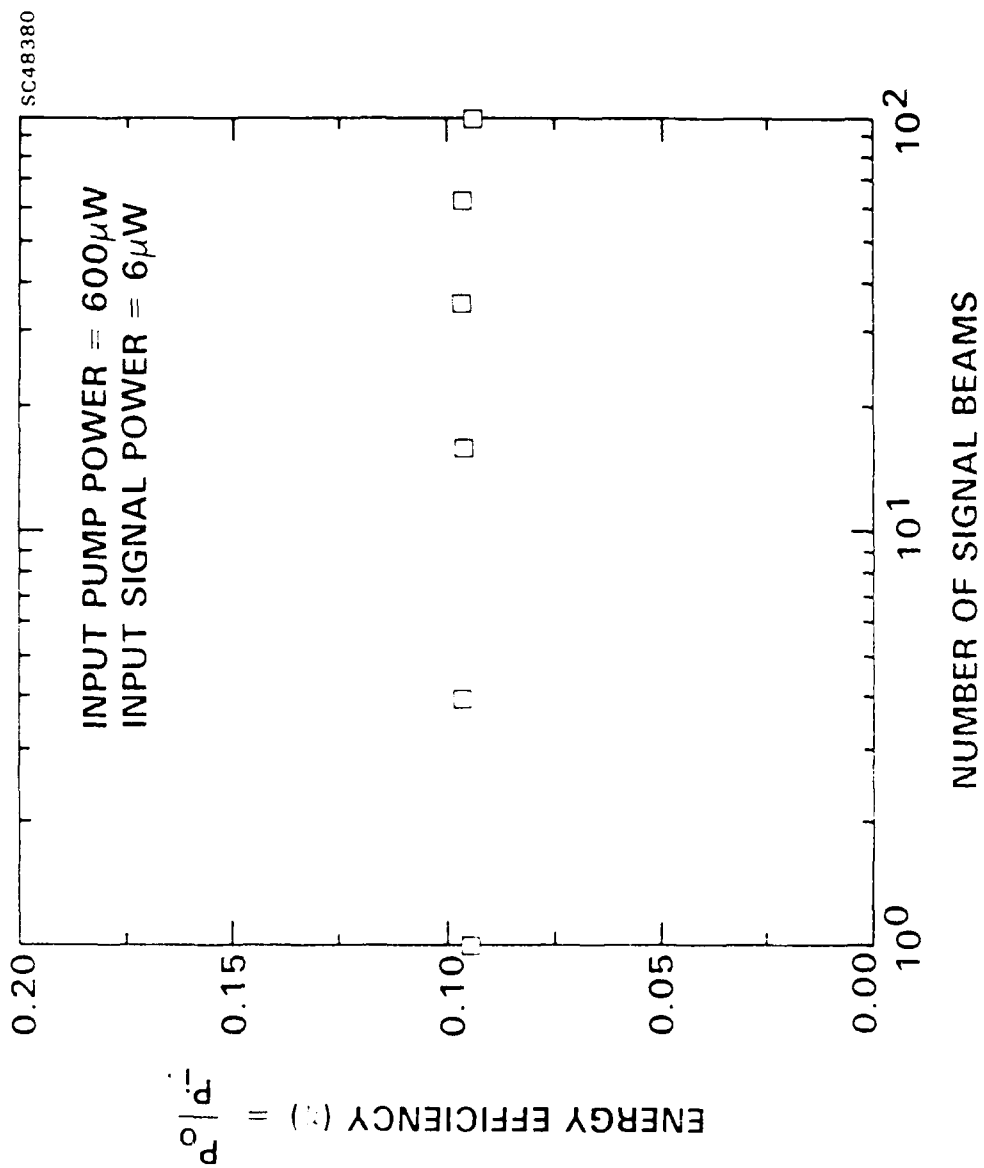
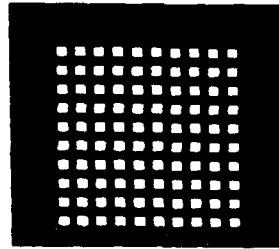


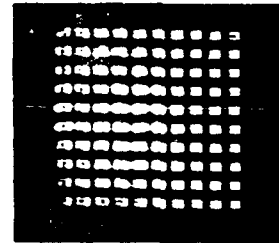
Fig. 8

SC49395

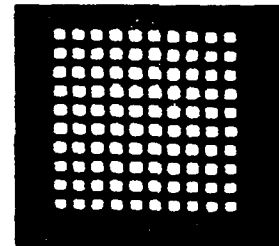
(a)



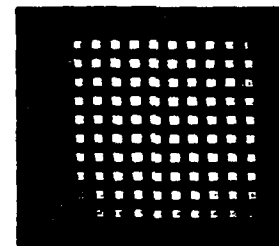
(b)



(c)



(d)



(e)

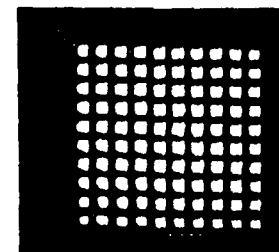
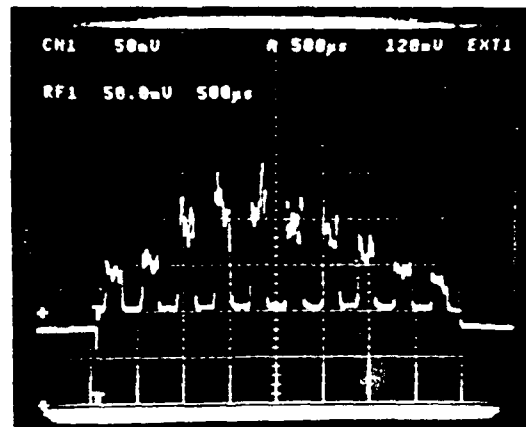
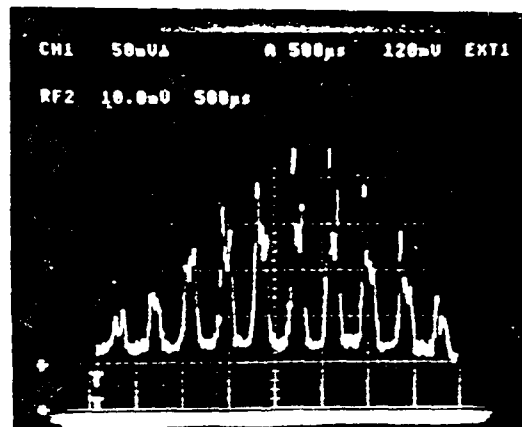


Fig. 9

(a)



(b)



(c)

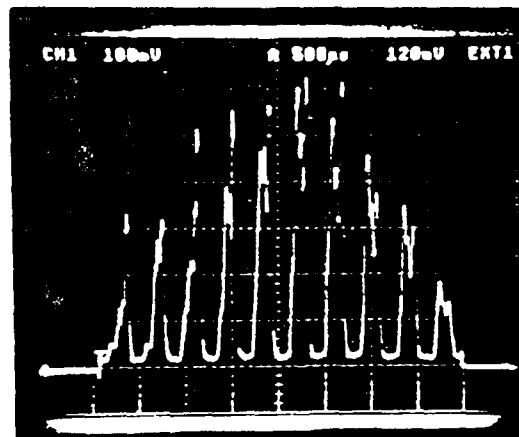
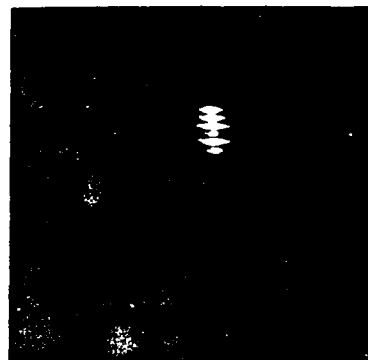
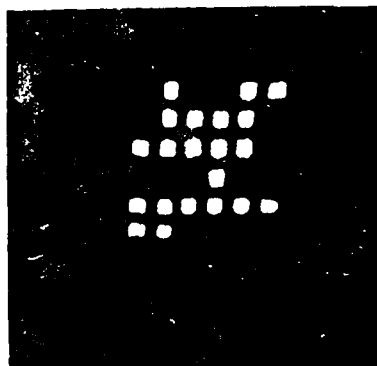


Fig. 10

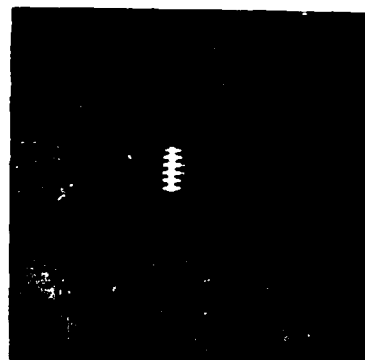
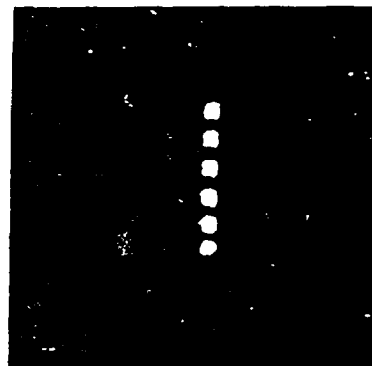
INTENSITY PATTERNS

IMAGE PLANE

CRYSTAL PLANE



SIGNAL



PUMP

Fig. 11



Rockwell International
Science Center

SC5502.FR

APPENDIX 5.8

On Image Amplification by Two-Wave Mixing in Photorefractive Crystals

On Image Amplification by Two Wave Mixing in Photorefractive Crystals

John H. Hong, Arthur E. Chiou, and Pochi Yeh
Rockwell Science Center
1049 Camino dos Rios, A25A
Thousand Oaks, CA 91360

Abstract

Coherent amplification of images by two wave mixing in photorefractive crystals is examined with attention given to processing in the Fourier domain. It is shown that the gain that is experienced as the probe image traverses the crystal is uniform across the image. The gain can be expressed as a well known function of the average probe to pump intensity ratio. Experimental verification is given to support the theory.

The phenomenon of energy transfer in two wave mixing in nonlinear optical media has been used effectively for the coherent amplification of images [1,2]. In diffusion driven photorefractive crystals, for example, it is known that the inherent 90° phase shift between the induced refractive index grating and the holographic intensity grating is responsible for the energy coupling. Shown in Fig. 1 is a typical image amplification experiment in which, with the correct geometry, the signal image wave becomes amplified at the expense of the pump wave intensity. The model that is currently being used to describe coherent image amplification is a simple one developed for the case of mixing two plane waves. Since the signal image wave can be expressed as a superposition of many plane waves whose propagation directions vary over a limited range (this range is small when compared to the difference between the average signal wave direction and the pump wave direction), the simple plane wave interaction model must be modified to be more accurately applicable. In this letter, we present a simple modification of the theory of two wave mixing involving image bearing beams and discuss in particular the amplification process when the crystal is placed at the Fourier transform plane of lens L1. Experimental evidence is also given to support the theory.

Shown in Fig. 2 is the image amplification geometry in which the amplitudes of the image bearing waves are represented by $\{E_j\}$, $j=1,2,\dots,N$, and the pump plane wave is denoted by E_p . In photorefractive crystals, the index modulation depends on the intensity interference pattern so that the present analysis begins with the intensity expression which is given by

$$I(\mathbf{r}) = I_0 \left\{ 1 + \frac{1}{I_0} \operatorname{Re} \left[E_p \sum_{m=1}^N E_m^* \exp[i(\mathbf{k}_p - \mathbf{k}_m) \cdot \mathbf{r}] + \sum_{q \neq m}^N \sum_{m=1}^N E_q E_m^* \exp[i(\mathbf{k}_q - \mathbf{k}_m) \cdot \mathbf{r}] \right] \right\}, (1)$$

where \mathbf{k}_p and \mathbf{k}_m are the wave vectors of the pump and the m th probe beams expressible, according to Fig. 2, by

$$\mathbf{k}_p = \frac{2\pi}{\lambda} (-\hat{x}\sin\theta + \hat{z}\cos\theta), \quad \mathbf{k}_m = \frac{2\pi}{\lambda} (\hat{x}\sin\theta_m + \hat{z}\cos\theta_m), \quad (2)$$

and the total intensity is $I_0 = |E_p|^2 + \sum_{m=1}^N |E_m|^2$. If the probe waves span a sufficiently small angular spectrum (much smaller than the angle between the pump and the average probe direction such that $N\delta\theta \ll \theta$), then the interference between the probe waves will induce index gratings which are much weaker than those written by the interference between the probe waves and the pump wave [3]. This is the scenario of interest, and the index distribution can then be approximated as

$$n = n_0 - \text{Re} \left\{ i \frac{n_1}{I_0} \sum_{m=1}^N E_p E_m^* \exp[-j(\mathbf{k}_p - \mathbf{k}_m) \cdot \mathbf{r}] \right\}, \quad (3)$$

where n_1 is the index modulation coefficient which is assumed to be the same for all of the gratings. The $\pi/2$ phase shift is due to the diffusion driven process. With this and the assumption of slowly varying amplitudes for each plane wave involved in the interaction, Maxwell's equations yield the following coupled system:

$$\begin{aligned} \frac{dE_p}{dz} &= -\frac{\gamma_p}{I_0} \sum_{m=1}^N |E_m|^2 E_p, & \gamma_p &= \frac{n_1 \lambda}{4 \cos \theta} \\ \frac{dE_m}{dz} &= \frac{\gamma_m}{I_0} |E_p|^2 E_m, \quad m=1,2,\dots,N, & \gamma_m &= \frac{n_1 \lambda}{4 \cos \theta_m}. \end{aligned} \quad (4)$$

The standard separation of intensity and phase equations is useful, and in particular, the intensities of the pump and probes, $I_p = |E_p|^2$ and $I_m = |E_m|^2$, are governed by

$$\begin{aligned} \frac{dI_p}{dz} &= -\frac{\Gamma_p}{I_0} \sum_{m=1}^N I_m I_p, & \Gamma_p &= 2\gamma_p \\ \frac{dI_m}{dz} &= \frac{\Gamma_m}{I_0} I_p I_m, \quad m=1,2,\dots,N, & \Gamma_m &= 2\gamma_m. \end{aligned} \quad (5)$$

In the assumed diffusion driven scenario, the phases of the beams are decoupled so that the intensity equations describe the two wave mixing process completely. To obtain the final desired result, we make one further approximation which is consistent with the assumptions made thus far. We have assumed that $\theta_m \approx \theta$, so that it is justified to approximate $\Gamma_p \approx \Gamma_m$. With this, the equations become

$$\begin{aligned}\frac{dI_p}{dz} &= -\frac{\Gamma}{I_0} \sum_{m=1}^N I_m I_p, \\ \frac{dI_m}{dz} &= \frac{\Gamma}{I_0} I_p I_m, \quad m=1,2,\dots,N.\end{aligned}\tag{5}$$

These equations are easily integrated to yield the following solutions.

$$\begin{aligned}I_p(z) &= \frac{\beta I_0 \exp(-\Gamma z)}{1 + \beta \exp(-\Gamma z)}, \\ \frac{I_m(z)}{I_m(0)} &= \frac{1 + \beta}{1 + \beta \exp(-\Gamma z)}, \quad \beta = \frac{I_p(0)}{\sum_{m=1}^N I_m(0)}\end{aligned}\tag{6}$$

The above is the main result of this letter. The solutions indicate that the probe waves are amplified uniformly with a gain factor which is a function of the ratio of the pump beam to the total intensity of the probes. Small deviations from this are expected as the coupling coefficient is a function of the actual probe beam angle, and also as harmonic distortions of the gratings result from the modulation depth approaching unity [4-6].

The uniformity of the amplification has been verified by the following experiment (see Fig. 3). An output beam from an argon laser (514.5 nm) is spatially filtered and expanded to pass through a rectangular aperture (RA: 2mm x 6mm). A variable beam splitter consisting of two half-wave plates and a polarizing beam splitter cube is used to split the incoming beam into two (the pump and the probe) and to vary the intensity ratio of the pump and the probe beams; the polarizer positioned after the half wave plate in the

reflected path ensures that both transmitted and reflected beams have the same polarizations. The probe beam is transmitted through five rectangular windows (0.5mm x 2mm each) in a mask (MA_1) to form 5 probe beamlets. In the other arm, the pump beam illuminates an identical rectangular window in a second mask (MA_2). Two spherical lenses (FL_1 and FL_2), one in each arm, are used to Fourier transform the two spatial patterns onto the crystal plane. A spherical lens (FL_3) is used to re-image the spatial pattern carried by the amplified probe beam onto the detector plane where the optical intensity profile is sampled by a linear detector array and monitored by a storage oscilloscope. We have varied the pump-to-total probe power ratio in the range $1000 \sim 1$ and observed that the energy transferred from the pump is equally distributed among the probe beamlets to within 20%. A typical example of the intensity profiles is shown in Fig. 4. The lower trace is the intensity profile of the five probe beamlets transmitted through the crystal when the pump is off. The upper trace represents the corresponding profile when the pump beam is turned on. For this specific case, the optical powers of the pump and the total probe are 0.6 mW and 0.2 mW, respectively. When all but one of the probe beamlets are blocked, almost all of the depleted pump energy, originally distributed among the five channels, redirects itself into the single unblocked channel.

The dynamics of grating adjustments made by multiple probe beams were observed in the following experiment. A $BaTiO_3$ crystal was placed at the intersection of two weak probe waves and a strong pump beam as shown in Fig. 5. As shown, the two probes were arranged so that they propagate with a small angle (~ 1 degree) between them in comparison with the angle between them and the pump beam (~ 30 degrees). The results are shown in Figs. 6a-b. The input intensities of the two probes were roughly the same ($P \sim 10 \mu W$) with the input pump power set at $P = 5 mW$. Shown in Fig. 6a are the probe intensities (after passage through the crystal as seen by detectors 1 and 2) as they are strobed on with shutters. The amount of pump power that is scattered into the probe detectors was small compared to the unamplified probe intensities and correspondingly

becomes negligible when compared to the amplified probe beams. Fig. 6b shows the amplified probe beams as the probes were strobed by the shutters (top trace=probe1, bottom trace=probe2; scale factor=1V/mW). The power sharing is clearly evident in the mid portion of the trace where both probes are on. When the order of events were changed so that probe 2 was turned on first, the results were the same so that no hysteresis effects were seen. Note that probe 1 is slightly stronger than probe 2. This is due to the fact that the two beam coupling constants (one for each probe) were not the same.

In conclusion, we have analyzed the two wave mixing phenomenon when a multitude of probe beams are used. The theoretical results shown indicate that the pump power is shared by the probe beams. Experimental evidence was given to validate this power sharing effect.

We acknowledge useful discussions with our colleagues, Fred Vachss and Ragini Saxena. Also, at the time of the submission of this paper, work [7] presented at the OSA annual meeting and another recently published [8] which dealt with similar subjects were brought to our attention. This work is supported primarily by the Defense Advanced Research Agency.

Reference

1. N. V. Kukhtarev, V. B. Markov, S. G. Odulov and M. S. Soskin, "Holographic storage in electro-optic crystals II. Self amplification," *Ferroelectrics* **22**, p.961 (1979).
2. J. P. Huignard and A. Marrakchi, "Coherent signal beam amplification in two-wave mixing experiments with photorefractive $\text{Bi}_{12}\text{SiO}_{20}$ crystals," *Opt. Comm.* **38**, p.249 (1981).
3. D. Z. Anderson and R. Saxena, "Theory of multimode operation of a unidirectional ring oscillator having photorefractive gain: weak field limit," *J. Opt. Soc. Am. B* **4**, p.164 (1987).
4. E. Ochoa, F. Vachss and L. Hesselink, "Higher-order analysis of the photorefractive effect for large modulation depths," *J. Opt. Soc. Am. A* **3**, p.181 (1986).
5. Ph. Refrigier, L. Solymar, H. Rajenbach and J. P. Huignard, "Two beam coupling in Photorefractive $\text{Bi}_{12}\text{SiO}_{20}$ crystals with moving gratings: theory and experiments," *J. Appl. Phys.* **58**, p.45 (1985).
6. F. Vachss and L. Hesselink, "Nonlinear photorefractive response at high modulation depths," *J. Opt. Soc. Am. A* **5**, p.690 (1988).
7. G. C. Gilbreath and F. M. Davidson, "Spatial light modulation using two-wave mixing properties of photorefractive materials," *Opt. Soc. Am. 1988 Ann. Meet. Tech. Digest (THU6)*, p 144.
8. J. Man, L. Liu, S. Wu, Z. Wang, L. Xu and B. Shu, "Multibeam coupling in photorefractive $\text{SBN}:\text{Ce}$," *Opt. Lett.* **13**, #11, p.1020 (1988).

Figure Captions

1. Typical image amplification experiment using two wave mixing in photorefractive crystals.
2. Two wave mixing with the crystal at the Fourier plane of the input image. The pump E_p is a plane wave and the image effectively consists of a set of point sources.
3. Experimental setup used to verify uniform gain. MA1 consists of five identical apertures and comprises the probe image to be amplified. Because of the gaussian illumination, the intensity pattern at MA1 is not uniform. MA2 is the pump image aperture.
4. Input (lower amplitude) and amplified (higher amplitude) intensity distributions. Each portion of the overall input distribution receives roughly the same gain.
5. Experimental setup used to record the dynamics of multiple grating buildup.
6. Dynamics of two gratings in the same volume. a) input probe intensities (upper corresponds to #1 and lower #2 in reference to Fig. 5). b) output amplified intensities (history: #1 turned on, #1 turned off, #2 turned on, #2 turned off, #1 turned on, #2 turned on, #1 turned off, ...).

SC47546

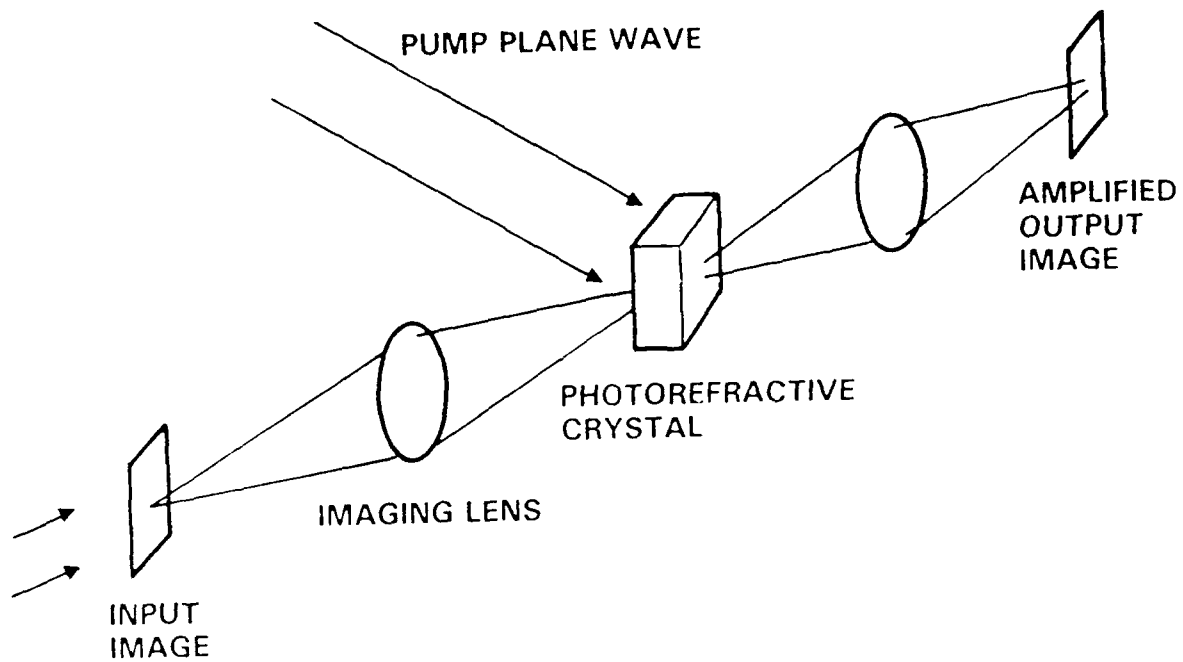


Fig. 1

SC47544

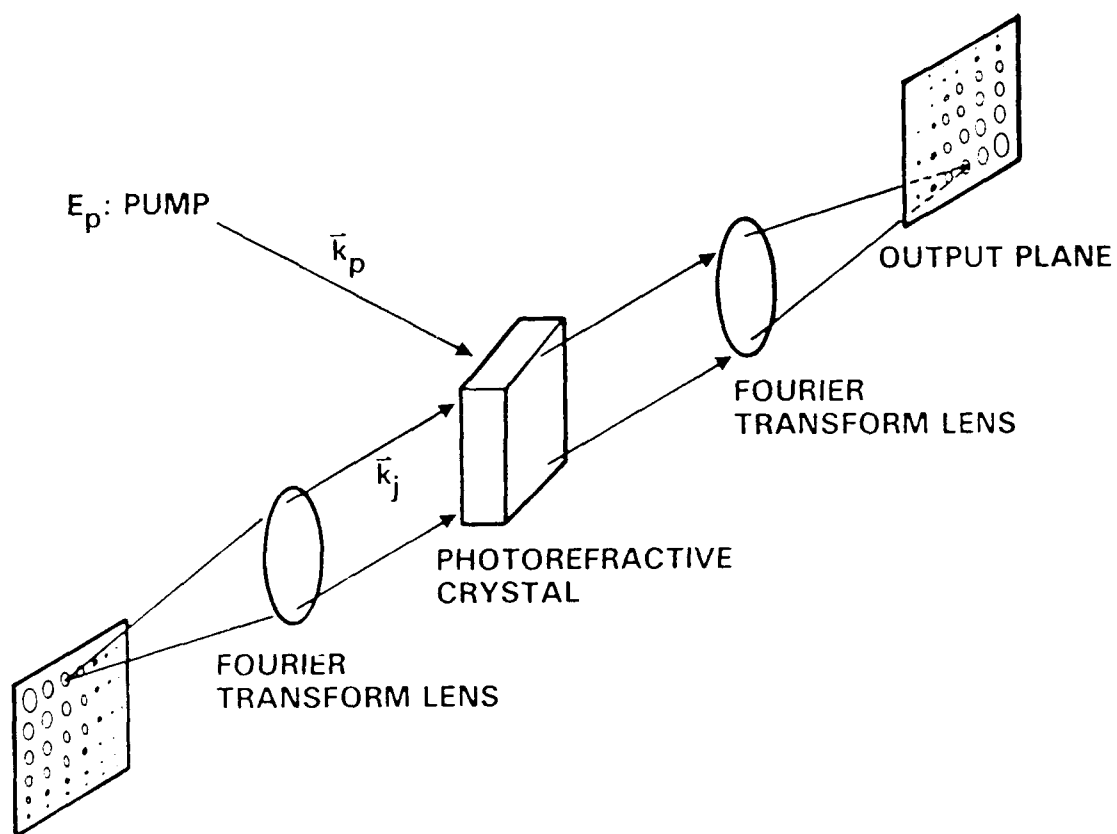


Fig. 2

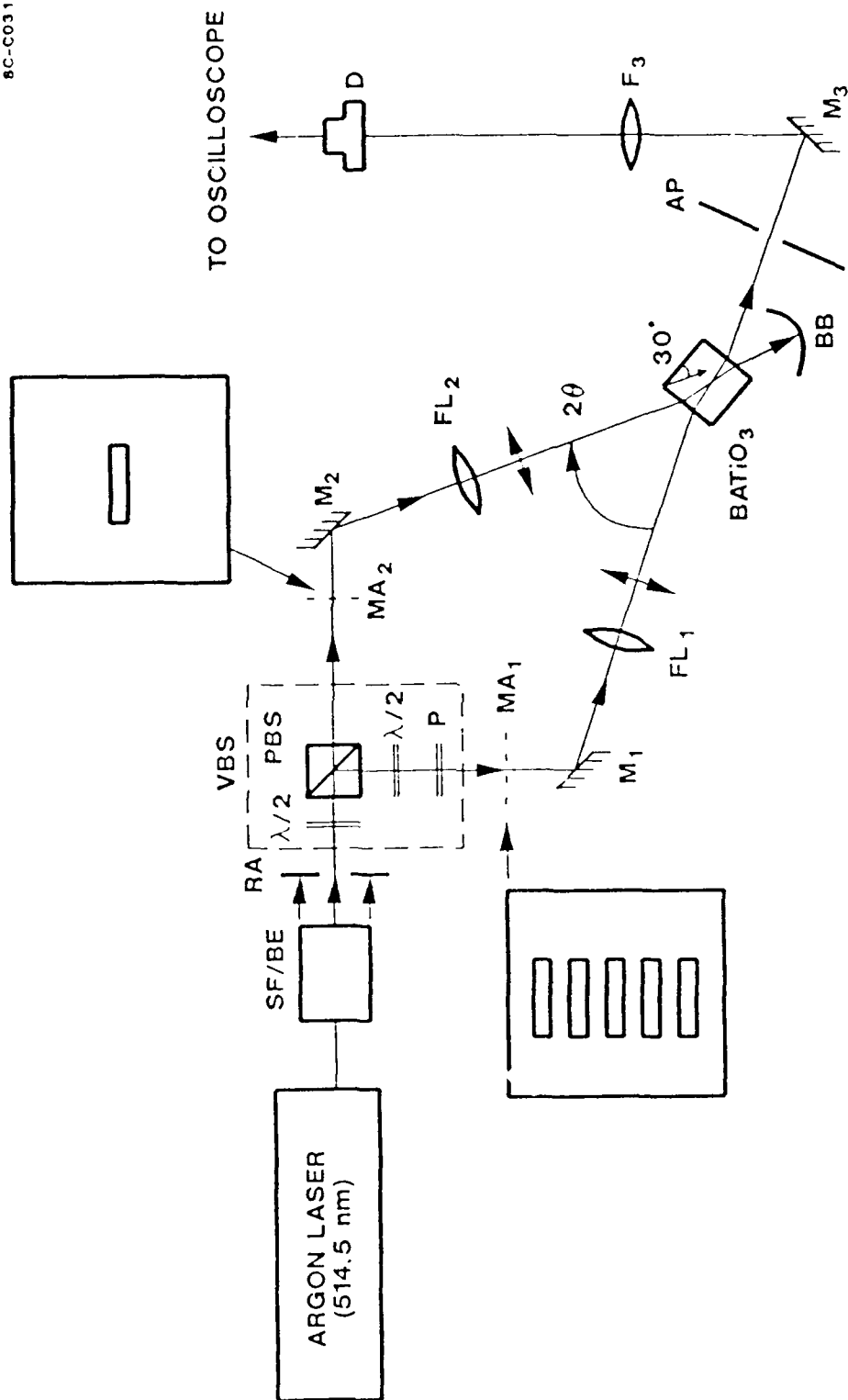


FIG. 3

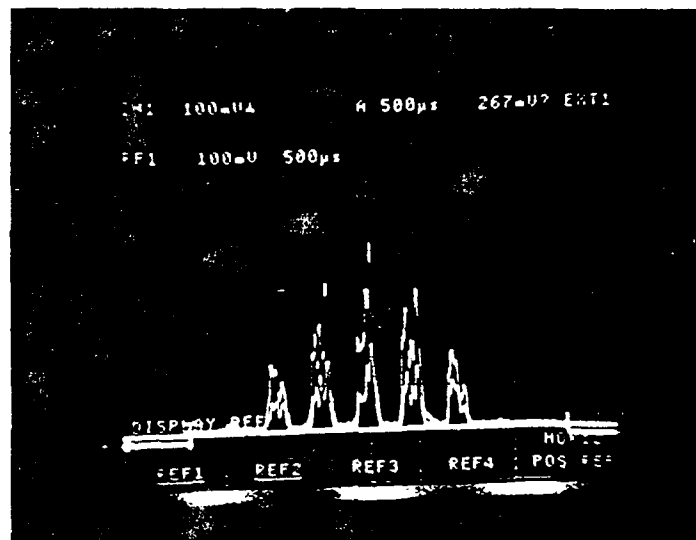


Fig. 4

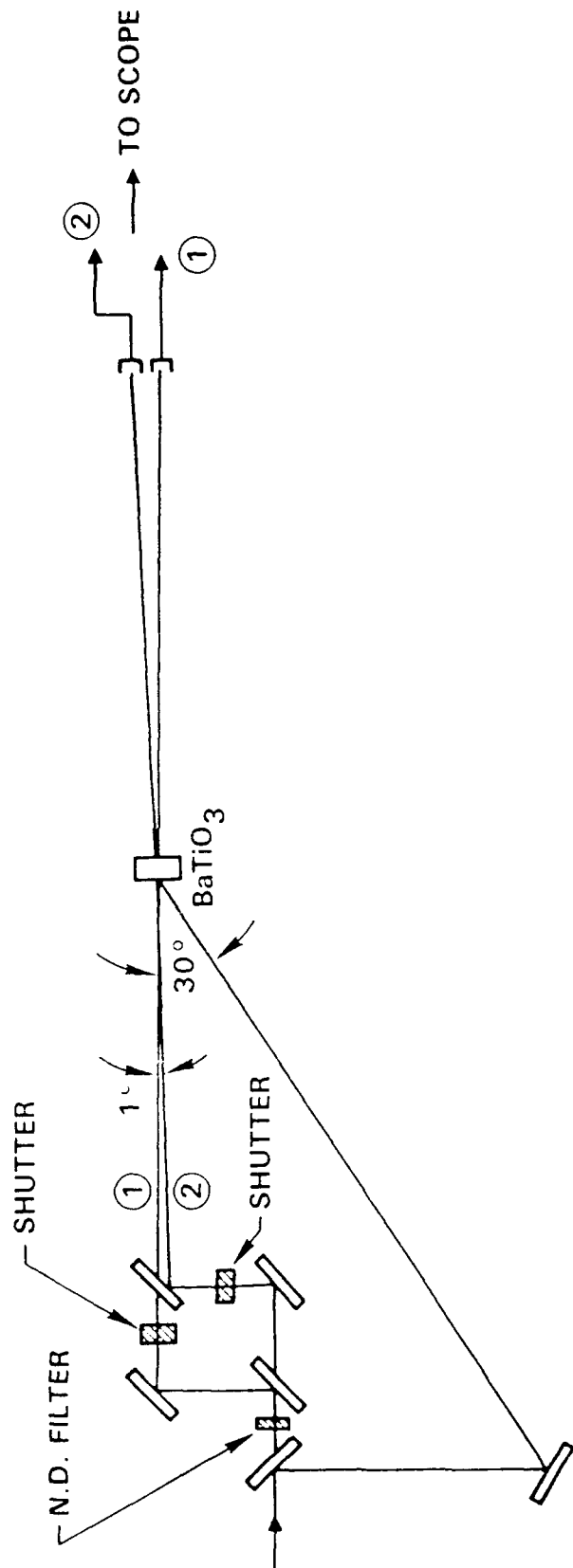


FIG. 5

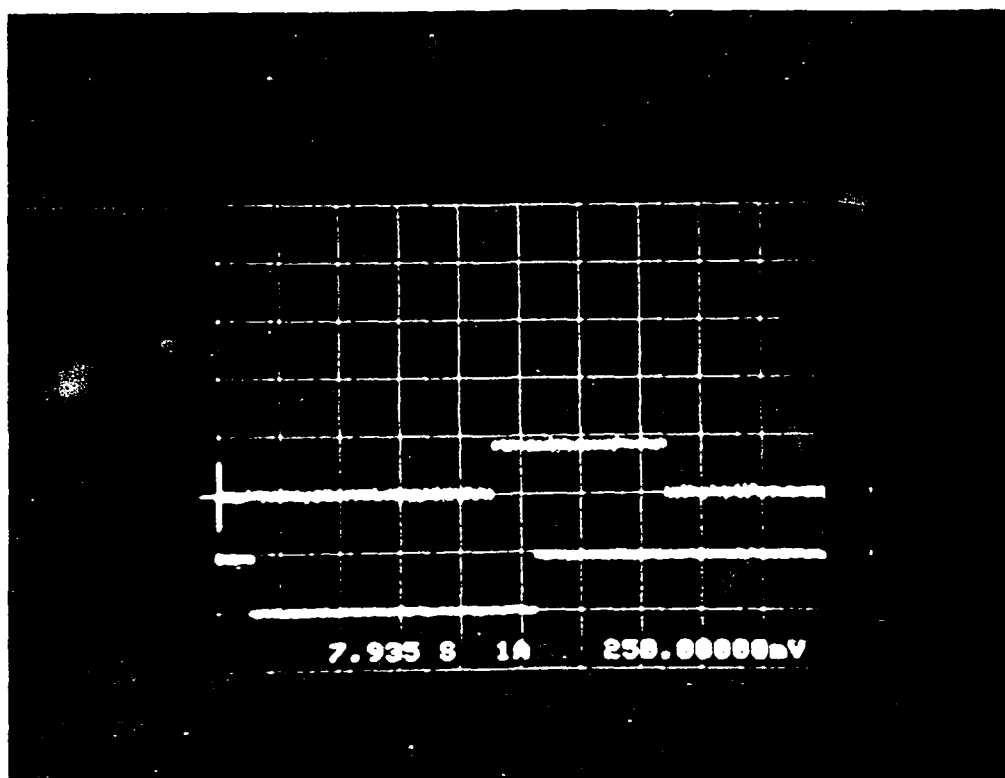


Fig. 6 (a)

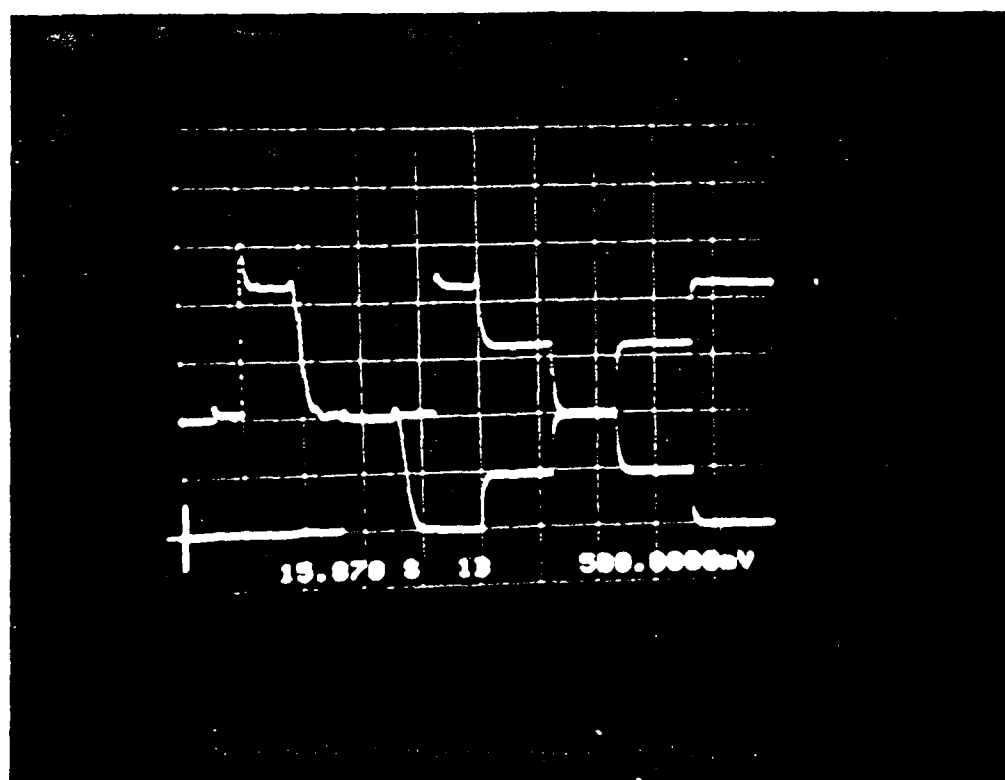


Fig. 6 (b)



Rockwell International
Science Center

SC5502.FR

APPENDIX 5.9

Reconfigurable Optical Interconnection Using Photorefractive Holograms

Reconfigurable optical interconnection using photorefractive holograms

Arthur Chiou, Pochi Yeh, Scott Campbell, and John Hong

Rockwell International Science Center
1049 Camino Dos Rios, Thousand Oaks, CA 91360

ABSTRACT

The use of photorefractive holograms in conjunction with a spatial light modulator (SLM) to realize a reconfigurable optical interconnection with very high energy efficiency is briefly discussed. In this approach, the SLM is used as a programmable binary matrix mask to encode the interconnection pattern to a coherent laser beam whereas the photorefractive crystal is used as a dynamic holographic medium to store the pattern and to efficiently diffract the readout beam into the selected channels at high speed. We report recent experimental results on issues such as energy efficiency, reconfiguration time, contrast, and uniformity.

1. INTRODUCTION

Optical interconnection between VLSI circuits, computing chips or boards plays an important role in parallel optical computing.^{1,2} Such a scheme of computing provides the potential of achieving extremely high speed because it uses the fast switching of electronics and the wide bandwidth and massive parallelism of optics for communication.³ A generalized optical crossbar switch can provide an arbitrary and reconfigurable interconnection^{4,5} between an array of N lasers and an array of N detectors. Conceptually, such an interconnection can be achieved by using optical matrix-vector multiplication,⁵⁻⁸

$$\mathbf{V}' = \mathbf{M}\mathbf{V}, \quad (1)$$

where \mathbf{V} is the input vector representing the signals carried by an array of N lasers and \mathbf{V}' is the output vector representing the signals received by the array of detectors. \mathbf{M} is an $N \times N$ binary matrix representing the interconnection pattern. Such an architecture provides the N^2 parallelism required for arbitrary interconnection. When an SLM is used as the matrix mask, the interconnection is reconfigurable.

The N^2 parallelism is accompanied with an intrinsic fan-out energy loss;^{4,9} the fan-out leads to an energy efficiency of $1/N$. For interconnection with large N (e.g., $N \sim 1000$), this large amount of energy loss is intolerable. We recently proposed and demonstrated a novel concept of reconfigurable optical interconnection^{9,10} which can provide very high energy efficiency. Using the nonreciprocal energy coupling in photorefractive crystals,¹¹⁻¹⁴ such a scheme of interconnection is capable of minimizing the fan-out energy loss; thus, it achieves extremely high energy efficiency. Although the basic concept has been validated^{9,10} using fixed binary matrix masks (or transparencies) and the energy efficiency has been measured and reported,^{15,16} the demonstration of reconfigurability with high energy efficiency and high signal-to-noise-ratio (S/N) using an SLM remains a subject of experimental investigation. This paper reports the results of the investigation on the contrast of reconfigurable optical interconnection using a liquid crystal television (LCTV) in conjunction with a photorefractive barium titanate crystal. The effect of finite contrast of the SLM on the performance of the holographic interconnection is also discussed.

In what follows, we will briefly review the basic principle of operation of the photorefractive interconnection. We will summarize some of our earlier results on energy efficiency measurement and on the use of Fourier transforms to achieve maximum beam

overlap in the photorefractive medium.¹⁶ We then discuss the results of our experimental investigations on the issue of contrast.

2. PRINCIPLE OF OPERATION

Figure 1 shows the basic idea of reconfigurable optical interconnection using photorefractive holograms. A beam splitter is used to split off a small portion of the beam which consists of beamlets each carrying information from one of the sources. This small portion of the beam will be called the signal beam. The beam splitter allows the majority of the energy to pass through. This major portion of the beam is called the pump beam. The signal beam is fanned by the cylindrical lens and then passes through the spatial light modulator (SLM) which contains the interconnection pattern. After passing through the SLM, the signal beam is imprinted spatially with the interconnection pattern. The pump beam does not pass through the spatial light modulator and thus suffers no energy loss due to the fan-out and all other loss mechanisms associated with the SLM.

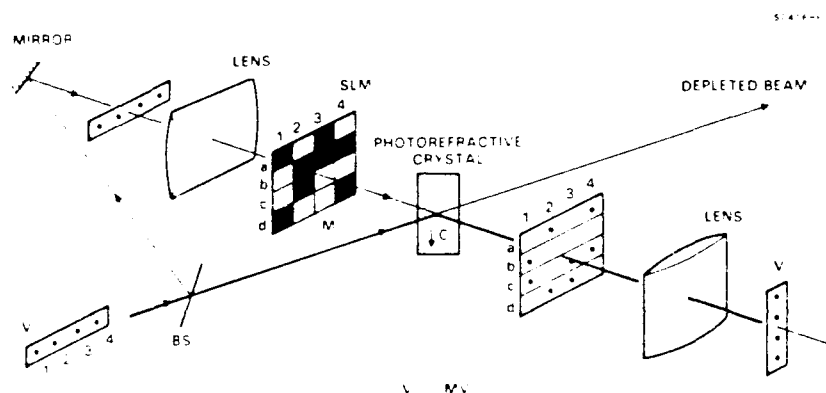


Fig. 1 A schematic diagram illustrating the basic idea of a reconfigurable optical interconnection using a photorefractive crystal in conjunction with a spatial light modulator.

The signal beam which contains the interconnection information is then recombined with the pump beam in a photorefractive crystal. Under the appropriate conditions, the signal beam can be amplified at the expense of the pump beam. Most of the energy of the pump beam will be transferred to the signal beam provided the length of interaction is large enough.^{13, 14}

Although photorefractive two-wave mixing is involved, such a scheme can also be considered as a real-time holographic interconnection with a very high diffraction efficiency. The combination of the beam splitter and the SLM in conjunction with the pump beam is used to record a hologram inside the photorefractive crystal. Such a hologram contains the interconnection as prescribed by the SLM. Once the hologram is formed, the pump beam can be diffracted off the hologram and be redirected into the array of detectors. The advantage here is that the recording and the readout occur simultaneously. This offers the possibility of reconfigurable interconnection by controlling the SLM.

To achieve maximum energy efficiency, it is important that the signal beam and the pump beam overlap completely. Specifically, beamlet 1 of the pump beam in Fig. 1 must overlap completely with column 1 of the signal beam. And similarly, beamlets 2, 3, and 4 must also overlap completely with their corresponding columns in the signal beam. Although the beamlets in the signal beam and the pump beam are intrinsically different because of the interconnection pattern, the individual pixels can have identical shape (e.g., square). Complete overlap is

possible in the Fourier domain, provided all the pixels are identical. The results of our experimental investigations of beam overlap and the energy efficiency were presented recently¹⁵ and discussed in detail in a separate paper.¹⁶ The key results pertinent to the energy efficiency are summarized in the next section.

3.0 ENERGY EFFICIENCY

We first investigated the energy efficiency due to beam coupling in a photorefractive crystal. Referring to Fig. 2, we define the efficiency (η) of energy transfer in photorefractive holograms as $\eta = P_o/P_i$, where P_i and P_o are the optical power of the input beam and the amplified signal beam, respectively. A theoretical expression of such an energy efficiency was derived earlier in reference 9. Using an uncoated barium titanate crystal ($\sim 5 \times 7 \times 7$ mm, 30° -cut, from Sanders Associates) as the photorefractive medium and an argon ion laser (514.5 nm) as the source, we have achieved an energy efficiency as high as 30%. Further improvement in energy efficiency can be achieved by coating the crystal surfaces with antireflection dielectric films and by using crystals with higher coupling constants. Ultimately, the energy efficiency is limited by the bulk absorption in the crystal.

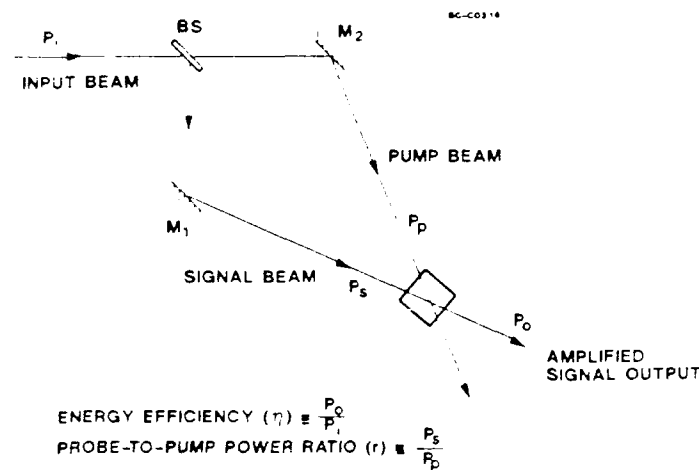


Fig. 2 An experimental configuration for measuring the energy efficiency in photorefractive two-beam coupling.

Using an experimental configuration as schematically illustrated in Fig. 3, we have also successfully demonstrated^{15,16} that :

- the energy efficiency is insensitive to the lateral position of the signal window in the SLM (shift-invariant).
- the energy efficiency is insensitive to the number of signal channels
- the energy distribution among all the signal channels is fairly uniform.

The properties listed above are due to matched amplification at the Fourier plane.¹⁶ As indicated in Fig. 3, each individual pixel of the signal beam is identical to that of the pump beam to ensure maximum beam overlap at the Fourier plane. Another desirable characteristic of two-wave mixing at the Fourier plane is the preservation of contrast of the input pattern. In the next section, we discuss the issue of contrast and a simple method to enhance the contrast.

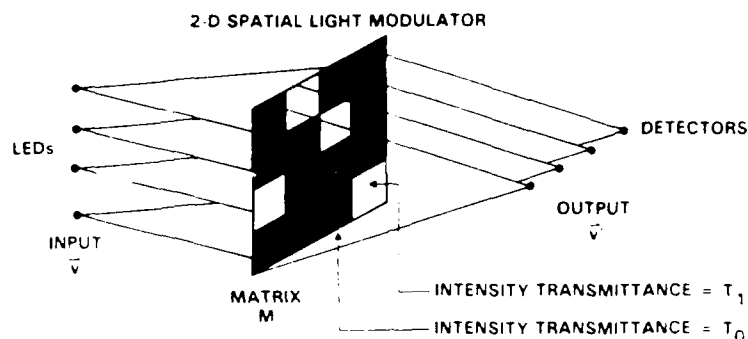


Fig.4 Reconfigurable interconnection using an SLM with finite contrast.

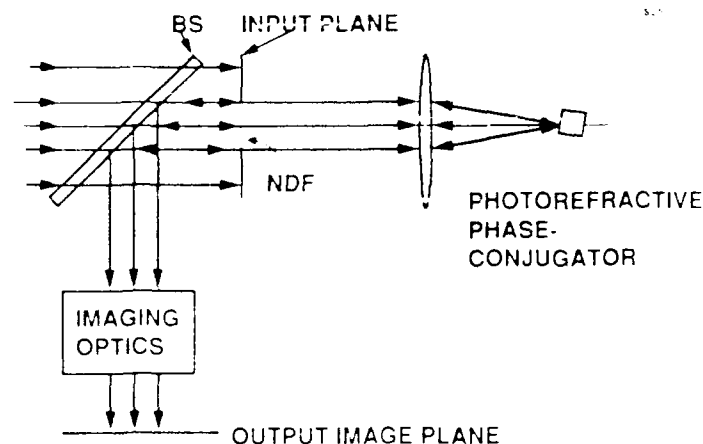


Fig. 5 An experimental configuration for contrast-enhancement by double-passage.

binary amplitude mask at the input plane. The transmitted beam is collected by a lens (L) and directed into a barium titanate crystal. The crystal is oriented so that the incoming beam is retro-reflected via self-pumped phase conjugation.¹⁹ After traversing through the aperture, the phase conjugated beam is sampled by a beam splitter through imaging optics which reimages the binary mask on the output plane. The input intensity distribution (i.e. single-passage through the mask) and the output intensity distribution (i.e., double-passage through the mask) are measured by scanning a detector with a small aperture (diameter $\approx 1\text{mm}$) across the beam diameter at the input and the output planes, respectively. The experimental results (for a mask with optical density $\text{OD} = 0.5$) are shown in Fig. 6(a) and (b). Apart from some imperfection at the edge of the output image, the output contrast ratio is approximately the square of that of the input as expected. Instead of a phase-conjugate mirror, a plane mirror can also be placed at the input plane immediately after the mask to retro-reflect the beam back through the binary mask. The resulting intensity distribution is shown in Fig. 6(c). We have repeated the same measurement with a different NDF ($\text{OD} = 1.0$) and also with a LCTV at the input plane; the results are tabulated in Table I. Photographs of the output image of an arbitrary binary pattern written on a LCTV are shown in Fig. 7(a) for mirror reflection and (b) for self-pumped phase conjugation. The phase conjugation has the key advantage of being intrinsically self-aligned. The grating formation time for self-pumped phase conjugation using a typical barium titanate

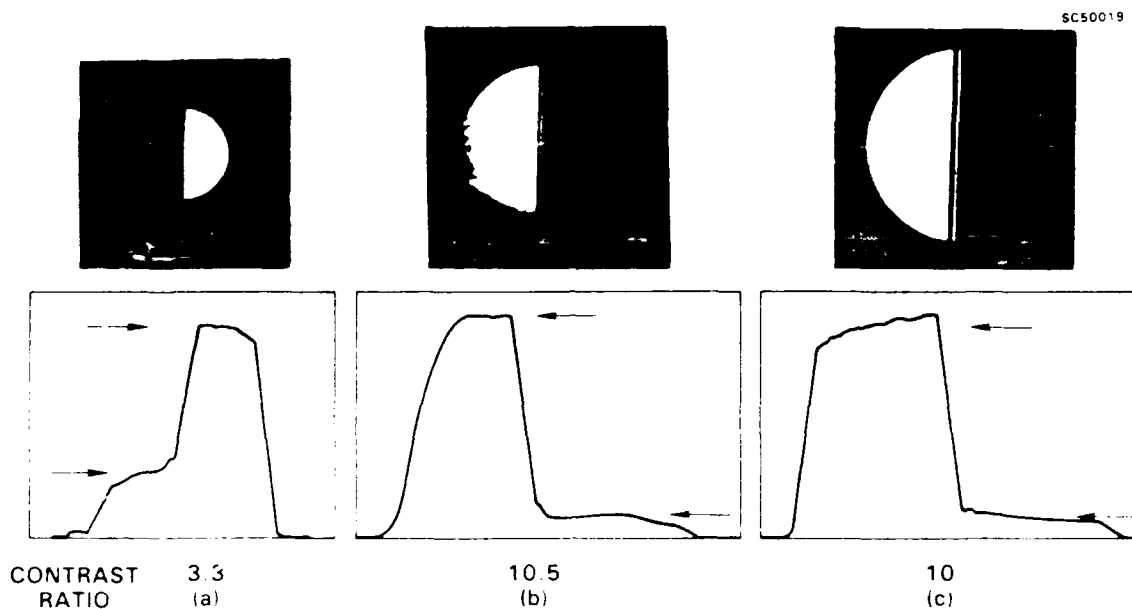


Fig.6 Intensity profiles and contrast of a binary image: (a) at the input plane, (b) at the output plane after double-passage via phase-conjugate reflection, (c) at the output plane after double-passage via mirror reflection. The arrows indicate the intensities (of the bright and dark regions) used for calculating the contrast ratio.

Table 1
Contrast Enhancement of Binary Images by Double-Passage

CONTRAST RATIO OF VARIOUS IMAGES

AMPLITUDE MODULATION	SINGLE PATH		DOUBLE PATH	
	INPUT	PHASE- CONJUGATE OUTPUT	PHASE- CONJUGATION	MIRROR REFLECTION
OD0.5	3.3	3.5	10.5	10.0
OD1.0	10.0	11.1	96	96
LCTV	14	20	~80	~100

crystal at a few tens of milliwatt of optical power is, however, relatively slow (a fraction of a second to several seconds). Note that the output obtained by mirror reflection is fairly uniform (see Fig.6(c) and Fig.7(a)) and the reflection is practically instantaneous.

The photorefractive interconnection holograms used to diffract the pump beam into the signal channels specified by the matrix mask do not degrade the contrast provided that the photorefractive crystal is placed at the Fourier plane.^(6,7) In contrast, photorefractive image amplification via two-wave mixing in the image plane tends to decrease the contrast of the



Fig.7 Double-passage image of a binary matrix pattern on a liquid crystal T.V. (a) via mirror reflection, (b) via phase-conjugate reflection.

input image.^{22,23} An experimental result verifying this contrast preserving property is given in Fig. 8. Intensity profiles of a binary image and its amplified output are shown in (a) and (b), respectively. Note that the contrast ratio of the input and the output image are almost identical and that the vertical scale in (b) is 20 times that of (a).

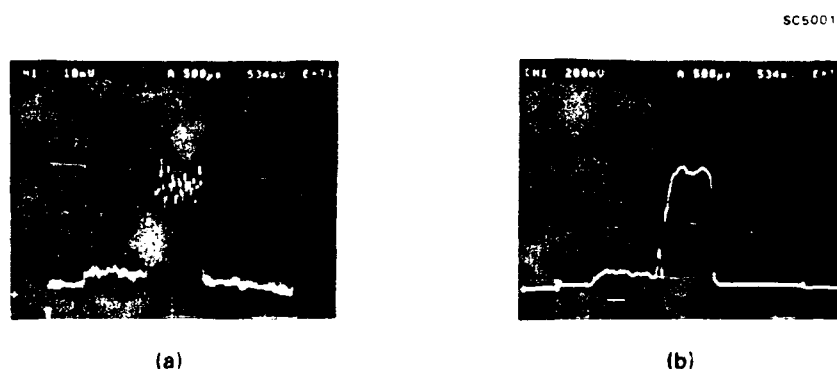


Fig.8 Experimental results showing contrast-preserving image amplification by photorefractive two-wave mixing at the Fourier domain; (a) input intensity profile, (b) amplified output intensity profile.

To extrapolate from the above discussion, if an SLM with a contrast ratio of the order of 100 (for example, a ferroelectric liquid crystal SLM) is used in the double passage mode, the maximum number of channels (M) of a $M \times M$ crossbar switch limited by the contrast ratio of the SLM can be as high as 10^4 .

5.0 EXPERIMENTAL DEMONSTRATION OF RECONFIGURABILITY

Using an experimental configuration similar to the one illustrated in Fig. 3, with the photographic mask (transparency) replaced by an SLM, we have demonstrated the reconfigurability of the interconnection by writing new interconnection patterns on the LCTV. The patterns are generated by an IBM PC and sent to the LCTV. With optical power of the order of tens of milliwatts, the frame rate is currently limited by the photorefractive response time to a few frames per second. The data rate, however, is not limited by the photorefractive response time and can be higher than several megahertz.⁹ To enhance the contrast of the binary pattern, the signal beam is passed through the SLM twice via a retroreflecting mirror (as described in Section 4.0) prior to interacting with the pump beam in a photorefractive barium titanate crystal.

6. SUMMARY

We have described a novel method for reconfigurable interconnections using photorefractive holograms in conjunction with an SLM. Several important features, including high energy efficiency ($> 30\%$), uniform energy distribution, and high data rate transmission ($> \text{several megahertz}$) of this dynamic holographic interconnection are discussed. We have also described the problem associated with the finite contrast of the SLM and have shown that the contrast can be greatly enhanced (i.e., squared) by double passage through the SLM either by a retro-reflecting mirror or by a phase-conjugator. We also report the demonstration of reconfigurability by using a LCTV in conjunction with a photorefractive barium titanate crystal.

7. ACKNOWLEDGEMENT

We thank F. Vachss for helpful technical discussions. This work is partially supported by DARPA/AFOSR under Contract No. F49620-87-C-0015.

8.0 REFERENCES

1. See, for example, J.W. Goodman, F.I. Leonberger, S.Y. Kung, and R.A. Athale, "Optical Interconnections for VLSI Systems," *Proc. IEEE* 72, pp. 850, 1984.
2. See, for example, J.A. Neff, Ed., Optical Computing, *Proc. SPIE* 625, pp. 109, 1986.
3. C. Mead, "Potential and Limitation of VLSI," Topical Meeting on Optical Computing, *Technical Digest 1985*, (Optical Society of America, Washington, D.C. 1985) MA2-1.
4. A.A. Sawchuk, and B.K. Jenkins, "Dynamic Optical Interconnections for Parallel Processors," *Proc. SPIE* 625, pp. 143, 1986.
5. A.A. Sawchuk, B.K. Jenkins, C.S. Raghavenura, and A. Varma, "Optical Crossbar Networks," *IEEE Computer* 20, No. 6, pp. 50, 1987.
6. J.W. Goodman, A.R. Dias, and L.M. Woody, "Fully Parallel, High-speed Incoherent Optical Method for Performing Discrete Fourier Transforms," *Opt. Lett.* 2, pp. 1, 1978.
7. W.T. Rhodes, "Optical Matrix-Vector Processors: Basic Concepts," *Proc. SPIE* 614, pp. 146, 1986.
8. R.A. Athale, "Optical Matrix Processors," *Proc. SPIE* 634, pp. 96, 1986.
9. P. Yeh, A.E.T. Chiou, and J. Hong, "Optical Interconnection Using Photorefractive Dynamic Holograms," *Appl. Opt.* 27, pp. 2093, 1988.
10. A.E. Chiou, P. Yeh, and J. Hong, "Energy Efficient Optical Interconnection Using Dynamic Holograms in Photorefractive Media," OSA Annual Meeting, *1988 Technical Digest Series*, Vol. 11, (Optical Society of America, Washington, D.C. 1988), pp. 178.
11. N.V. Kukhtarev, et al, "Holographic Storage in Electrooptic Crystal. I. Steady State," *Ferroelectrics* 22, pp. 949, 1979.
12. P. Gunter, "Holography, Coherent Light Amplification and Optical Phase Conjugation with Photorefractive Materials," *Physics Report*, 93, pp. 199, 1982.
13. N.V. Kukhtarev, et al, "Holographic Storage in Electrooptic Crystal. II. Beam Coupling, - Light Amplification," *Ferroelectrics*, 22, pp. 961, 1979.
14. J.P. Huignard, and A. Marrakchi, "Coherent Signal Beam Amplification in Two-Wave Mixing Experiments with Photorefractive $\text{Bi}_{12}\text{SiO}_{20}$ Crystals," *Opt. Commun.* 38, pp. 249, 1981.
15. A.E. Chiou, and P. Yeh, "Energy Efficiency of Optical Interconnection Using Photorefractive Dynamic Holograms," Optical Computing, *1989 Technical Digest Series*, Vol. 9, (Optical Society of America, Washington, D.C. 1989), pp. 128.
16. A.E. Chiou and P. Yeh "Energy Efficiency of Optical Interconnection Using Photorefractive Holograms," submitted to *Appl. Opt.*
17. A.D. Fisher, and J.N. Lee, "The Current Status of Two-Dimensional Spatial Light Modulator Technology," *Proc. SPIE* 634, pp. 352, 1986.
18. C. Warde, and A.D. Fisher, "Spatial Light Modulators: Applications and Functional Capabilities," in *Optical Signal Processing*, J. Horner, Ed., Academic Press (1987).

19. J. Feinberg, "Self-Pumped, Continuous-Wave Phase Conjugation Using Internal Reflection," *Opt. Lett.* 7 (10), pp. 486, 1982.
20. J.H. Hong, A.E. Chiou, and P. Yeh, "On Image Amplification by Two Wave Mixing in Photorefractive Crystal," submitted to *Appl. Opt.*
21. J. Ma, et al., "Multibeam Coupling in Photorefractive SBN:Ce," *Opt. Lett.* 13(11), pp. 1020, 1988.
22. Y. Fainman, E. Klancnik, and S. Lee "Optimal Coherent Image Amplification by Two-Wave Coupling in Photorefractive BaTiO₃," *Opt. Eng.* 25(2), pp. 228, 1986.
23. H. Rajbenbach, "Digital Optical Processing with Photorefractive Materials: Applications of a Parallel Half-Adder Circuit to Algorithmic State Machines," *J. Appl. Phys.* 62(12), pp. 4675, 1987.